NASA Technical Paper 1350

Flight-Determined Stability and Control Derivatives for the F-111 Tact Research Aircraft

Alex G. Sim and Robert E. Curry

OCTOBER 1978

NASA

NASA Technical Paper 1350

Flight-Determined Stability and Control Derivatives for the F-111 Tact Research Aircraft

Alex G. Sim and Robert E. Curry
Dryden Flight Research Center
Edwards, California

National Aeronautics
and Space Administration

Scientific and Technical Information Office

1978

FLIGHT-DETERMINED STABILITY AND CONTROL DERIVATIVES FOR THE F-111 TACT RESEARCH AIRCRAFT

Alex G. Sim and Robert E. Curry
Dryden Flight Research Center

INTRODUCTION

The F-111 transonic aircraft technology (TACT) aircraft is the latest of a series of research aircraft to incorporate supercritical wing technology. Unlike previous supercritical wing designs, the TACT wing was designed to provide improvements in transonic maneuver capability without degrading the F-111A aircraft's cruise and supersonic performance.

A research program was conducted jointly by the National Aeronautics and Space Administration (NASA) and the U.S. Air Force. During the envelope-expansion phase of the flight program, the flight-determined derivatives were used to update the analysis of the vehicle dynamics to insure safety of flight. One goal of the TACT program was to provide stability and control derivatives to establish a data base with which experimental and analytical prediction techniques could be improved for this class of aircraft. To lend credence to the flight-determined derivatives and to indicate the deviation from potential theory, some of the major derivatives were calculated based on computer models of the aircraft's geometry. These are referred to in this report as analytical model derivatives.

This report presents the flight derivative data base for the F-111 TACT research aircraft. The flight derivatives are correlated with the analytical model derivatives for specific flight conditions and aircraft configurations.

SYMBOLS

The stability and control derivatives, as presented, are partial derivatives representing standard NASA coefficients of forces and moments. A right-hand sign convention is used to determine the direction of forces, moments, angular displacements, and velocities. Except for angle of attack, the data are referenced to the vehicle body axis. Angle of attack is referenced to the wing reference plane for consistency with wind tunnel data and other TACT flight data, and thus, it is 1° higher than it would be if it were referenced to the vehicle body axis.

Physical quantities are given in the International System of Units and parenthetically in U.S. Customary Units.

CLB	rolling moment coefficient with respect to angle of sideslip, per degree
CLDA	rolling moment coefficient with respect to aileron deflection, per degree
CLDR	rolling moment coefficient with respect to rudder deflection, per degree
CLDS	rolling moment coefficient with respect to spoiler deflection, per degree
CLP	rolling moment coefficient with respect to rolling rate, per radian
CLR	rolling moment coefficient with respect to yawing rate, per radian
CMA	pitching moment coefficient with respect to angle of attack, per degree
CMDE	pitching moment coefficient with respect to elevator deflection, per degree
CMQ	pitching moment coefficient with respect to pitching rate, per radian
CNA	untrimmed normal-force coefficient with respect to angle of attack, per degree
CNB	yawing moment coefficient with respect to angle of sideslip, per degree
CNDA	yawing moment coefficient with respect to aileron deflection, per degree
CNDE	untrimmed normal-force coefficient with respect to elevator deflection, per degree
CNDR	yawing moment coefficient with respect to rudder deflection, per degree
CNDS	yawing moment coefficient with respect to spoiler deflection, per degree
CNP	yawing moment coefficient with respect to rolling rate, per radian
CNR	yawing moment coefficient with respect to yawing rate, per radian
CYB	side-force coefficient with respect to angle of sideslip, per degree

CYDA	side-force coefficient with respect to aileron deflection, per degree
CYDR	side-force coefficient with respect to rudder deflection, per degree
CYDS	side-force coefficient with respect to spoiler deflection, per degree
c_{n_α}	section normal-force slope, per degree
M	Mach number
α	angle of attack with respect to wing reference plane, degrees
λ	angle of wing leading-edge sweep, degrees

AIRCRAFT DESCRIPTION

The TACT modifications to the F-111A baseline vehicle included a new wing planform with a supercritical airfoil and a new high-lift system, a modified wing seal, a modified overwing fairing, and a fixed-structure glove. The general arrangement of the F-111 TACT aircraft is shown in figure 1, and the aircraft's physical characteristics are given in table 1. Additional description of the TACT aircraft, as well as a comparison with the F-111A baseline vehicle, is given in references 1 and 2.

The TACT aircraft's control surfaces were controlled by an irreversible hydraulic system. The pilot controlled the aircraft through a conventional center stick and rudder pedals. For pitch control, the horizontal stabilizer was deflected symmetrically by either the pilot or the rate command augmentation system. A similar arrangement with the rudder was used for yaw control. However, for roll control, the pilot's inputs activated both the differential horizontal stabilizer and the spoilers, while the rate command augmentation system activated only the differential stabilizer.

INSTRUMENTATION

Data were obtained at 20 samples per second through a 10-bit pulse code modulation system. All the data were calibrated and analyzed after the flight using a ground-based computer.

Angle of attack and angle of sideslip were measured using a vane flow angularity sensor system. This system and its calibration are described in reference 3.

In addition, angle of attack was estimated along with the flight derivatives for correlation with the measured angle of attack. Angular positions were measured with a stable platform, angular rates were measured using rate gyros, and linear accelerations were determined from linear accelerometers. Control positions were measured using control position transducers.

Corrections were applied to the airspeed data to obtain true velocity, Mach number, and dynamic pressure. Linear accelerations, angle of attack, and angle of sideslip were corrected for displacement from the center of gravity.

FLIGHT CONDUCT

Before each flight, a detailed flight plan (checklist) specifying particular maneuvers was prepared. The flight was then monitored by chase aircraft pilots and control room personnel. This procedure not only insured safety of flight but also allowed the research engineer to monitor the flight data in real time, thus giving him insight into the adequacy of the maneuvers and the instrumentation data quality. The flight plan flexibility was sufficient to allow a maneuver to be repeated if necessary.

Longitudinal and lateral-directional maneuvers from which aircraft data were obtained were performed throughout the flight envelope. Data were obtained for angles of attack from approximately 3° to 14° for a Mach number range from approximately 0.25 to 1.70. The data for the higher angles of attack were obtained at elevated load factors. The longitudinal maneuver consisted of a horizontal stabilizer doublet, followed by 2 to 3 seconds of no pilot input, followed by a second horizontal stabilizer doublet. Because the vehicle normally exhibited an overdamped longitudinal response, the second doublet was necessary to increase the amount of statistically significant transient response information.

One of the objectives in the lateral-directional mode analysis was to obtain independent derivatives with respect to spoiler and aileron (rolling tail). However, it was difficult to separate the aileron and spoiler derivatives with the roll augmentation off because the two control surfaces operated nearly in phase. Because the roll augmentation acted only through the aileron, out-of-phase aileron and spoiler motion could be obtained with the roll augmentation on. With both roll and yaw augmentation on, the resulting airplane motion was heavily damped. The maneuver finally selected (fig. 2) was performed with the roll augmentation on and the yaw augmentation off. It consisted of two pilot-initiated roll doublets followed by a rudder doublet. This maneuver proved to be adequate for the derivative extraction process.

One flight was made without the use of the spoilers during maneuvers to evaluate the possibility of obtaining more consistent sets of derivatives with lower uncertainties. Better results were obtained from these maneuvers.

Some of the maneuvers analyzed were not performed to obtain derivatives. Examples of these include structural excitation (using stick raps) and handling quality evaluations. Although specific derivatives could be obtained from these maneuvers, a consistent, complete set of high-quality derivatives could not.

DERIVATIVE ANALYSIS

Flight Data

A digital computer program employing a maximum likelihood estimator method was used to determine sets of derivatives and uncertainty levels for the longitudinal and lateral-directional modes from flight data. This computer program and its theory, mathematical model, and practical application are documented in references 4 to 6.

The derivative analysis was usually performed within a week of the flight using a "best estimate" set of moments of inertia. After the completion of the derivative-extraction flights, the moments of inertia were experimentally determined using the Air Force Flight Test Center's Moment of Inertia Facility. The derivatives for presentation in this report were adjusted to reflect the experimentally determined moments of inertia. In addition, the derivatives were adjusted to a reference longitudinal center of gravity. The reference center of gravity varied as a function of wing sweep, and the variation is documented in table 2. A variable reference was used to provide a derivative data set consistent with the performance flight data. These reference values represent an average flight center of gravity for each wing sweep.

Geometric Models

Analytical model derivatives were obtained from two large computer programs based on a grid determined by dividing the aircraft geometry into constant pressure panels. Integration of these pressures yielded the forces and moments. Both programs assume inviscid, incompressible (with Prandtl-Glauert corrections), attached flow. They differ in the way they represent the aircraft geometry and in the solution for the constant pressure panels.

The first program, referred to as the WING-BODY program, models both lifting surfaces (wings) and a body. It is a potential-doublet panel program in which the wing-body combination is represented by a large number of distributed singularities which are used to satisfy the linearized potential equations. It can be used for both supersonic and subsonic analysis. Further information on the theory and use of the program is given in references 7 and 8, respectively.

For the second program, referred to as the VORTEX-LATTICE program, the lifting surface planforms are represented with a lattice of horseshoe vortexes. By solving the flow boundary condition of each horseshoe vortex, the elemental lift of each panel can be determined. The program is used for subsonic analysis. It can be used to compute the potential as well as the vortex leading- and side-edge components of forces and moments; however, only the potential solution was used for these studies. Further information on the theory and use of similar programs is given in references 9 to 11.

In using the above programs, an attempt was made to model the geometry in a basic, conceptual manner. This was done to best represent the manner in which these programs are mechanized to minimize computer time. A WING-BODY panel model that was used to obtain rolling tail control effectiveness is shown in figure 3. Only the right half of this model was used for the typical case where vehicle symmetry is assumed. The panel coordinates are the basic inputs to the program. A typical VORTEX-LATTICE planform model is shown in figure 4. The panels are not shown since paneling is an internal process of the program. Only the planform view is shown since, for this case, the wings are coplanar. It was not necessary to model wing camber in either program.

DATA PRESENTATION

The majority of the flight data were obtained over the airplane's Mach number and angle of attack ranges, predominantly at wing sweep angles of 26°, 35°, and 58° with the airplane in a clean configuration (that is, landing gear and flaps retracted). Additional flight data were obtained at low speeds (Mach numbers from 0.25 to 0.45) with various combinations of landing gear and flap positions for wing sweep angles of 16°, 20°, and 26°. All the data are presented as a function of angle of attack for specific Mach number ranges. Where possible, a recommended fairing is given to aid in the interpretation of the flight derivatives. In addition, certain derivatives that are strong functions of Mach number as well as angle of attack are presented as functions of Mach number for a given angle of attack.

Uncertainty levels are shown for all flight data. These uncertainty levels are proportional to the Cramèr-Rao bounds described in reference 5 and were obtained by multiplying the Cramèr-Rao bounds of reference 5 by a simple scale factor of 5. The factor is justified in reference 6. In a more general sense, the uncertainty level can be interpreted as a measure of the relative accuracy of each derivative value.

The analytical model derivatives were computed for the clean configuration at a Mach number of 0.60 for wing sweep angles of 26°, 35°, and 58° and at a Mach number of 1.20 for a wing sweep angle of 58°. These derivatives are only presented where the assumptions used to compute them are considered valid. Thus, due to the assumption of attached flow, the analytical model data are only valid, and hence only presented, for low angles of attack.

RESULTS AND DISCUSSION

Since a primary purpose of this report is to provide a stability and control data base, many of the results are presented without discussion.

Longitudinal Derivatives

The clean-configuration longitudinal derivatives for a wing sweep angle of 26° are shown in figure 5 as a function of angle of attack and in figure 6 as a

function of Mach number. For angles of attack less than 7°, the flight and analytical model values for *CNA* are in good agreement. Above an angle of attack of approximately 8°, the magnitude of the flight *CNA* decreases significantly as compared to the analytical model values obtained from linearized potential theory. The trend exhibited in the flight-determined *CNA* values is substantiated by figure 7, which shows a reduction in the section normal-force slope, c_{n_α}, with increasing angle of attack for four wingspan locations. These section data were obtained independently by integrating the flight-determined wing pressure coefficients.

Even though *CNA* has been shown to decrease with angle of attack, the actual angle of attack at which the break in the slope occurs can be easily misinterpreted from the data in figure 5(a). The maximum likelihood estimator used to obtain the flight derivatives provides a linearized derivative from the transient motion of the aircraft. For longitudinal derivatives, the average angle of attack is used as the independent variable; the actual angle of attack, being a state variable, will typically vary ±2° from trim. The resulting linearized derivative (in this case, *CNA*) tends to acquire an average slope over the angle of attack range for the maneuver. This, in effect, filters any sharp breaks in the coefficient. Thus, even though the first indications of a break in the data of figure 5(a) occur at an angle of attack of approximately 7°, the actual break occurs at an angle of attack between 8° and 9°, as shown in figure 8, which was taken from reference 12. Note that in this reference, the normal-force slope break is correlated with buffet intensity rise, which is an indication of flow separation.

The flight-determined *CMA* values (fig. 5(a)) decrease with angle of attack while the analytical model values do not. This lack of linearity for the flight values is related to the similar reduction in *CNA*. The apparent scatter in *CMA* is a Mach number effect, as shown in figure 6(a).

CNDE and *CMDE* are presented in figure 5(b). The flight values for *CMDE* are significantly lower than the analytical model values. The analytical model predictions for *CMDE* can be considered the theoretical upper limit for this planform configuration because they do not account for the reduction in dynamic pressure on the horizontal tail, which is caused by the wing wake.

Although the flight values of *CMQ* appear to contain considerable scatter (fig. 5(c)), much of this apparent scatter is a Mach number effect, as shown in figure 6(b). The correlation between the flight and analytical model derivatives is considered to be good even though the flight values are higher, because *CMQ* is historically difficult to estimate theoretically.

The clean-configuration longitudinal derivatives for a wing sweep angle of 35° are shown in figure 9 as a function of angle of attack and in figure 10 as a function of Mach number. In general, the previous discussion for a wing leading-edge sweep angle of 26° also applies to the 35° wing sweep data.

Figures 11 and 12 present the clean-configuration longitudinal derivatives for a wing sweep angle of 58° as a function of angle of attack and as a function of Mach number, respectively. As shown in figure 11(a), *CNA* increases slightly with angle

of attack. This is due to the formation of a leading-edge vortex, which is characteristic of aircraft with highly swept wings.

The subsonic flight values of *CMDE* included in figure 11(b) are slightly lower than the prediction. However, the analytical model greatly overpredicts *CMDE* at Mach 1.20, which is a result of the overestimation of the aft movement of the center of pressure on the horizontal stabilizer due to an assumption of established supersonic flow. This discrepancy may indicate that the flow over the horizontal tail of the flight vehicle is not established supersonic flow.

The longitudinal derivatives obtained with various combinations of landing gear and flap positions at wing sweep angles of 16°, 20°, and 26° are shown in figure 13. All these data were obtained at Mach numbers less than 0.45. The flaps-deflected configuration consisted of having the Krueger leading-edge flaps deployed and the Fowler trailing-edge flaps deflected 30°. Of particular significance is the increase in *CMA* due to flap deflection at a wing sweep angle of 26°.

Lateral-Directional Derivatives

The clean-configuration lateral-directional derivatives for a wing sweep angle of 26° are shown in figure 14 as a function of angle of attack and in figure 15 as a function of Mach number. These flight derivatives exhibit more scatter and higher uncertainty levels than the clean-configuration lateral-directional derivatives at other wing sweeps. For a low-sweep configuration, greater uncertainty would be expected at higher angles of attack where buffet and flow separation exist. However, figure 15 shows that the scatter in these derivatives exists at an angle of attack of 4° and increases with increasing Mach number. The pilot's comments indicate that a low level of buffet exists at these low angles of attack, beginning at a Mach number as low as 0.85. This slight indication of flow separation on the wing was not of sufficient magnitude to affect the flying qualities. Its primary effect appears to be an increase in the uncertainty in the flight derivative analysis for a wing sweep angle of 26°.

The VORTEX-LATTICE program was used to compute analytical model values for *CNB* and *CYB* by representing the side view of the body and the vertical tail as wing planforms and disregarding the wing. As shown in figures 14(a) and 14(g), these analytical model derivatives are reasonably close to the flight values. A similar analysis could have been conducted using the WING-BODY program, but the implementation would have been more complex because of the input requirements. Analytical model values for *CNDA* and *CLDA* were computed using both programs. Using the VORTEX-LATTICE program, *CLDA* was computed based on the horizontal tail lift and center of pressure. To compute *CNDA*, it was assumed that *CNDA* is a result of the differential drag from the horizontal stabilizer. Assuming the far field solution for drag due to the incremental horizontal stabilizer lift, the following expression was obtained:

$$CNDA = (CLDA)(\tan \alpha)$$

To compute the two derivatives using the WING-BODY program, the airplane was modeled as shown in figure 2. The resulting rolling and yawing moments were

direct outputs from the program. The analytical model and flight derivatives are shown in figure 14(d). This figure shows that the WING-BODY program computed a value for *CLDA* close to the flight value and that the value for *CNDA* based on the results from the VORTEX-LATTICE program is a good estimate.

The flight and analytical model values for *CNDR* and *CLDR* are shown in figure 14(e). For the VORTEX-LATTICE analysis, the rudder was modeled as aft camber in the side views of the vertical tail. When modeling a control surface of the aft camber type with the WING-BODY program, it is common procedure to scale down the resulting control derivatives to compensate for the WING-BODY program's historical tendency to overpredict the effects of aft camber. For this report, a scale factor of one-half was selected; however, an analysis of the results indicates that a scale factor of about two-thirds would have been more appropriate. The flight derivatives are generally within the boundaries of the predicted values.

The clean-configuration lateral-directional derivatives for wing sweep angles of 35° and 58° are shown in figures 16 to 19. The analytical model derivatives were computed using the same techniques discussed for the 26° wing sweep data. The correlations between the flight and analytical model derivatives follow the same trends. Of particular interest in these data are the nonlinearities in *CLB*, *CLP*, and *CLDS* with respect to angle of attack (figs. 16 to 18, parts (a), (b), and (f)). All three of these derivatives have primary effects on the handling qualities.

The lateral-directional derivatives obtained with either the landing gear extended or the flaps deflected at a wing sweep angle of 16° or 26° are shown in figure 20. The Mach number range and the flaps-deflected configuration were the same as those for the longitudinal derivatives of figure 13. To determine the incremental effects of the landing gear and flap configurations as compared with the clean configuration, the data of figure 20 should be compared with those of figure 14. Of the derivatives presented, *CNB*, *CLP*, *CLDS*, and *CNDS* show the most significant effects. A definite, and expected, decrease in *CNB* results from the extension of the landing gear. *CLP* increases when the flaps are deflected as a result of the increase in the actual wing area. *CLDS* and *CNDS* also increase when the flaps are deflected as a result of having higher levels of lift to decrease.

To check the validity of the angle of attack measurement, angle of attack was calculated based on the value of sin α. The value and uncertainty of sin α were obtained from the maximum likelihood estimator used to compute the flight derivtives. The calculated angle of attack includes the 1° angle between the angle of attack reference axis and the vehicle body axis.

In figure 21, calculated angle of attack is correlated with reference angle of attack for Mach numbers near 0.70. These data indicate that the reference angle of attack is correct from 3° to 10°. At higher angles of attack, the results are inconclusive because the uncertainties are high and the values were obtained from high load factor maneuvers, which undoubtedly induced aeroelastic effects.

CONCLUDING REMARKS

A flight investigation was conducted to provide a stability and control derivative data base for the F-111 transonic aircraft technology (TACT) research aircraft. Both longitudinal and lateral-directional derivatives were obtained for the clean configuration (that is, landing gear and flaps retracted) at wing sweep angles of 26°, 35°, and 58°. In addition, the effects of landing gear extension and flap deflection were obtained for several low speed and low wing sweep conditions. Data were obtained for angles of attack from approximately 3° to 14° for a Mach number range from approximately 0.25 to 1.70.

The VORTEX-LATTICE and WING-BODY analysis programs were used to predict selected derivatives based on vehicle geometry. These derivatives, referred to as the analytical model derivatives, were obtained for wing sweep angles of 26°, 35°, and 58° at a Mach number of 0.60 and for a wing sweep angle of 58° at a Mach number of 1.20.

A correlation between the flight-determined and analytical model derivatives indicated both the strengths of the prediction methods and the variation of the flight derivatives from potential theory. Of particular significance was the break in the flight normal-force slope which occurred at a relatively low angle of attack. This break was correlated with data from two independent sources.

The validity of the angle of attack measurement was verified independently at a Mach number of 0.70 for angles of attack from 3° to 10°.

Dryden Flight Research Center
National Aeronautics and Space Administration
Edwards, Calif., November 17, 1977

REFERENCES

1. Marquardt, R. F.: Transonic Aircraft Technology - TACT Aircraft Geometric Characteristics. MAIR 595-19, General Dynamics, April 16, 1973.

2. Hallissy, James B.; and Ayers, Theodore G.: Transonic Wind-Tunnel Investigations of the Maneuver Potential of the NASA Supercritical Wing Concept. Phase I. NASA TM X-3534, 1977.

3. Sakamoto, Glenn M.: Aerodynamic Characteristics of a Vane Flow Angularity Sensor System Capable of Measuring Flightpath Accelerations for the Mach Number Range From 0.40 to 2.54. NASA TN D-8242, 1976.

4. Maine, Richard E.; and Iliff, Kenneth W.: A FORTRAN Program for Determining Aircraft Stability and Control Derivatives From Flight Data. NASA TN D-7831, 1975.

5. Iliff, Kenneth W.; and Taylor, Lawrence W., Jr.: Determination of Stability Derivatives From Flight Data Using a Newton-Raphson Minimization Technique. NASA TN D-6579, 1972.

6. Iliff, Kenneth W.; and Maine, Richard E.: Further Observations on Maximum Likelihood Estimates of Stability and Control Characteristics Obtained From Flight Data. AIAA Paper 77-1133, Aug. 1977.

7. Woodward, Frank A.: Analysis and Design of Wing-Body Combinations at Subsonic and Supersonic Speeds. J. Aircraft, vol. 5, no. 6, Nov.-Dec. 1968, pp. 528-534.

8. Gustavsson, S. Anders L.: A Computer Program for the Prediction of Aerodynamic Characteristics of Wing-Body-Tail Combinations at Subsonic and Supersonic Speeds. Part 2. Report AU-635, Flygtekniska Försöksanstalten (The Aeronautical Research Institute of Sweden), 1972.

9. Margason, Richard J.; and Lamar, John E.: Vortex-Lattice FORTRAN Program for Estimating Subsonic Aerodynamic Characteristics of Complex Planforms. NASA TN D-6142, 1971.

10. Lamar, John E.; and Gloss, Blair B.: Subsonic Aerodynamic Characteristics of Interacting Lifting Surfaces With Separated Flow Around Sharp Edges Predicted by a Vortex-Lattice Method. NASA TN D-7921, 1975.

11. Luckring, James M.: Some Recent Applications of the Suction Analogy to Asymmetric Flow Situations. Vortex-Lattice Utilization, NASA SP-405, 1976, pp. 219-236.

12. Monaghan, Richard C.: Flight-Measured Buffet Characteristics of a Supercritical-Wing and a Conventional Wing on a Variable-Sweep Airplane. NASA TP-1244, 1978.

TABLE 1.—PHYSICAL CHARACTERISTICS OF F-111 TACT RESEARCH AIRCRAFT

Fuselage length, m (ft)	22.39 (73.47)
Wing—	
Reference planform area, m^2 (ft^2)	56.1 (603.9)
Reference longitudinal length, m (ft)	3.65 (10.4875)
Reference span, m (ft)	18.1 (59.3)
λ, deg	10 to 58
Taper ratio at $\lambda = 16°$	0.542
Aspect ratio at $\lambda = 16°$	5.82
Dihedral, deg	0
Horizontal tail—	
Area (movable), m^2 (ft^2)	14.2 (153)
Span, m (ft)	8.94 (29.3)
λ, deg	57.5
Deflection, elevator is average symmetric deflection where trailing edge up is negative and aileron is right (movable area) minus left (movable area), deg	15 to -30
Vertical tail—	
Area, m^2 (ft^2)	10.4 (112)
Span, m (ft)	2.71 (8.90)
λ, deg	55
Rudder—	
Area, m^2 (ft^2)	2.72 (29.3)
Span, m (ft)	2.43 (7.98)
Deflection, trailing edge left positive, deg	±30
Spoilers (two per side)—	
Type	Flap
Total area, m^2 (ft^2)	2.47 (26.6)
Deflection (maximum), average right minus average left where trailing edge up is negative, deg	45
Leading-edge flaps (three sections per wing)—	
Type	Krueger
Total area, m^2 (ft^2)	5.11 (55.0)
Deflection (maximum), deg	45
Trailing-edge flaps (four per side)—	
Type	Fowler, single slotted
Total area, m^2 (ft^2)	12.54 (135)
Deflection (maximum), deg	30

TABLE 2.—REFERENCE CENTER OF GRAVITY AS A FUNCTION OF WING SWEEP

λ, deg	Reference center of gravity
10	0.245
16	0.255
26	0.275
30	0.280
35	0.290
45	0.305
50	0.310
58	0.320

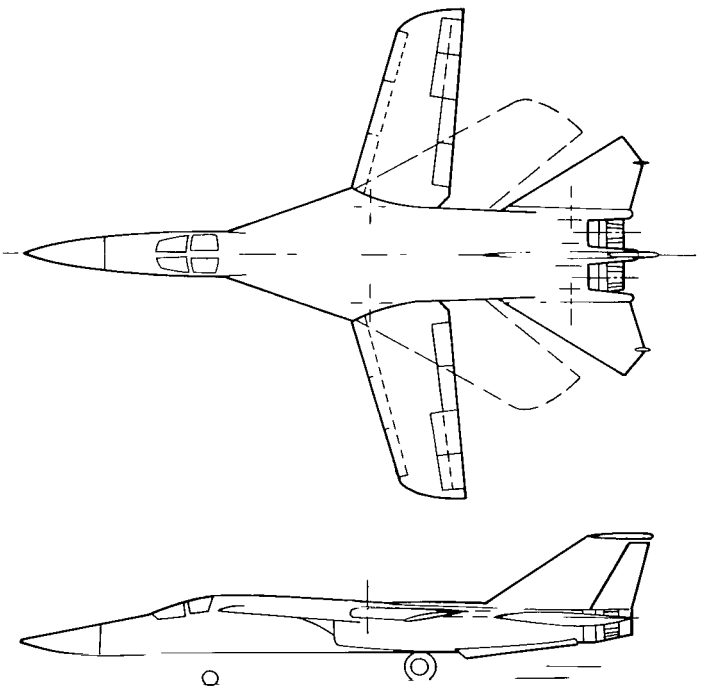

Figure 1. F-111 TACT aircraft.

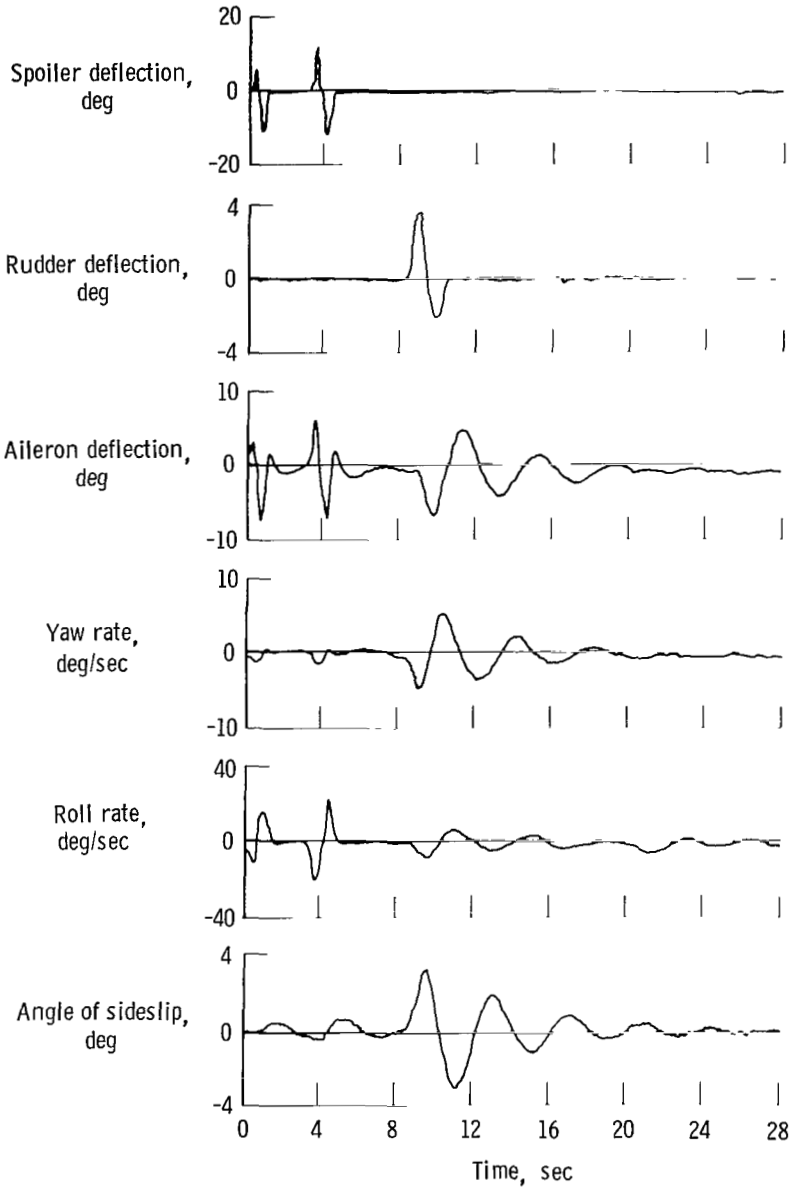

Figure 2. Typical lateral-directional maneuver used for derivative extraction.

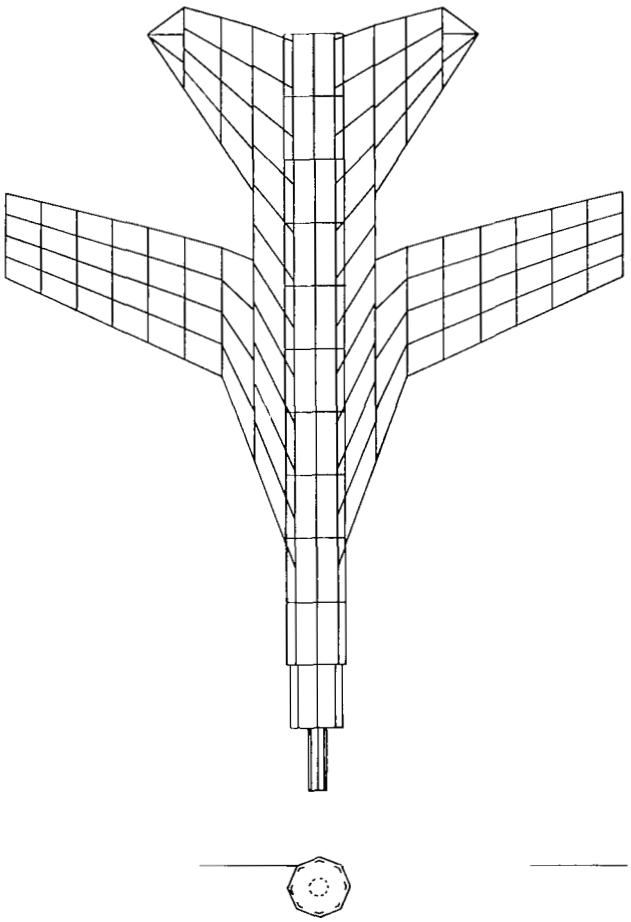

Figure 3. WING-BODY model of F-111 TACT aircraft. $\lambda = 26°$.

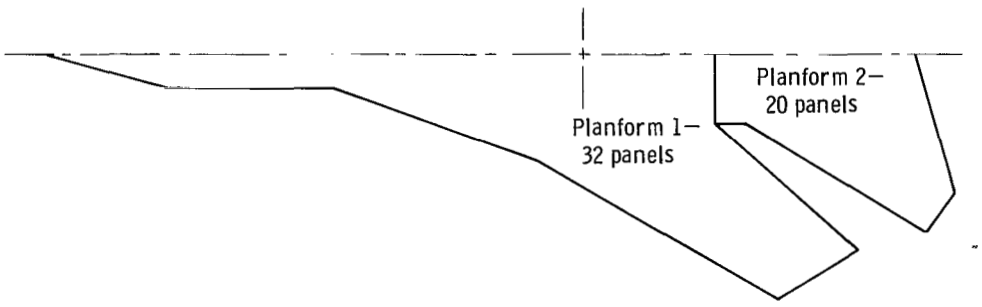

Figure 4. Typical VORTEX-LATTICE planform model.

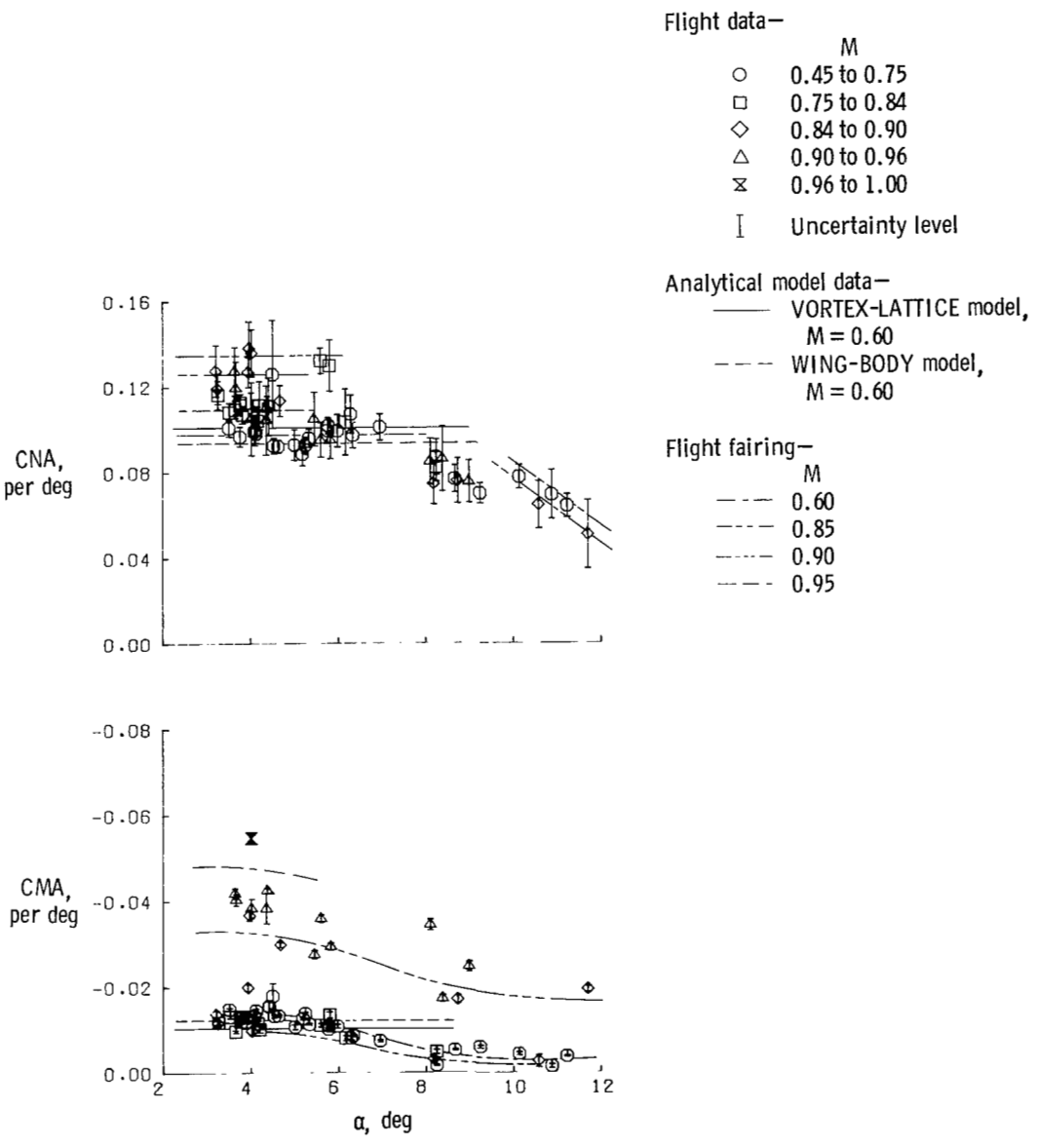

(a) CNA, CMA.

Figure 5. Longitudinal derivatives obtained from flight data as a function of angle of attack and comparison with analytical model results. λ = 26°; clean configuration.

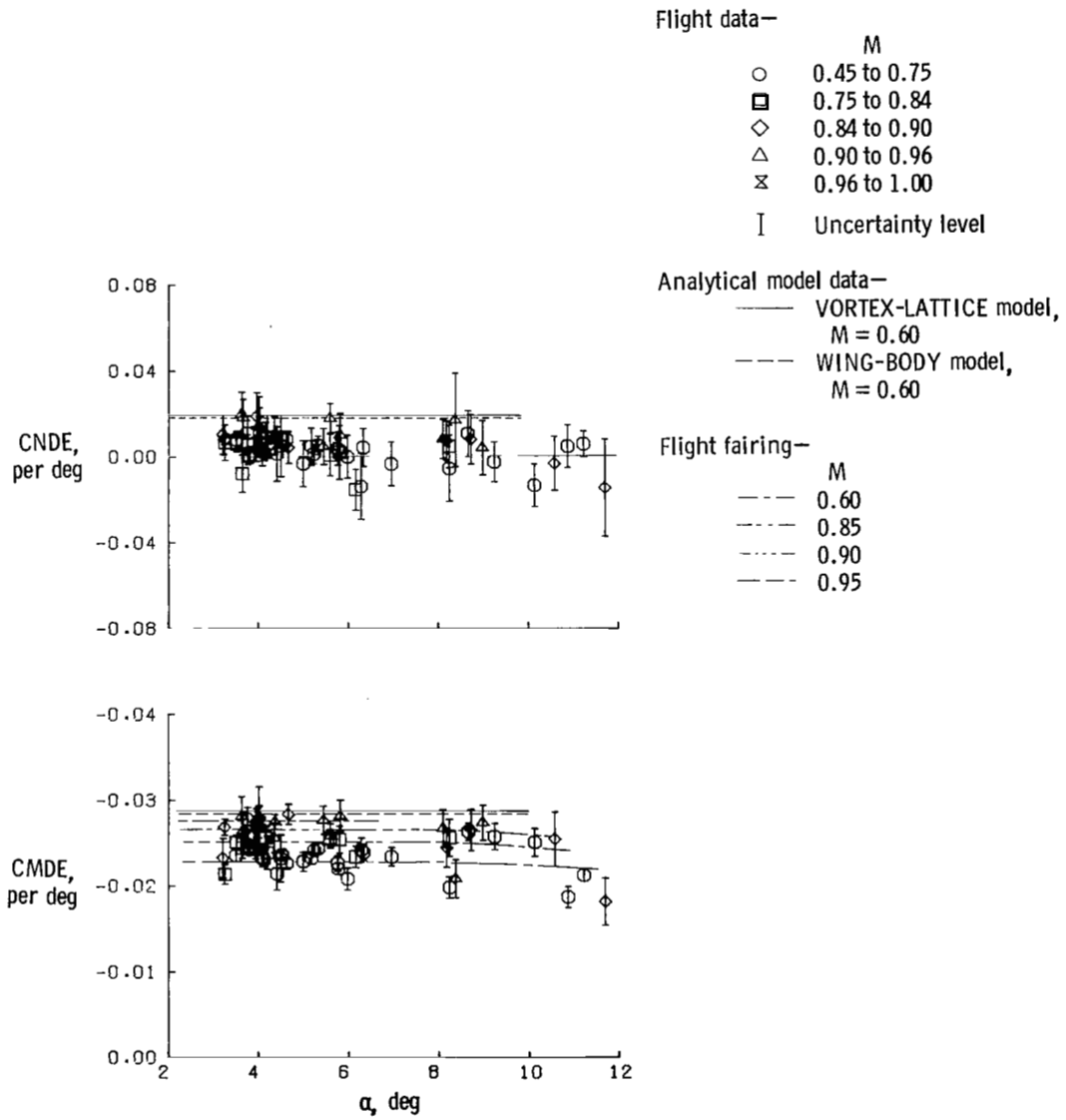

(b) CNDE, CMDE.

Figure 5. Continued.

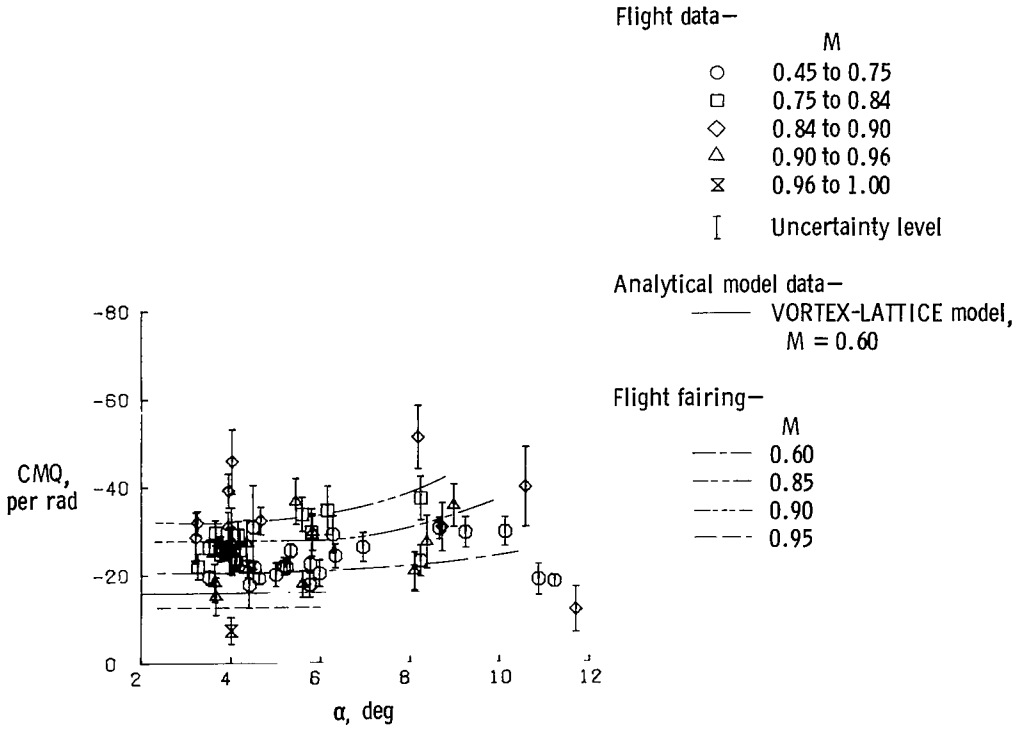

(c) CMQ.

Figure 5. Concluded.

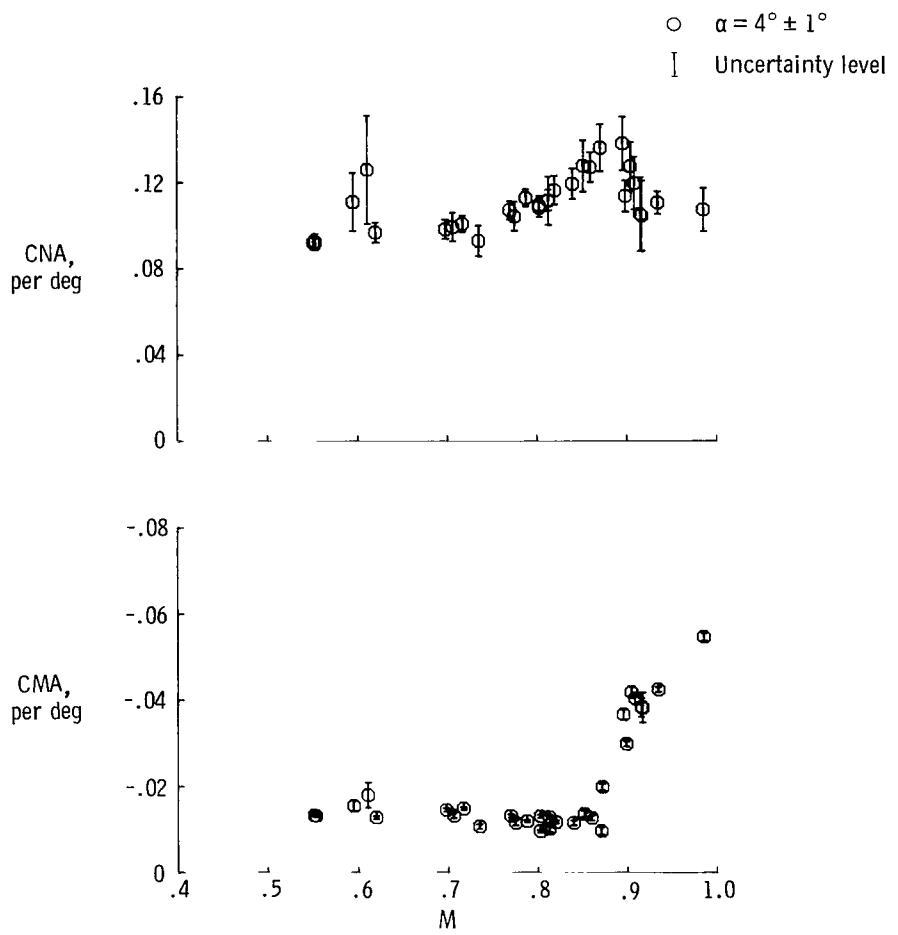

(a) CNA, CMA.

Figure 6. Longitudinal derivatives obtained from flight data as a function of Mach number. λ = 26°; clean configuration.

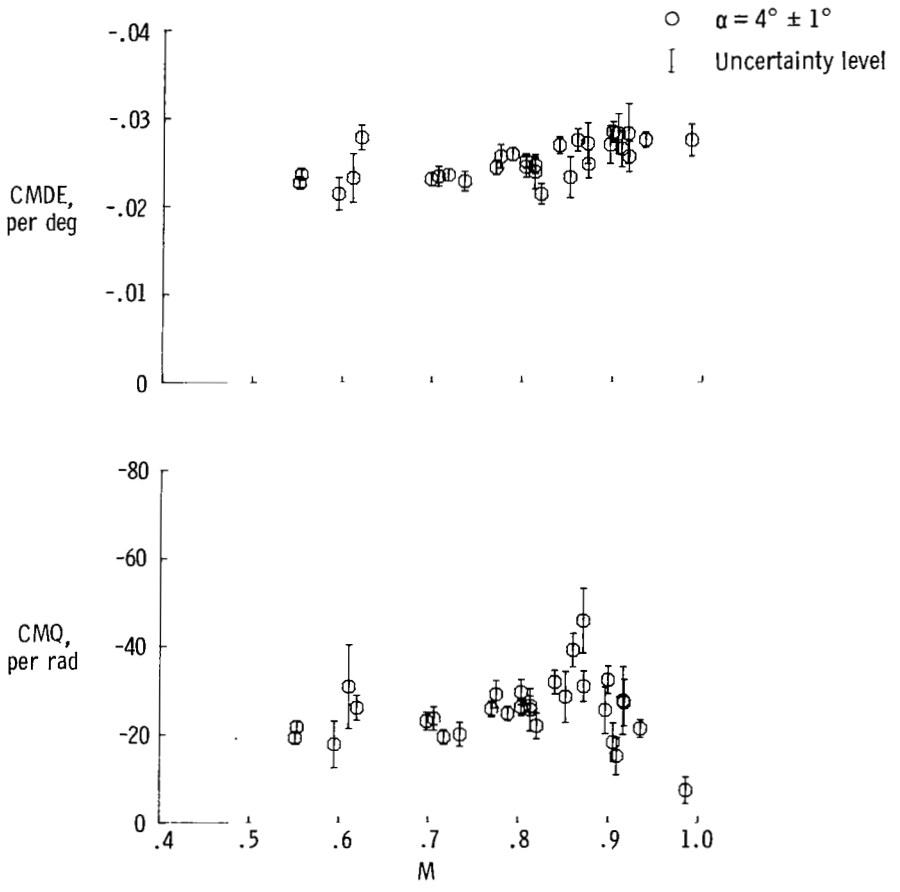

(b) CMDE, CMQ.

Figure 6. Concluded.

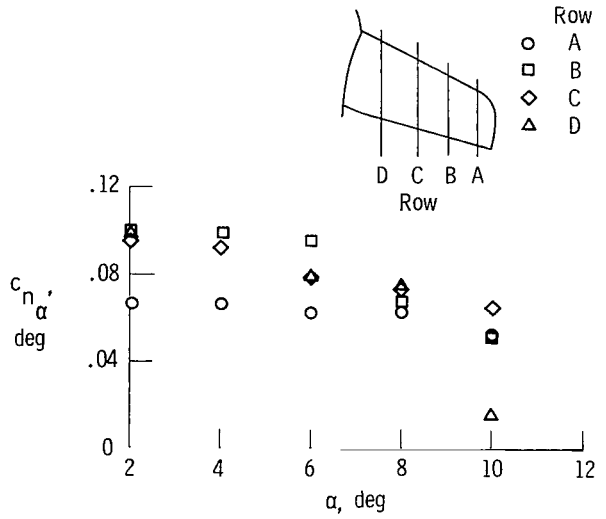

Figure 7. Section normal-force slope as a function of angle of attack. M = 0.60; λ = 26°.

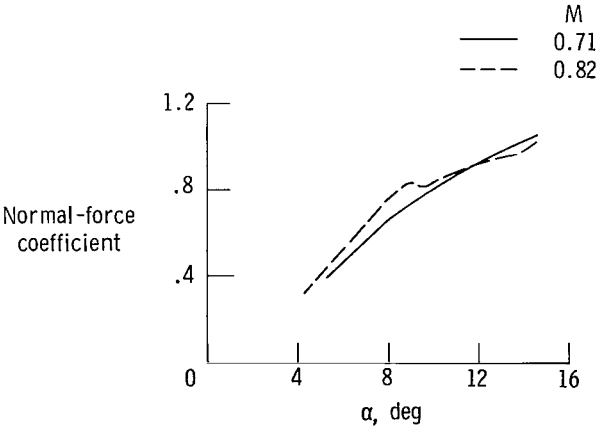

Figure 8. Normal-force coefficient as a function of angle of attack (from ref. 12).

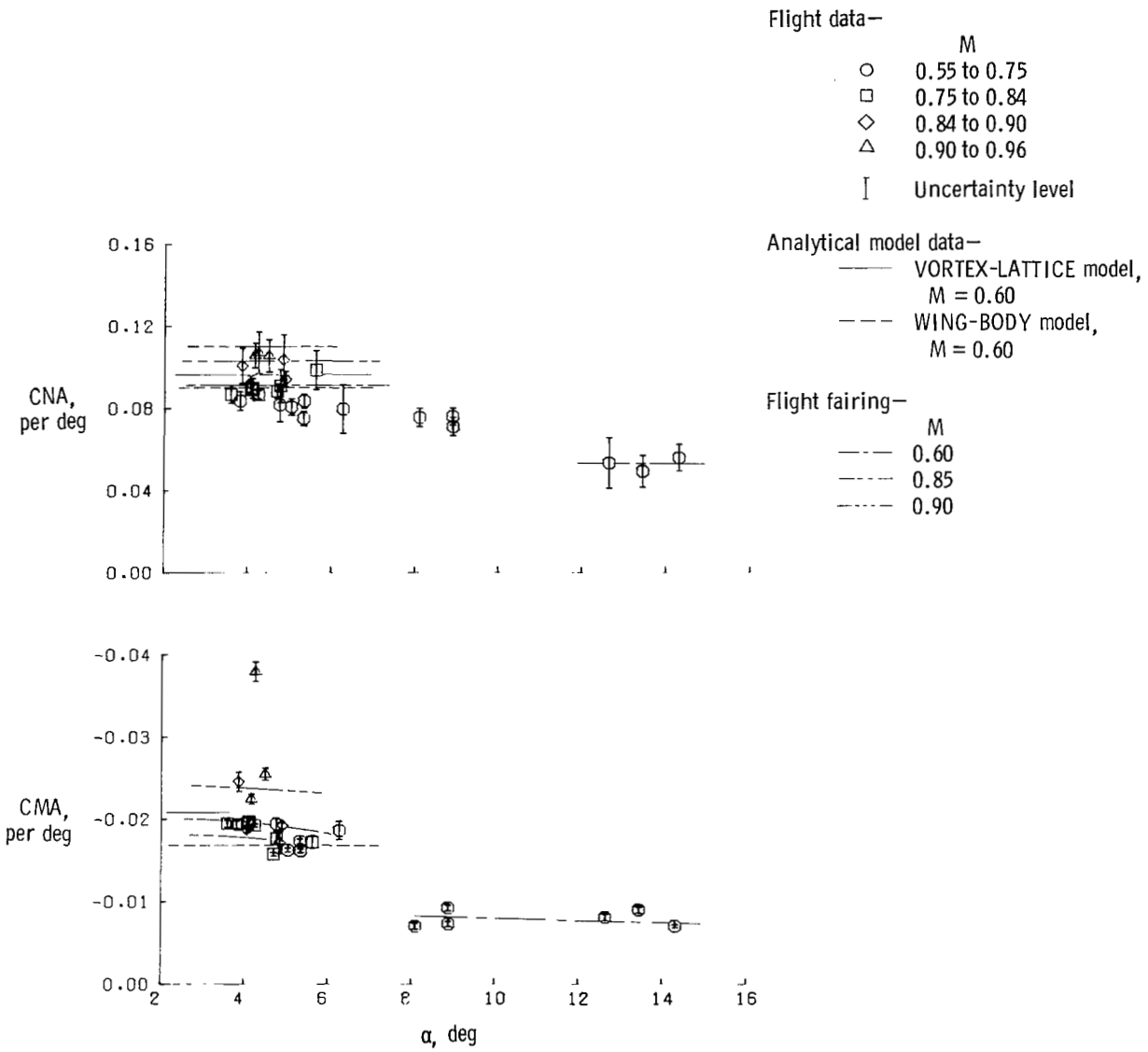

(a) CNA, CMA.

Figure 9. Longitudinal derivatives obtained from flight data as a function of angle of attack and comparison with analytical model results. λ = 35°; clean configuration.

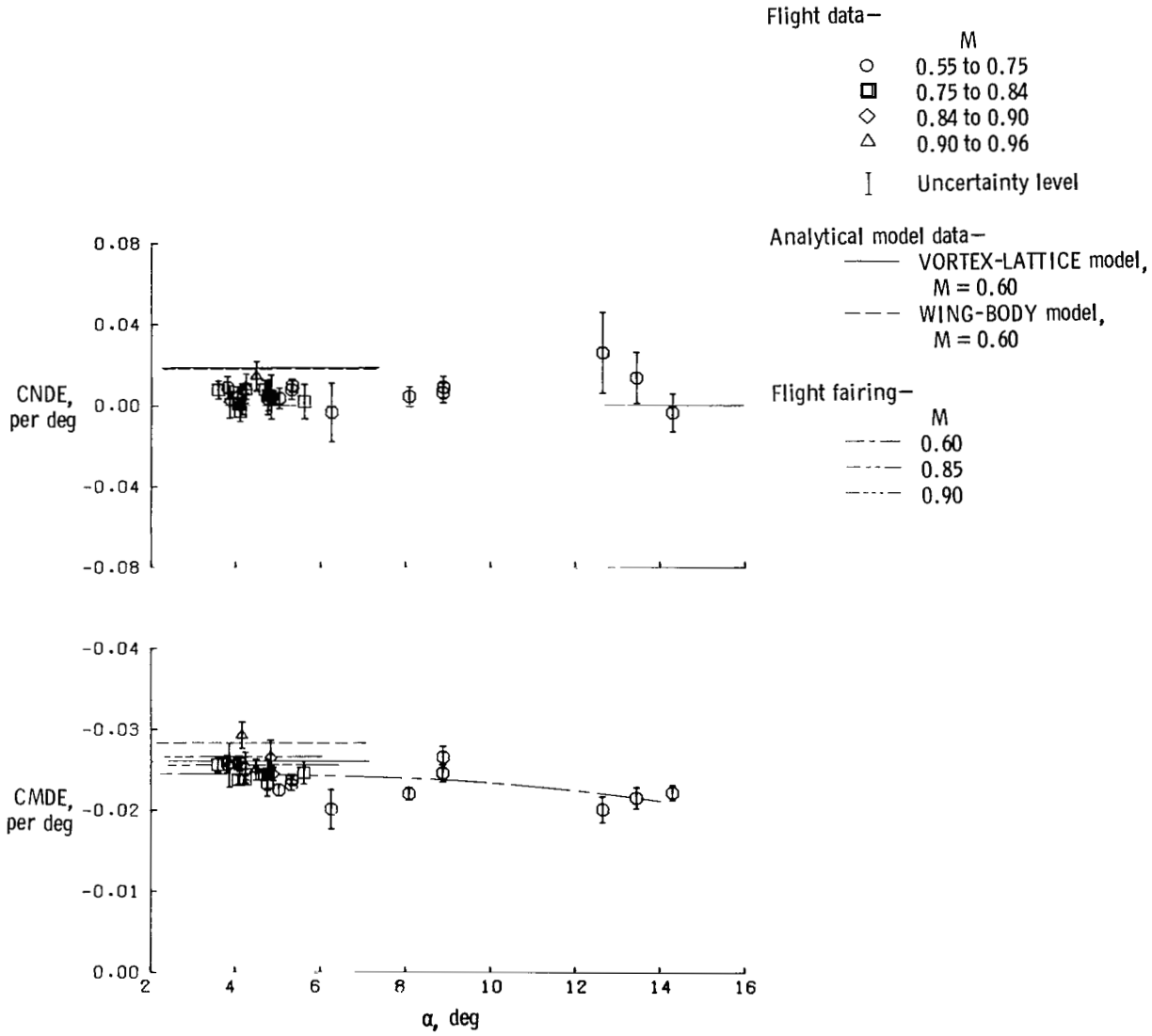

(b) CNDE, CMDE.

Figure 9. Continued.

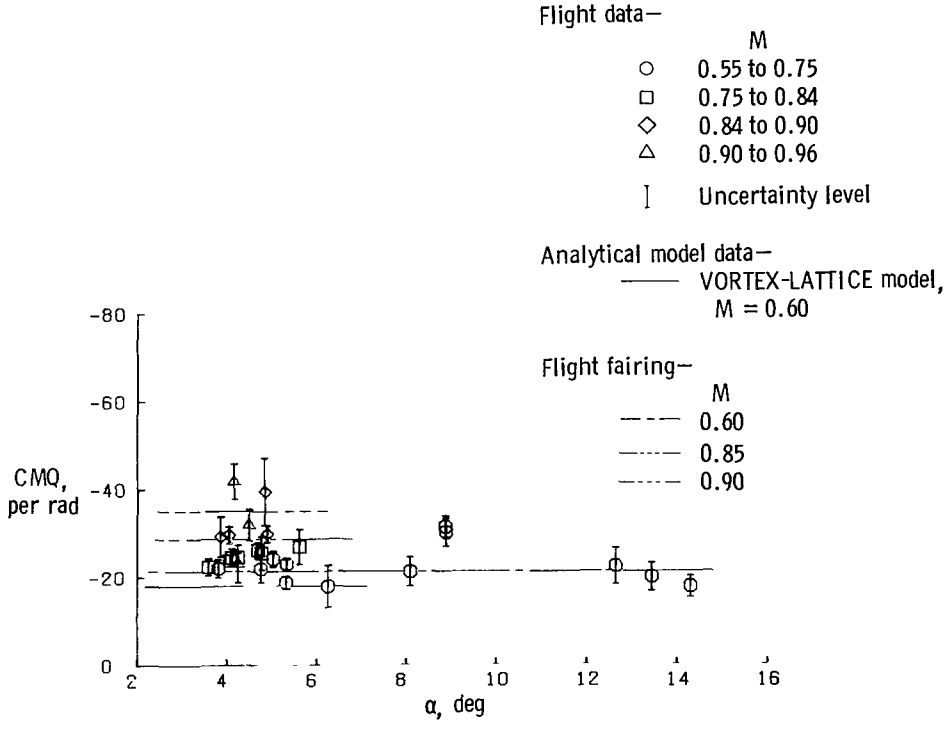

(c) CMQ.

Figure 9. Concluded.

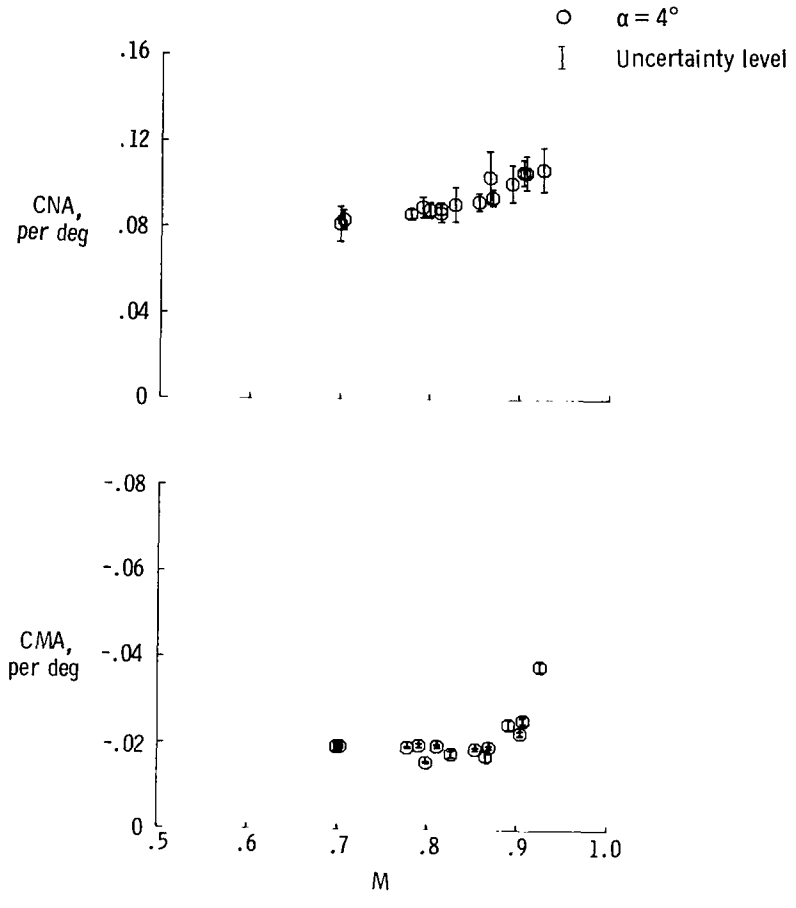

(a) CNA, CMA.

Figure 10. Longitudinal derivatives obtained from flight data as a function of Mach number. λ = 35°; clean configuration.

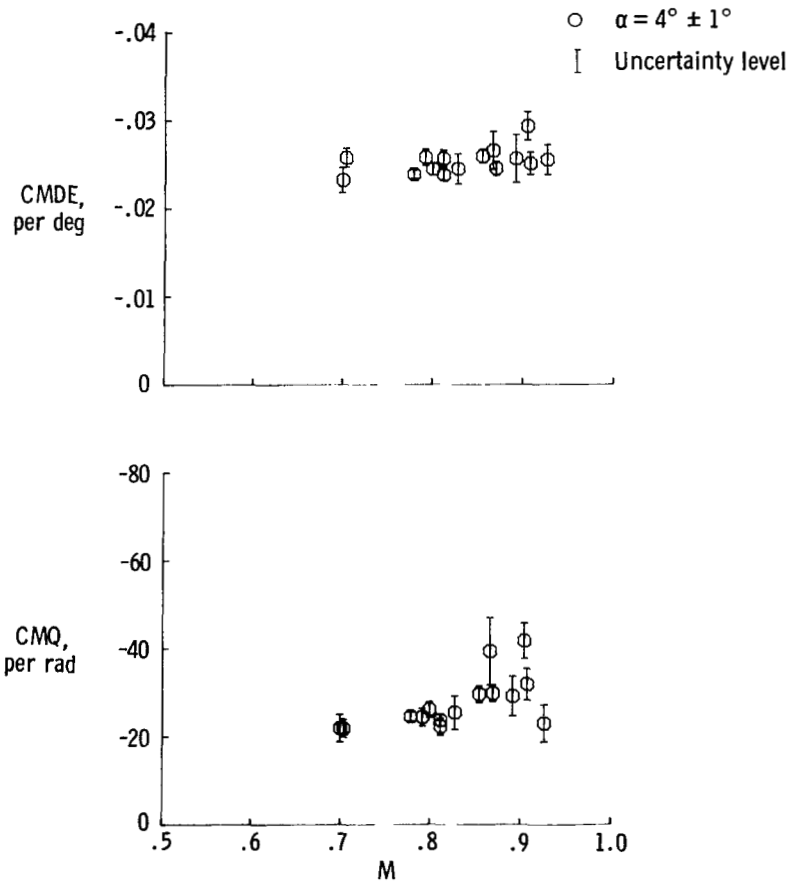

(b) CMDE, CMQ.

Figure 10. Concluded.

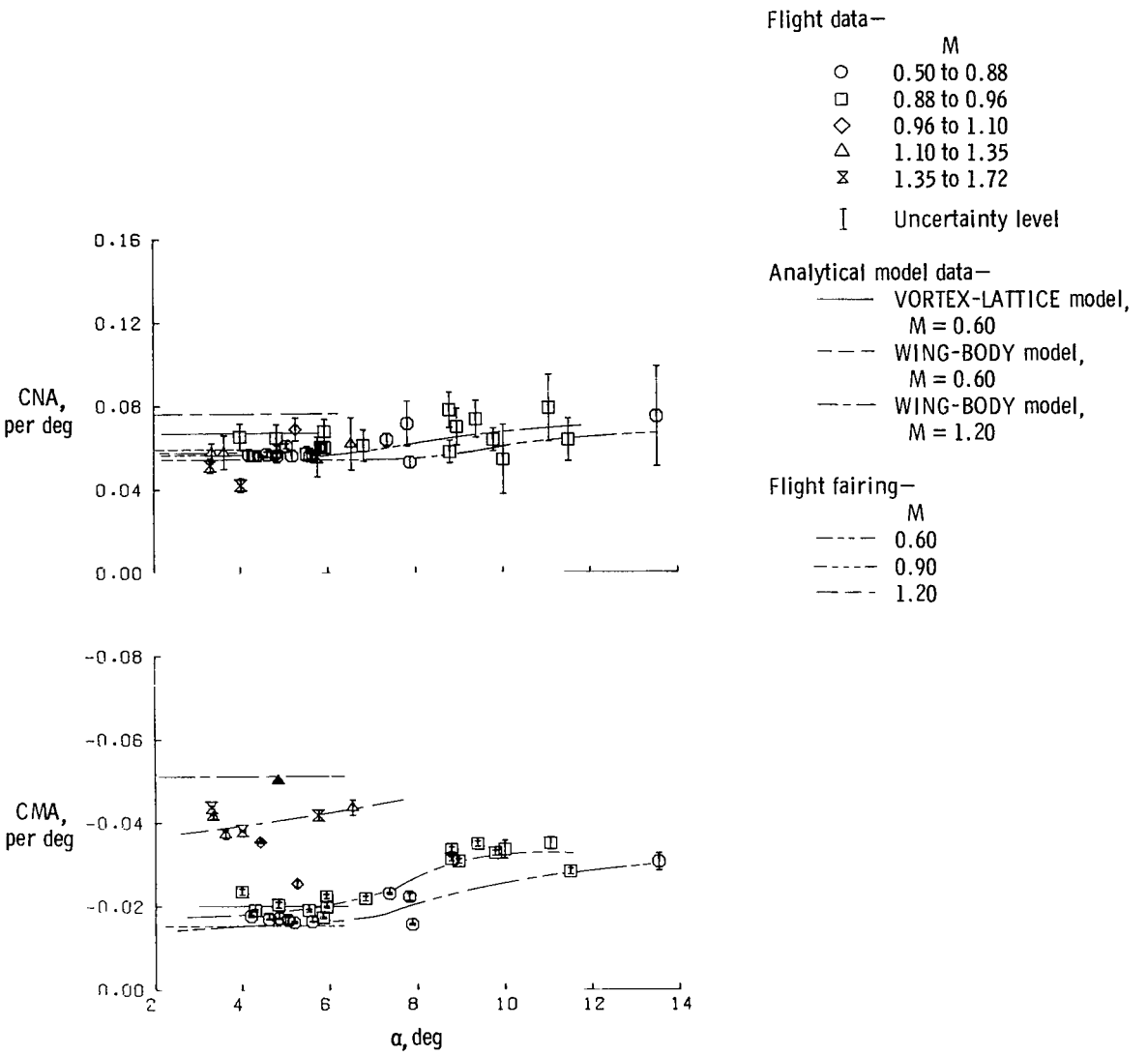

(a) CNA, CMA.

Figure 11. Longitudinal derivatives obtained from flight data as a function of angle of attack and comparison with analytical model results. λ = 58°; clean configuration.

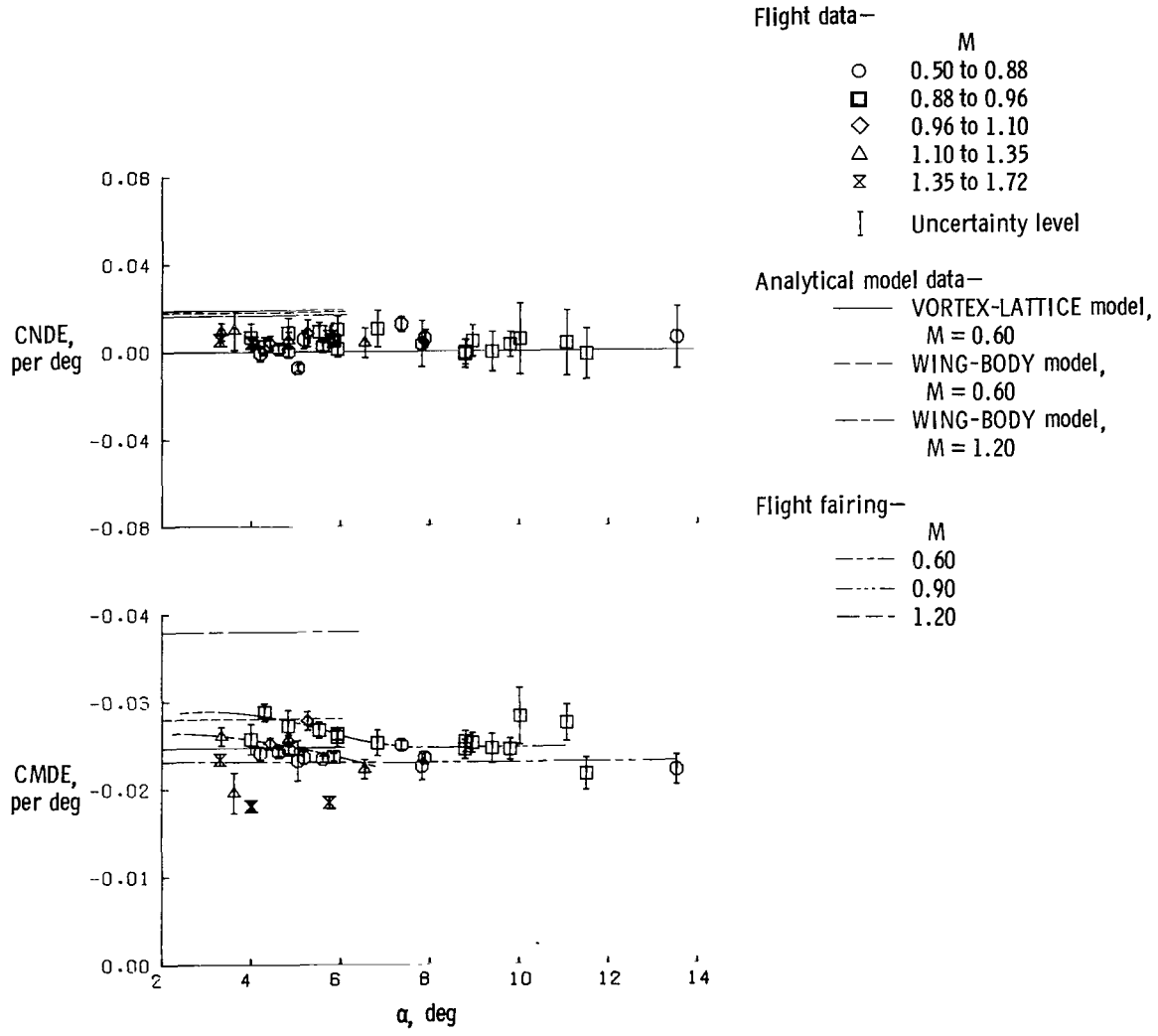

(b) CNDE, CMDE.

Figure 11. Continued.

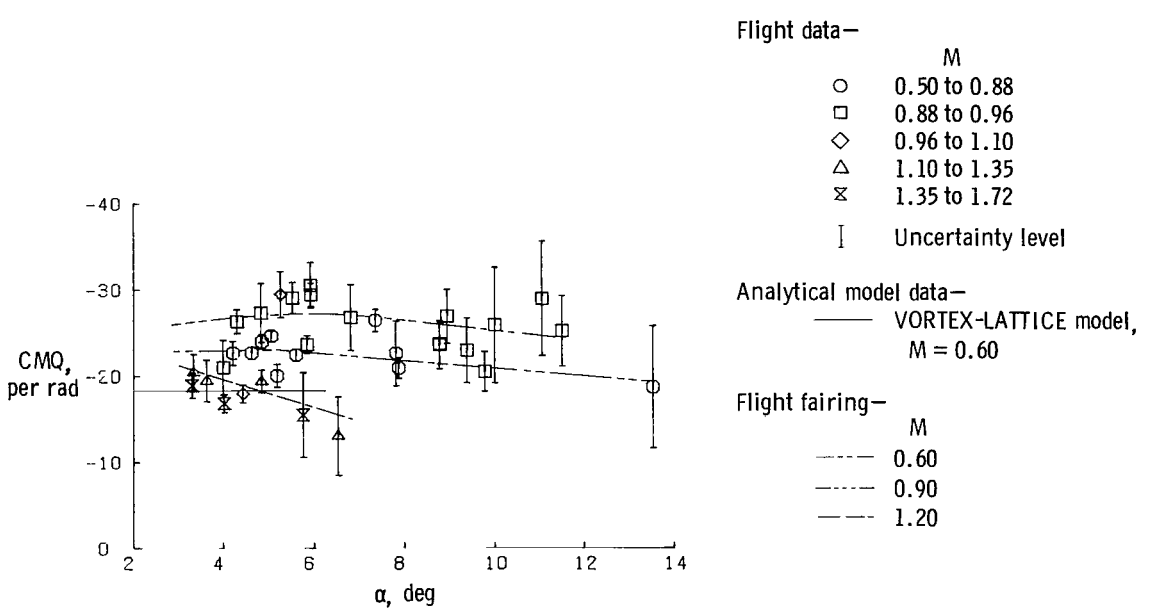

(c) CMQ.

Figure 11. Concluded.

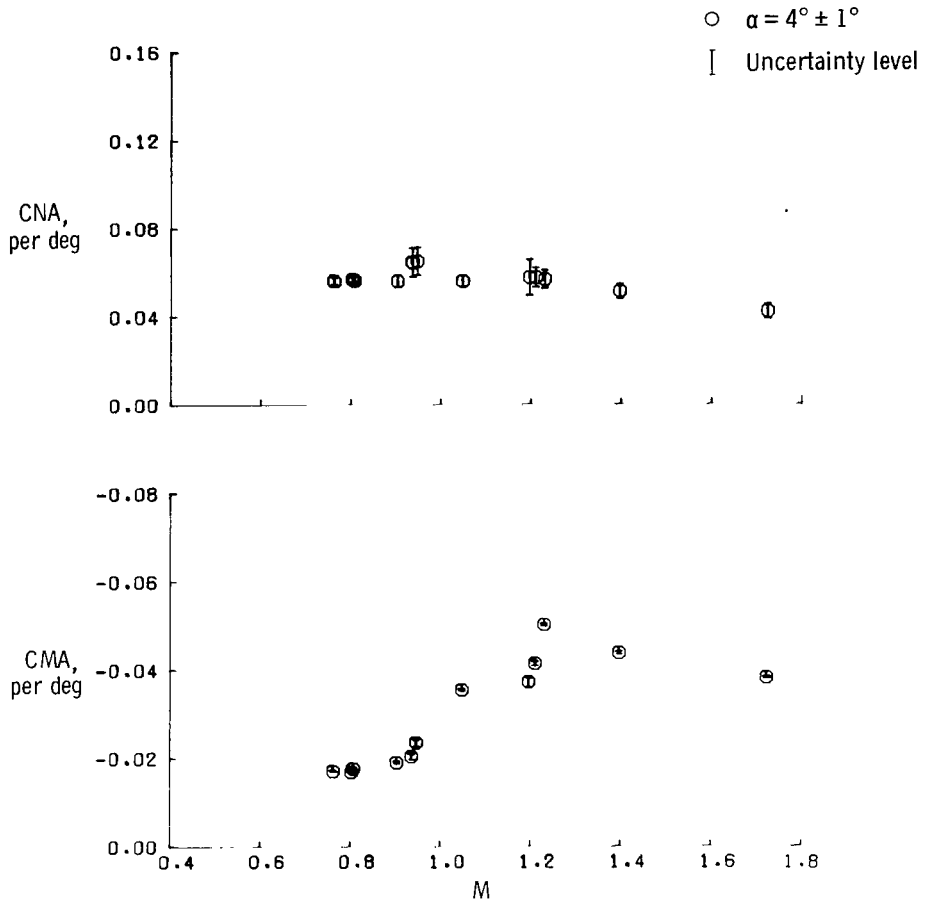

(a) CNA, CMA.

Figure 12. Longitudinal derivatives obtained from flight data as a function of Mach number. λ = 58°; clean configuration.

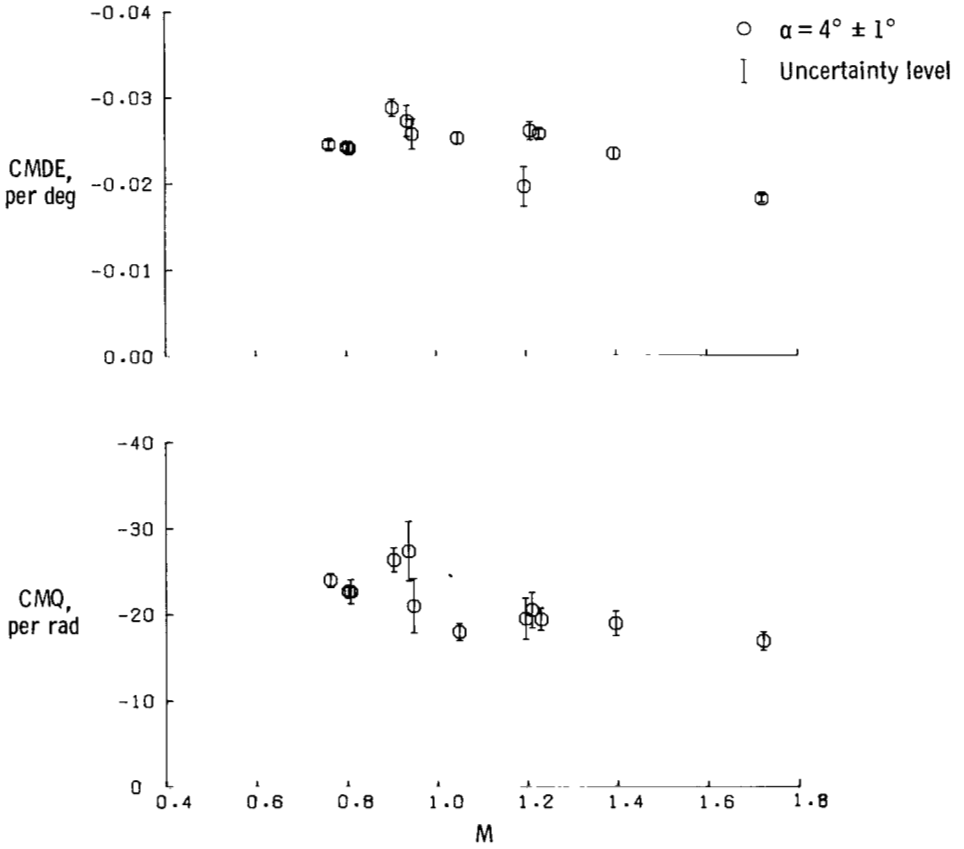

(b) CMDE, CMQ.

Figure 12. Concluded.

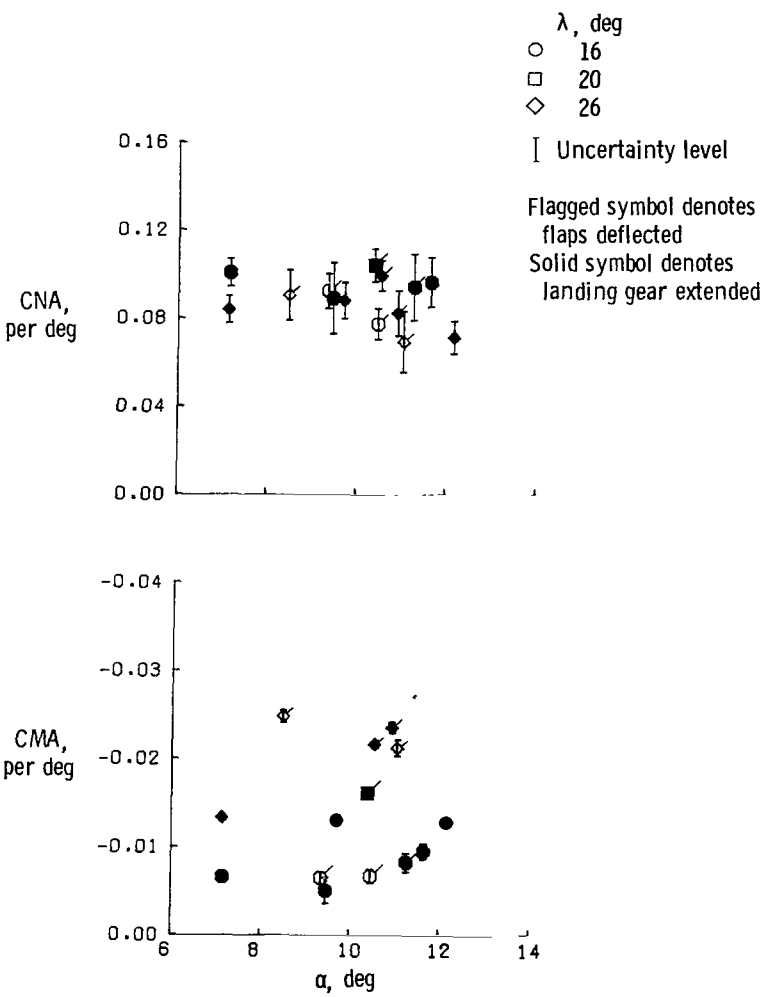

(a) CNA, CMA.

Figure 13. Longitudinal derivatives obtained from flight data for various combinations of landing gear and flap positions. Low speed.

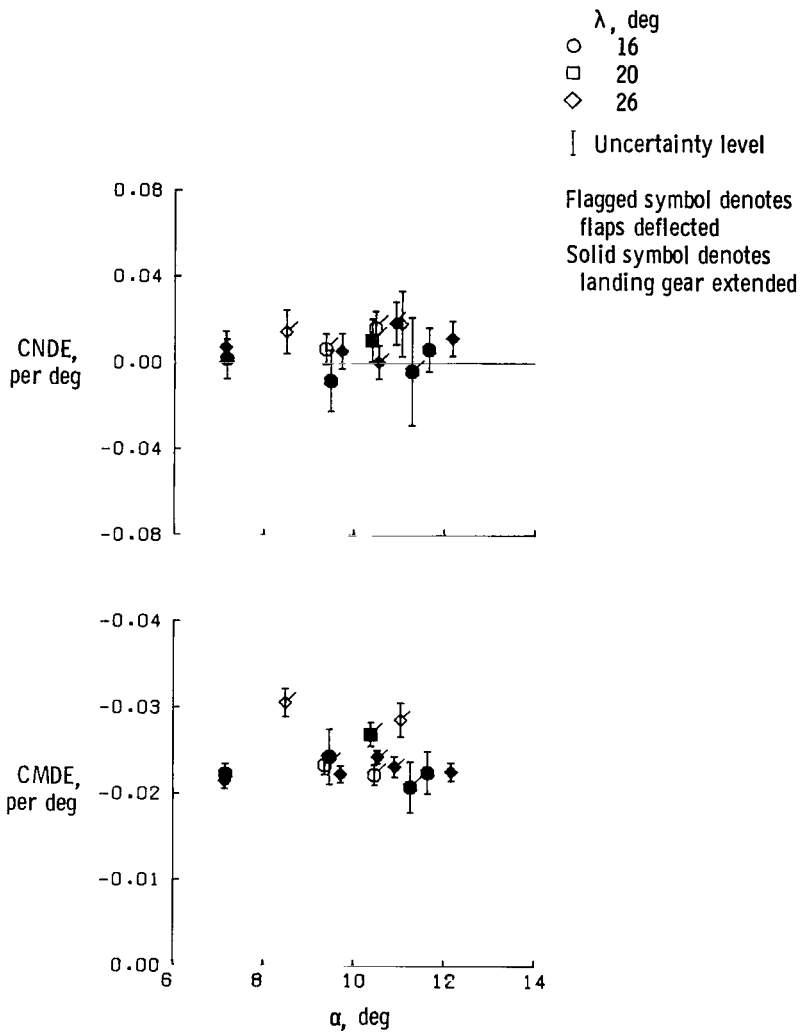

(b) CNDE, CMDE.

Figure 13. Continued.

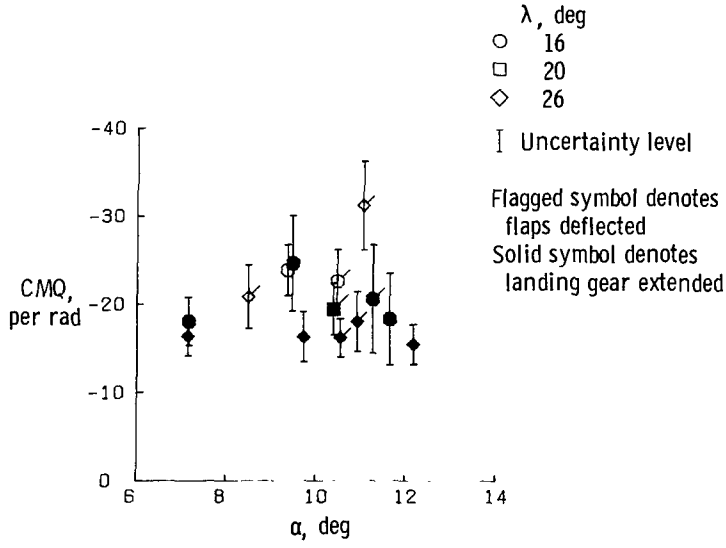

(c) CMQ.

Figure 13. Concluded.

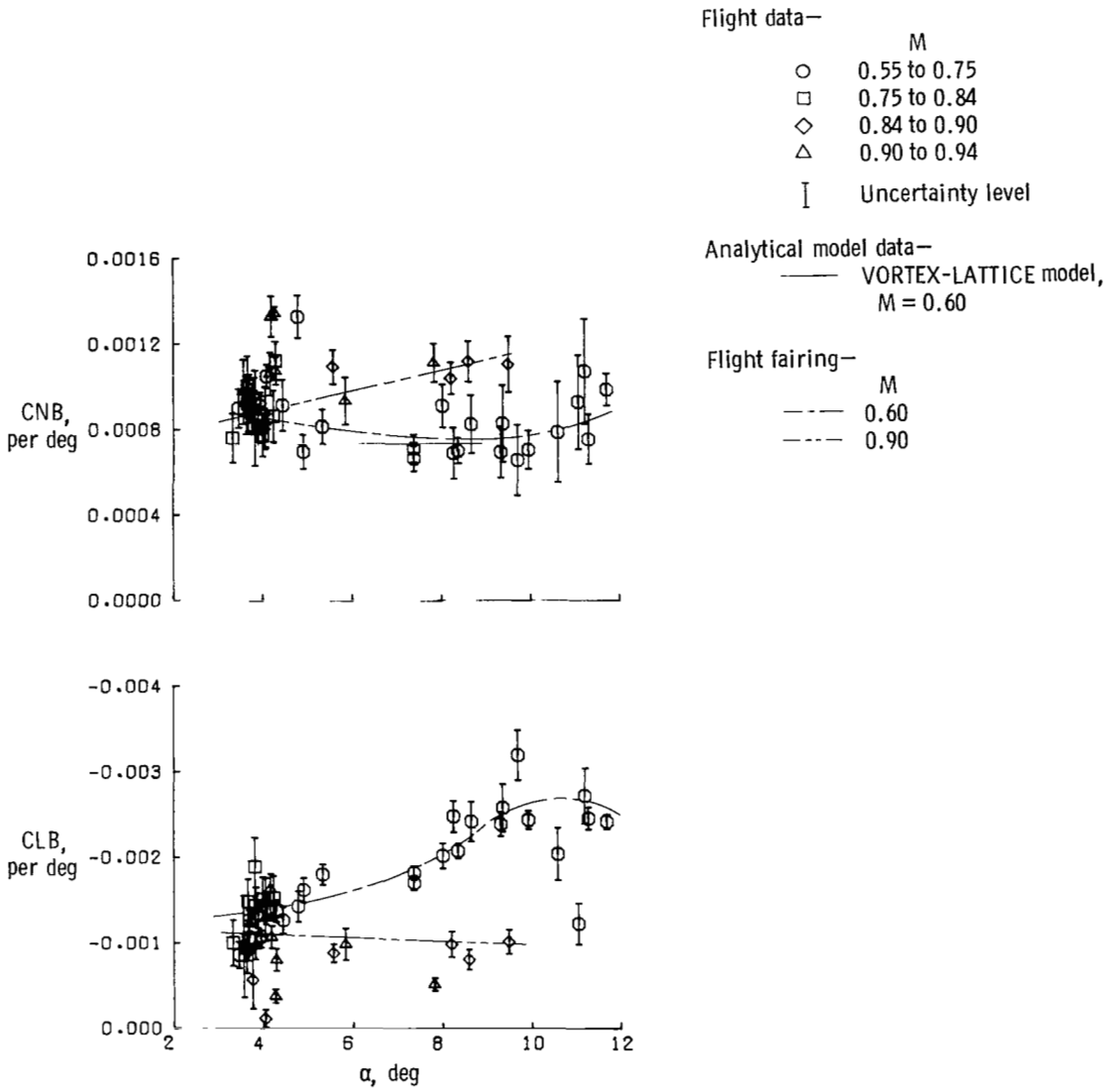

(a) CNB, CLB.

Figure 14. Lateral-directional derivatives obtained from flight data as a function of angle of attack and comparison with analytical model results. λ = 26°; clean configuration.

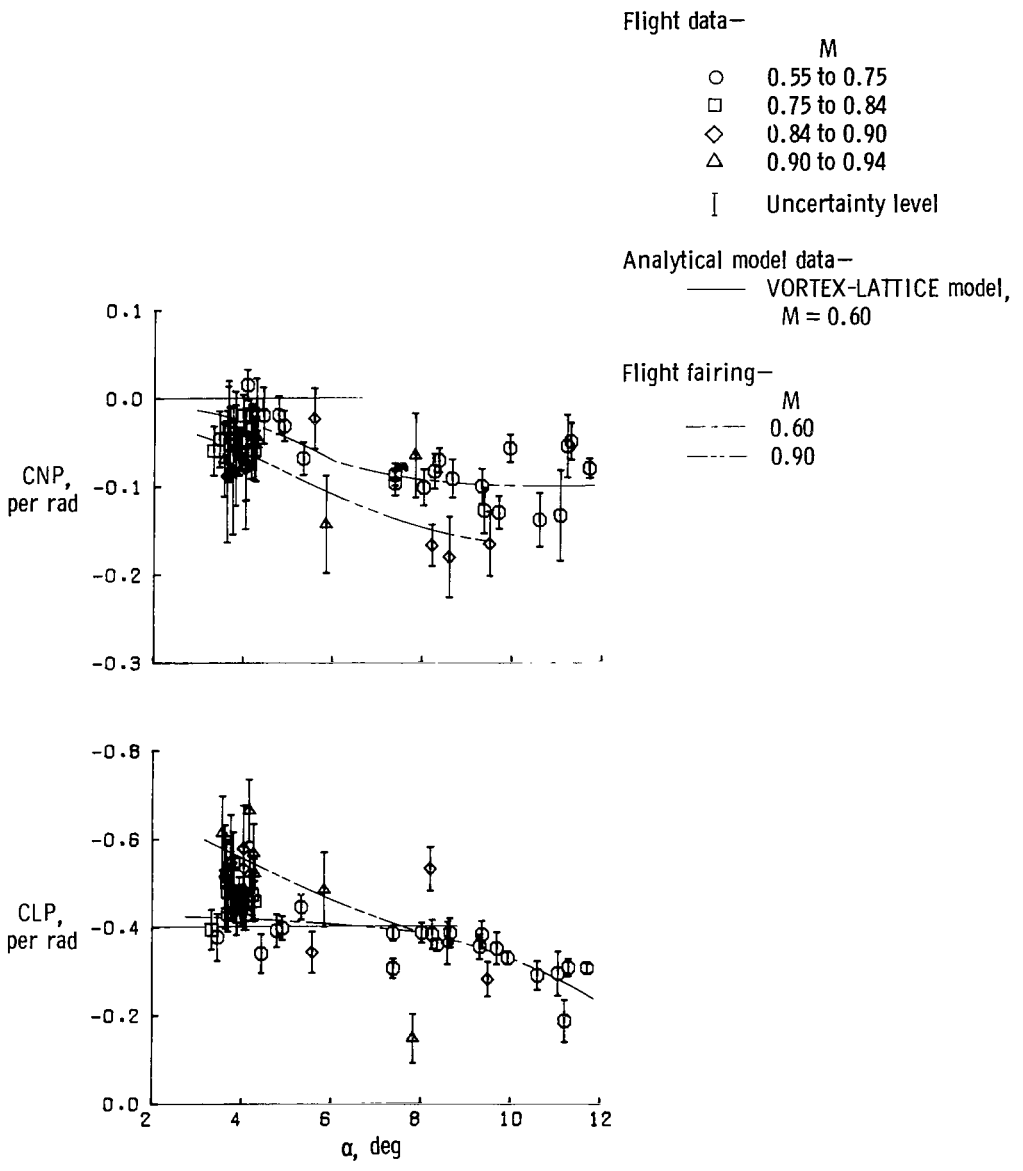

(b) CNP, CLP.

Figure 14. Continued.

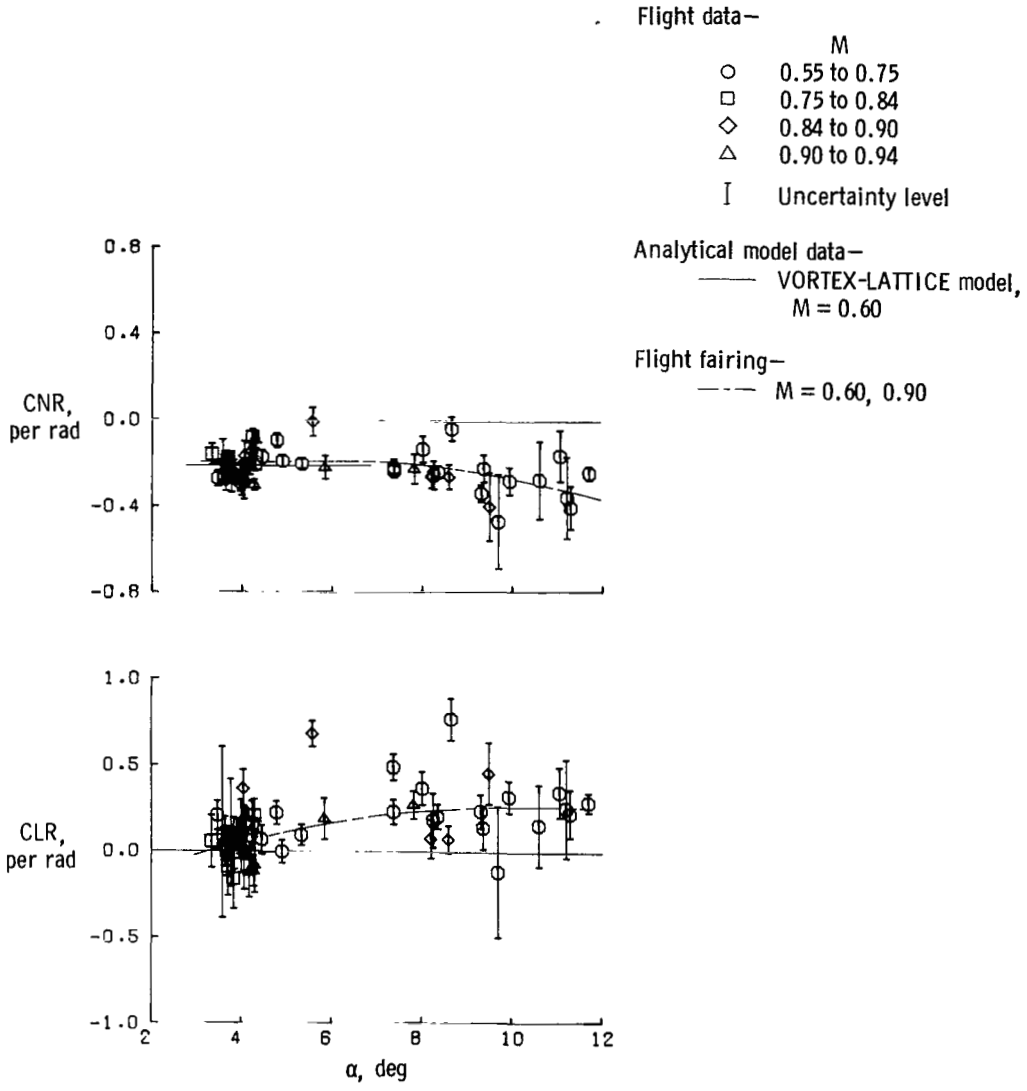

(c) CNR, CLR.

Figure 14. Continued.

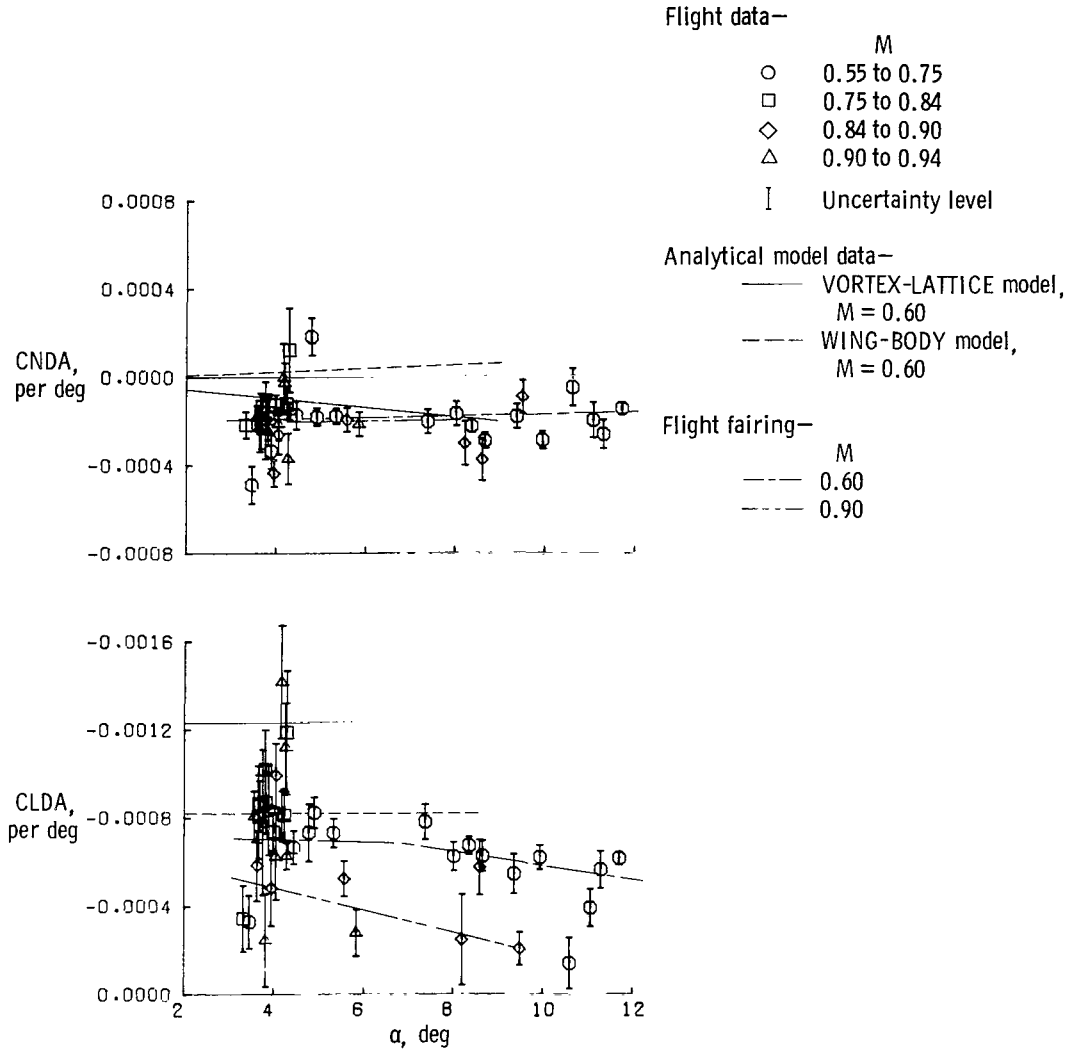

(d) CNDA, CLDA.

Figure 14. Continued.

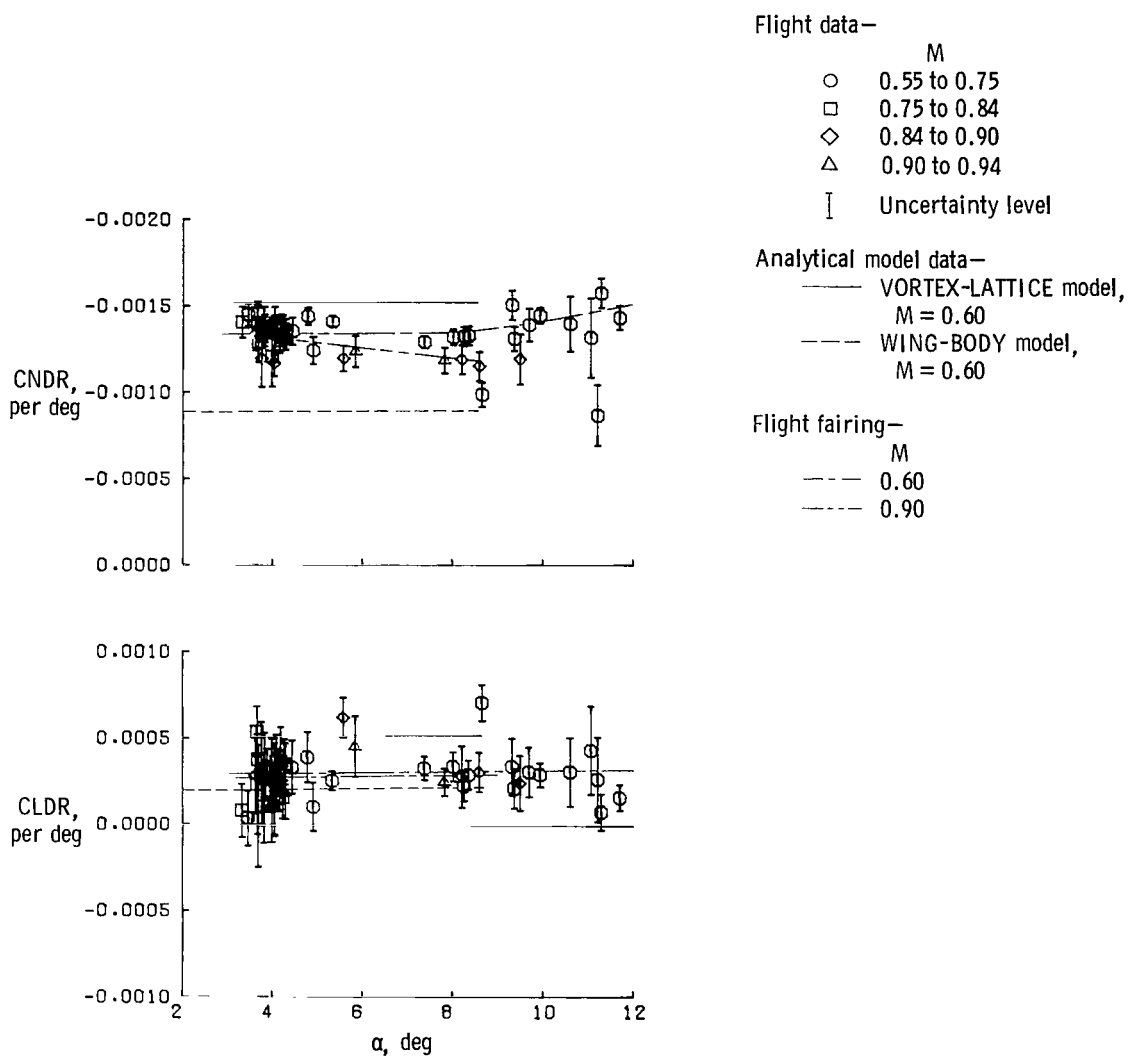

(e) CNDR, CLDR.

Figure 14. Continued.

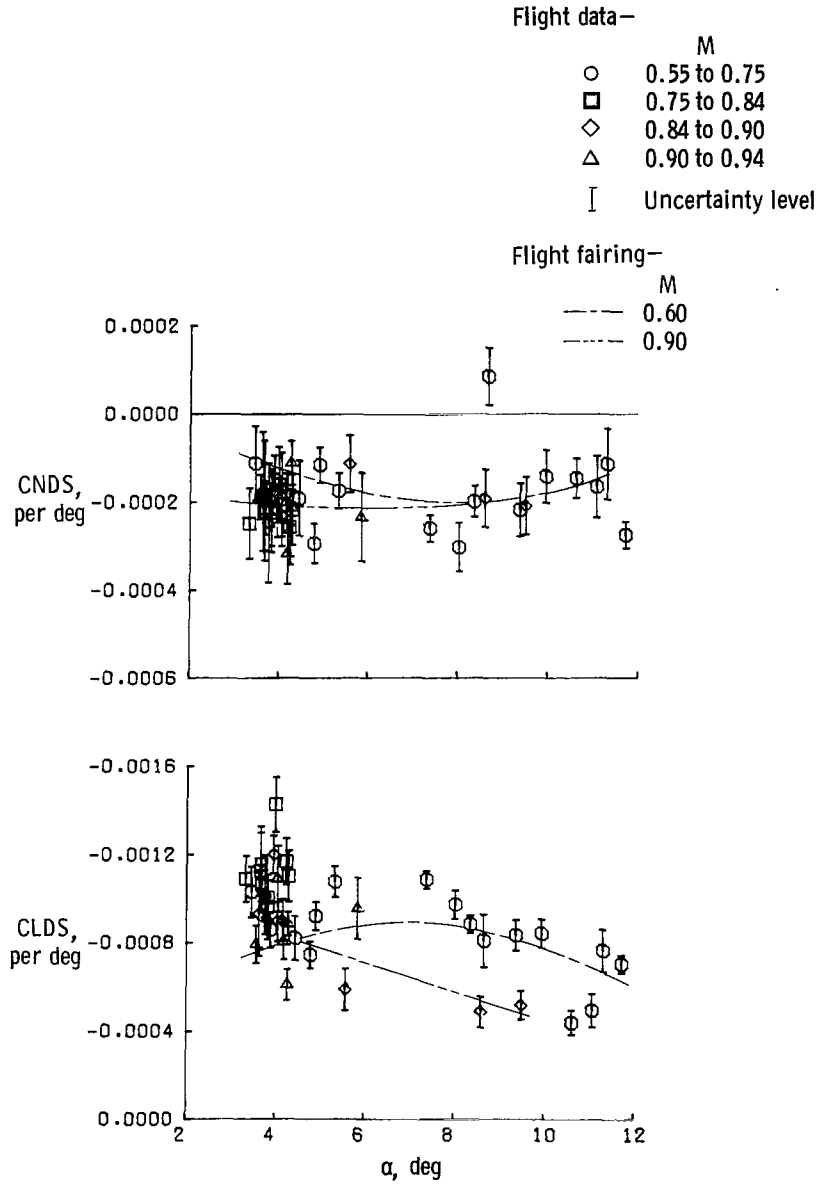

(f) CNDS, CLDS.

Figure 14. Continued.

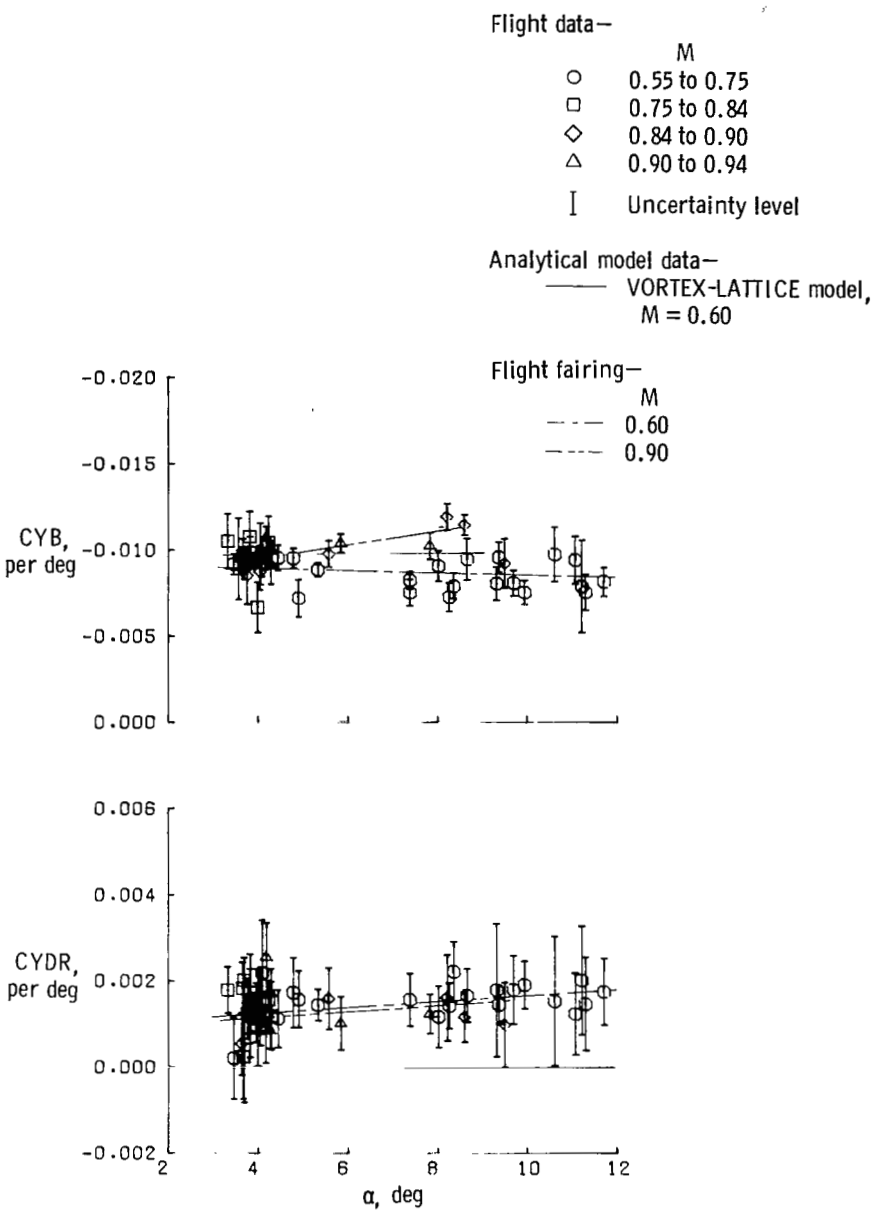

(g) CYB, CYDR.

Figure 14. Continued.

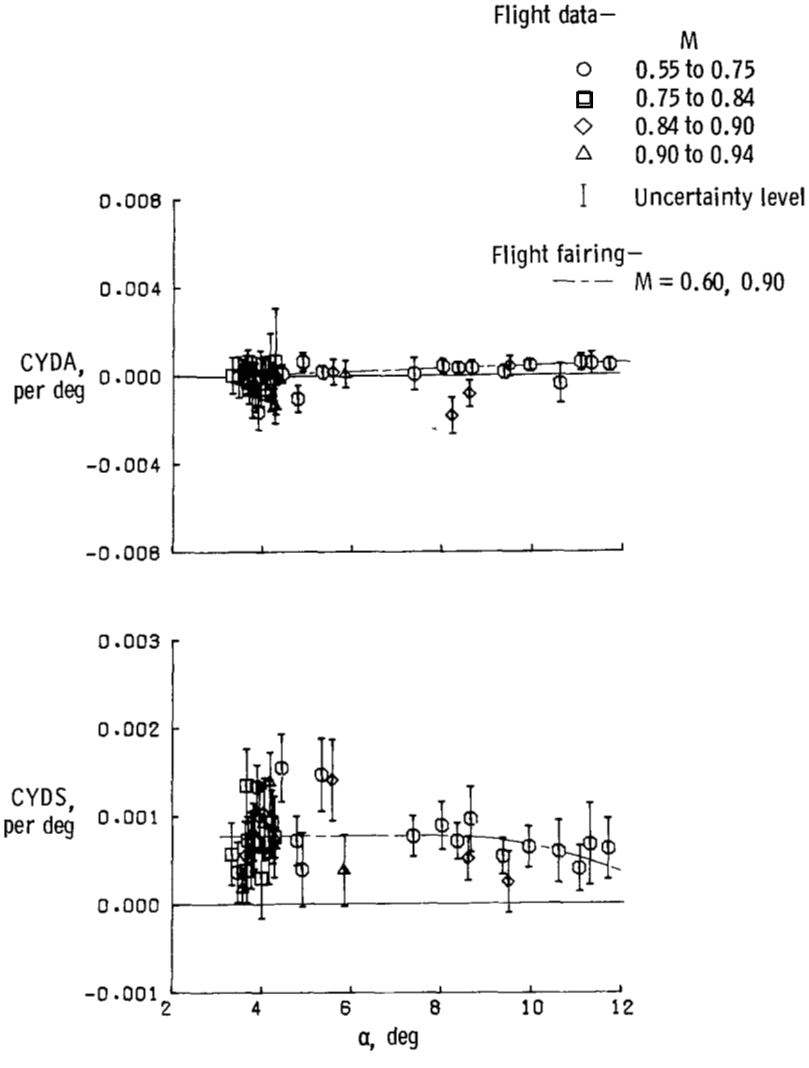

(h) CYDA, CYDS.

Figure 14. Concluded.

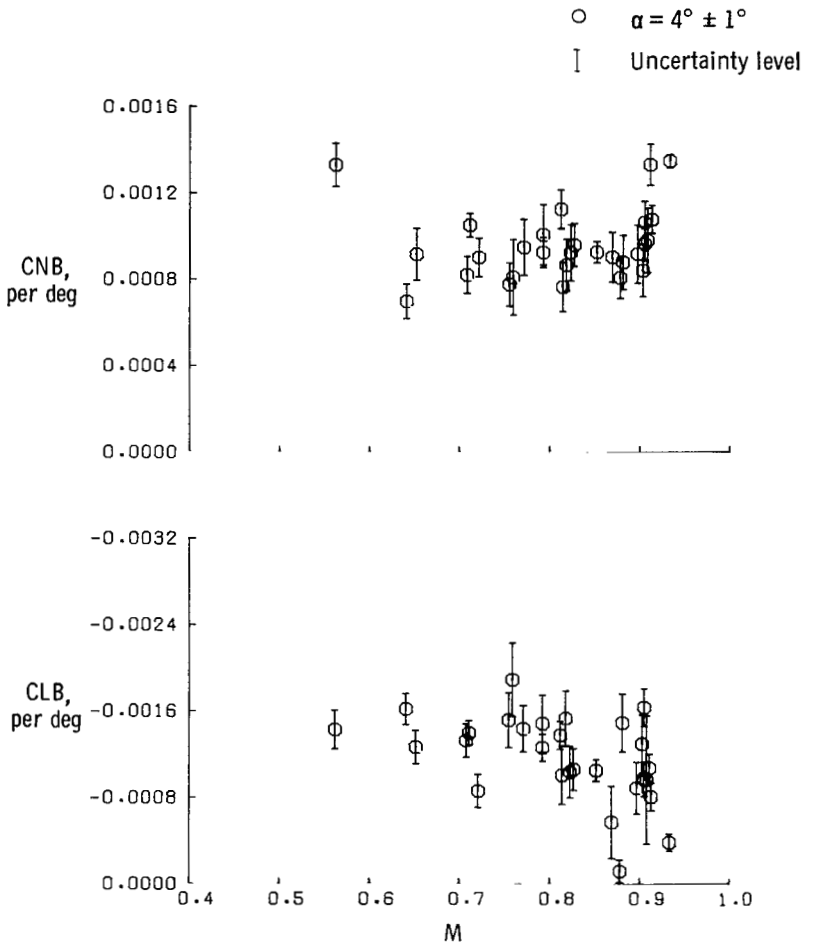

(a) CNB, CLB.

Figure 15. Lateral-directional derivatives obtained from flight data as a function of Mach number. λ = 26°; clean configuration.

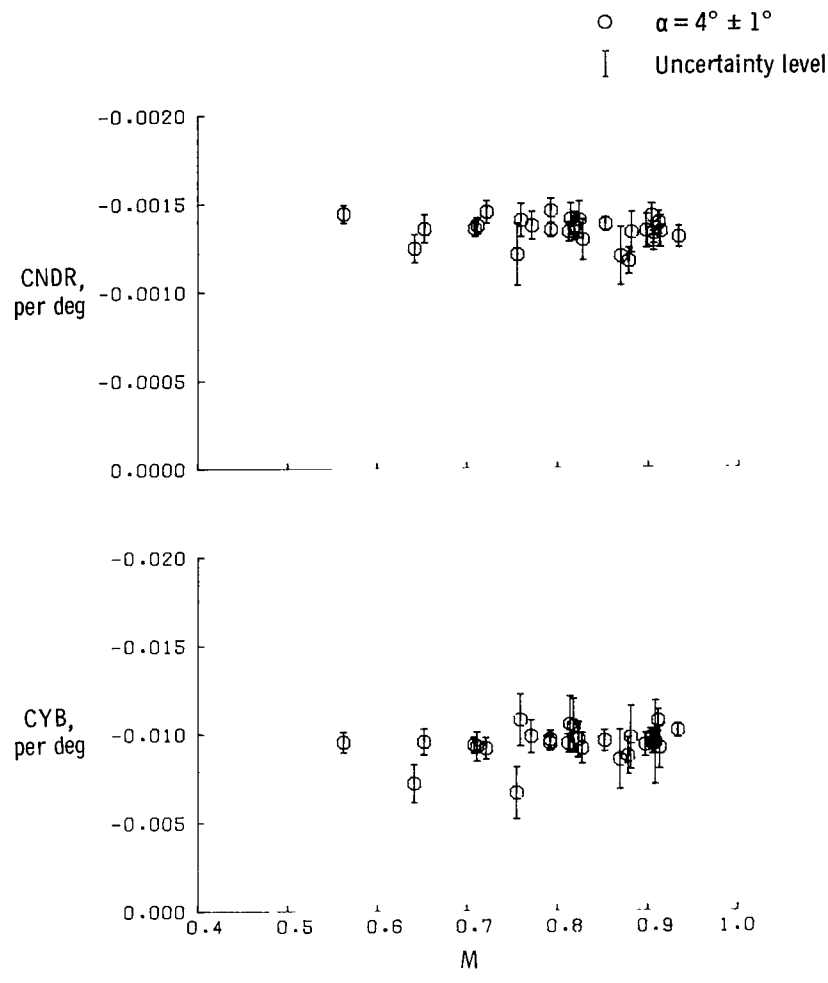

(b) CNDR, CYB.

Figure 15. Continued.

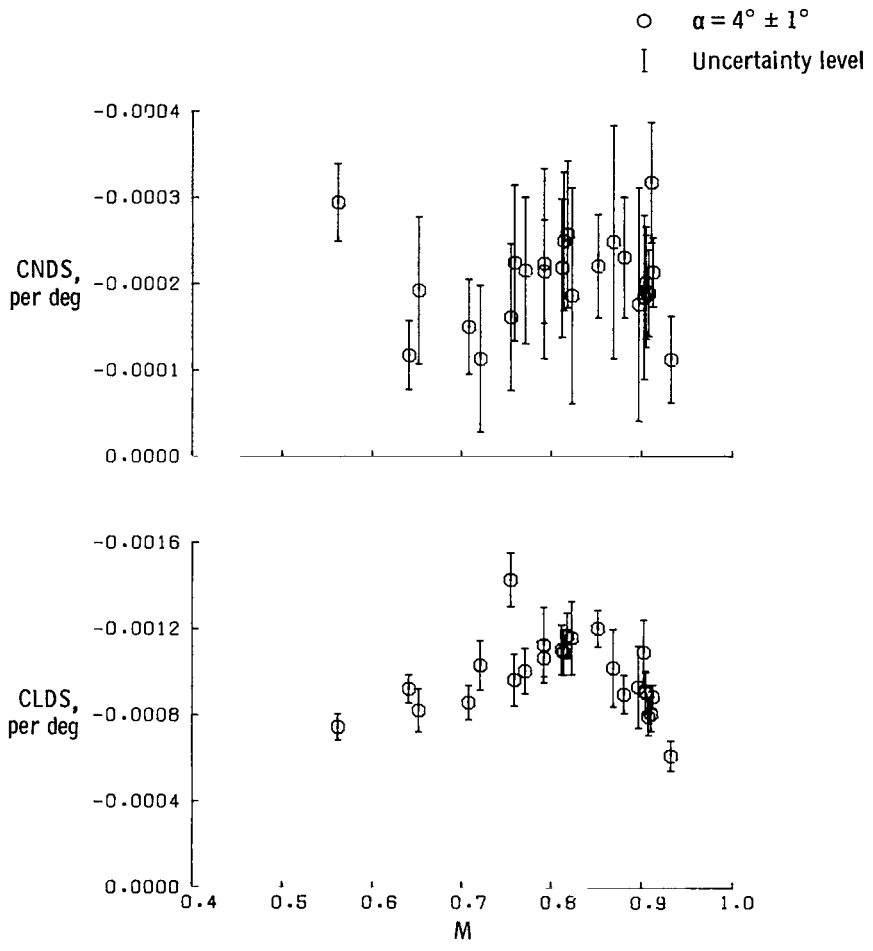

(c) CNDS, CLDS.

Figure 15. Concluded.

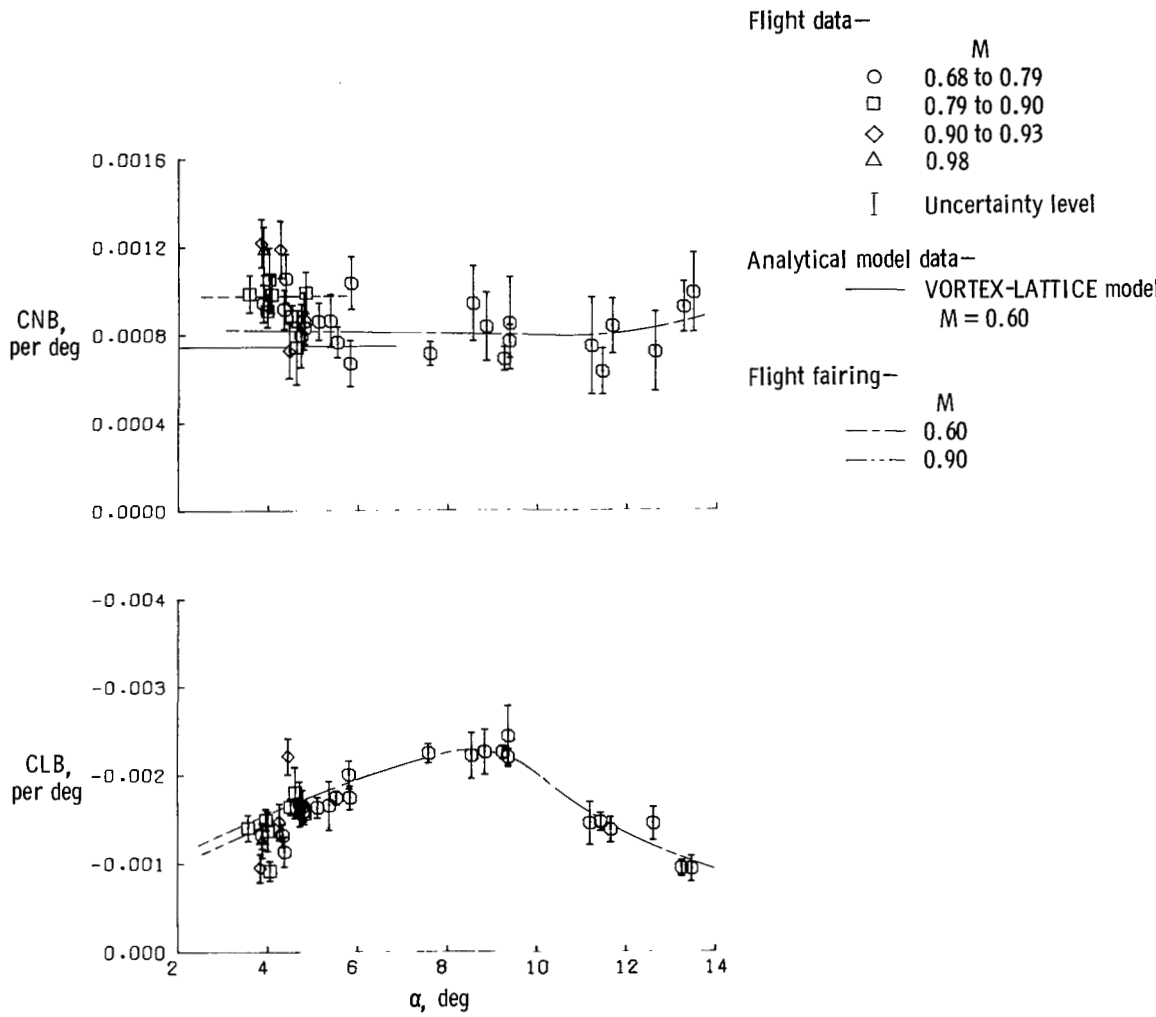

(a) CNB, CLB.

Figure 16. Lateral-directional derivatives obtained from flight data as a function of angle of attack and comparison with analytical model results. λ = 35°; clean configuration.

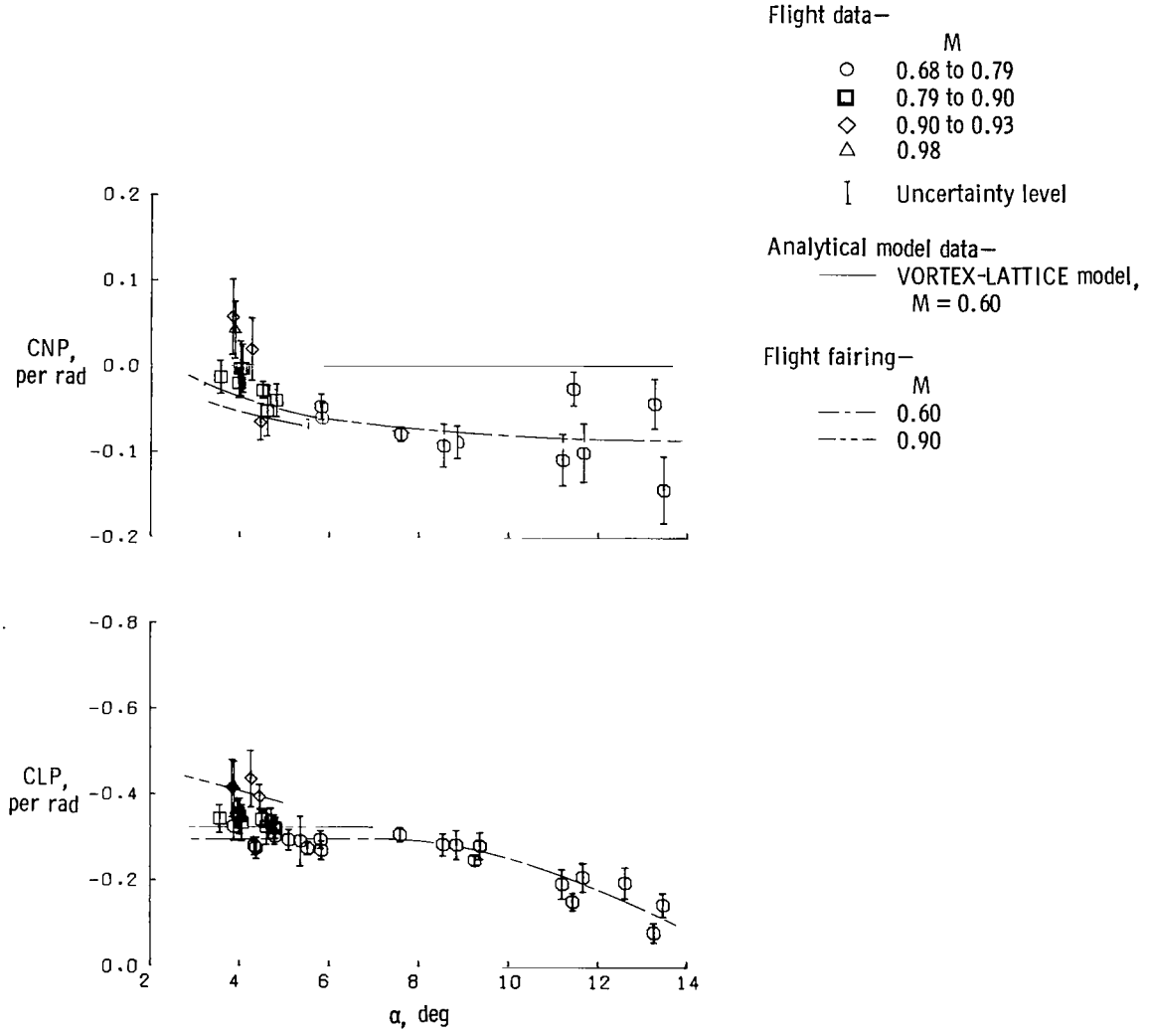

(b) CNP, CLP.

Figure 16. Continued.

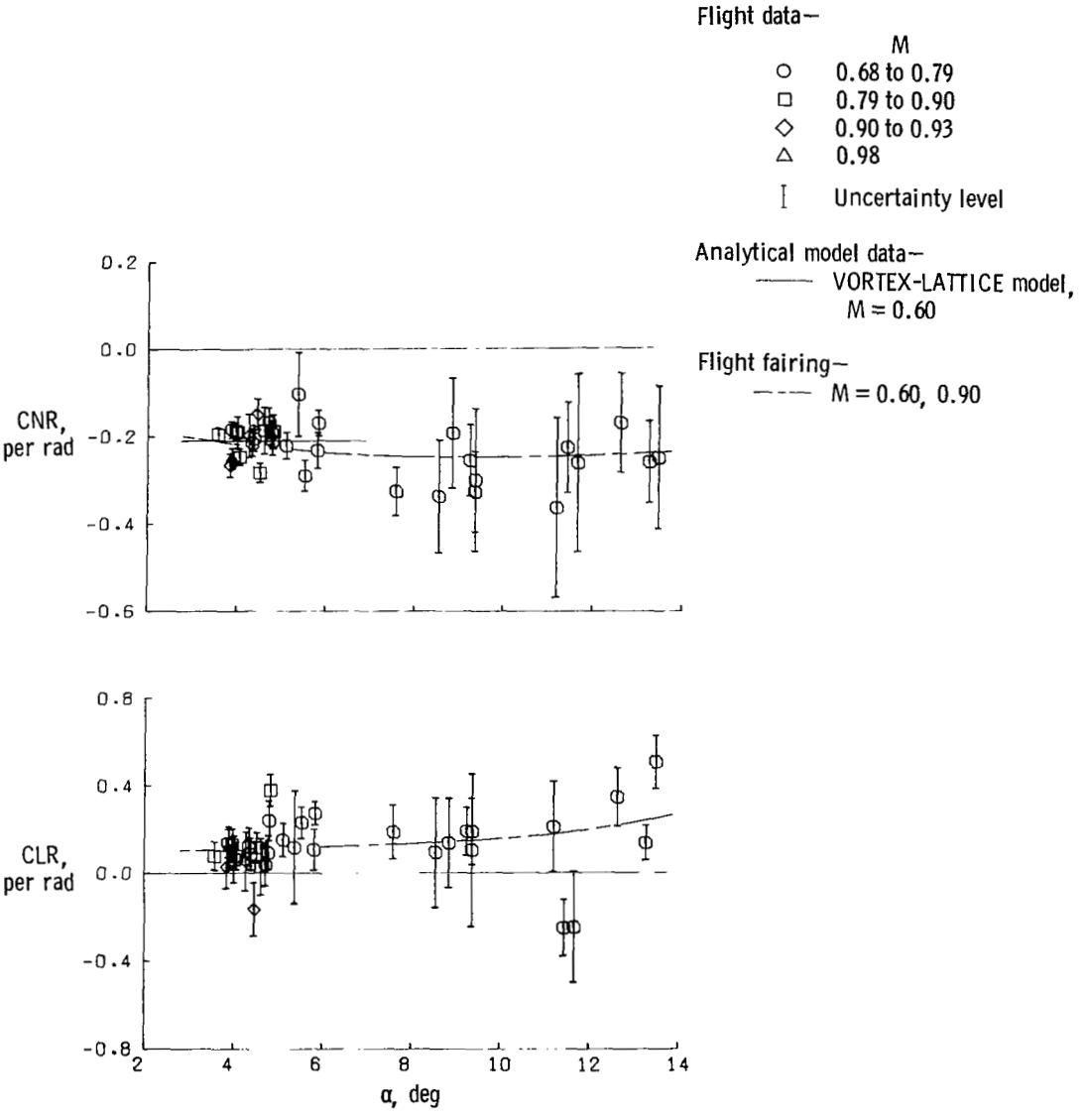

(c) CNR, CLR.

Figure 16. Continued.

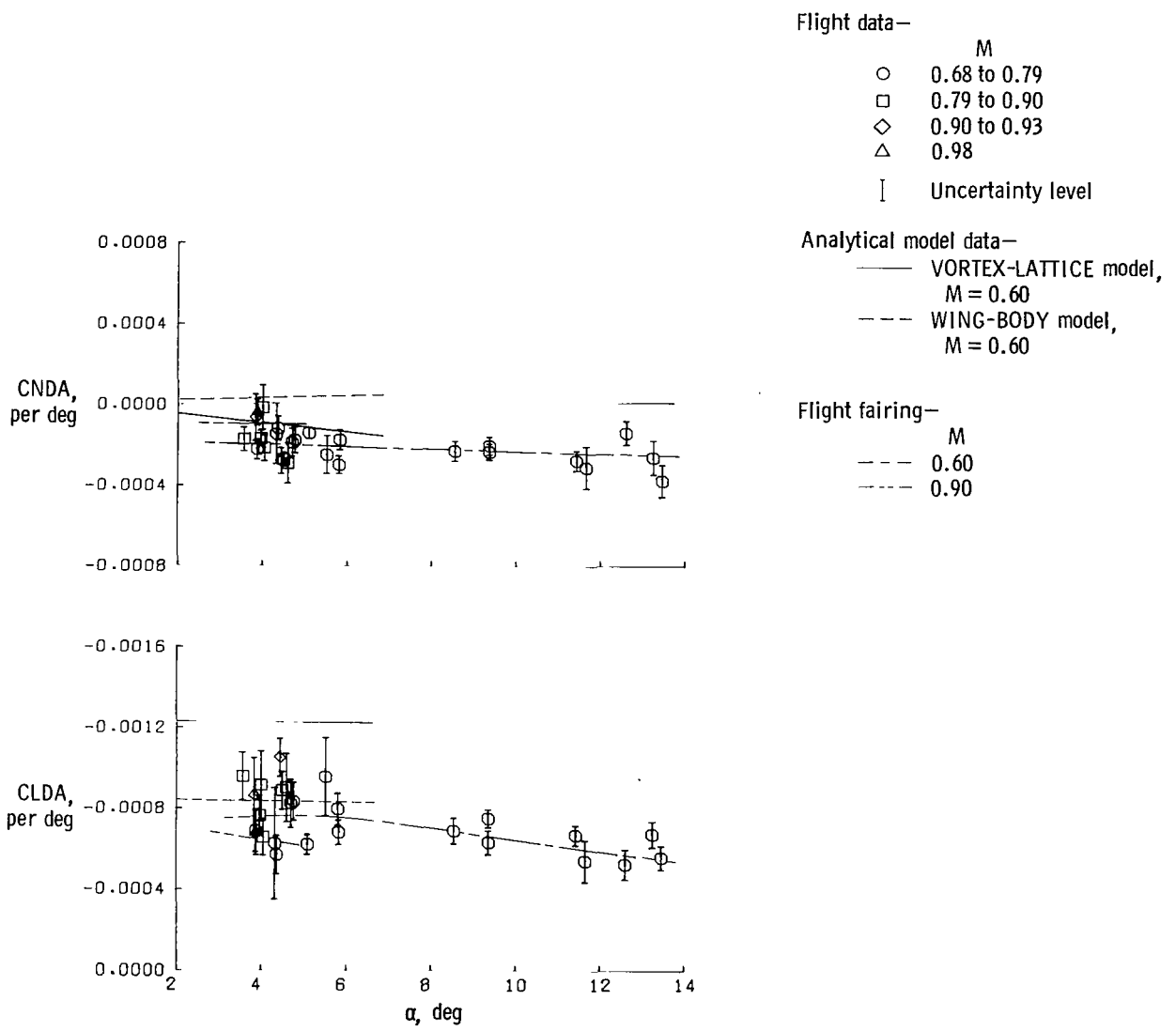

(d) CNDA, CLDA.

Figure 16. Continued.

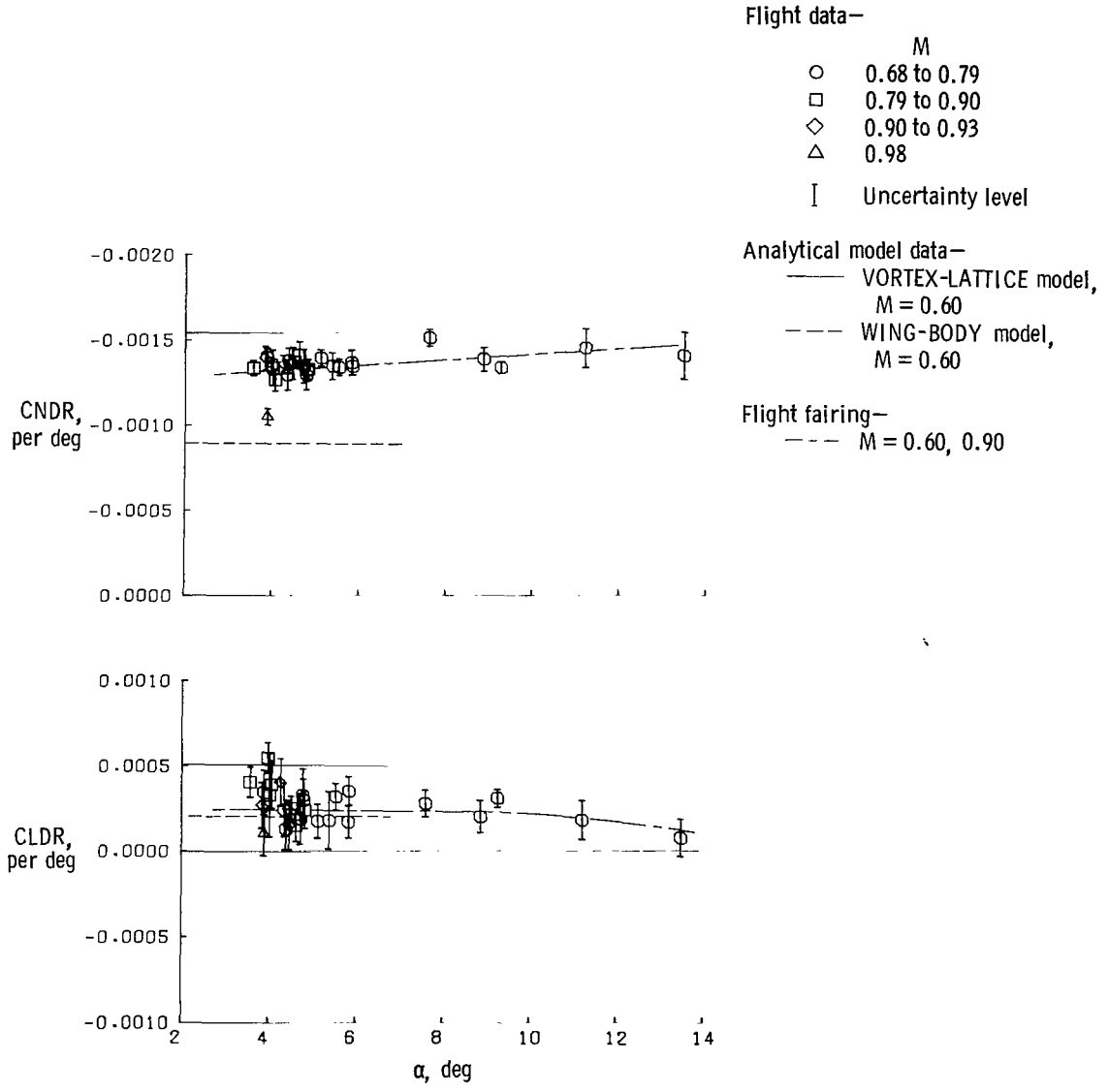

(e) CNDR, CLDR.

Figure 16. Continued.

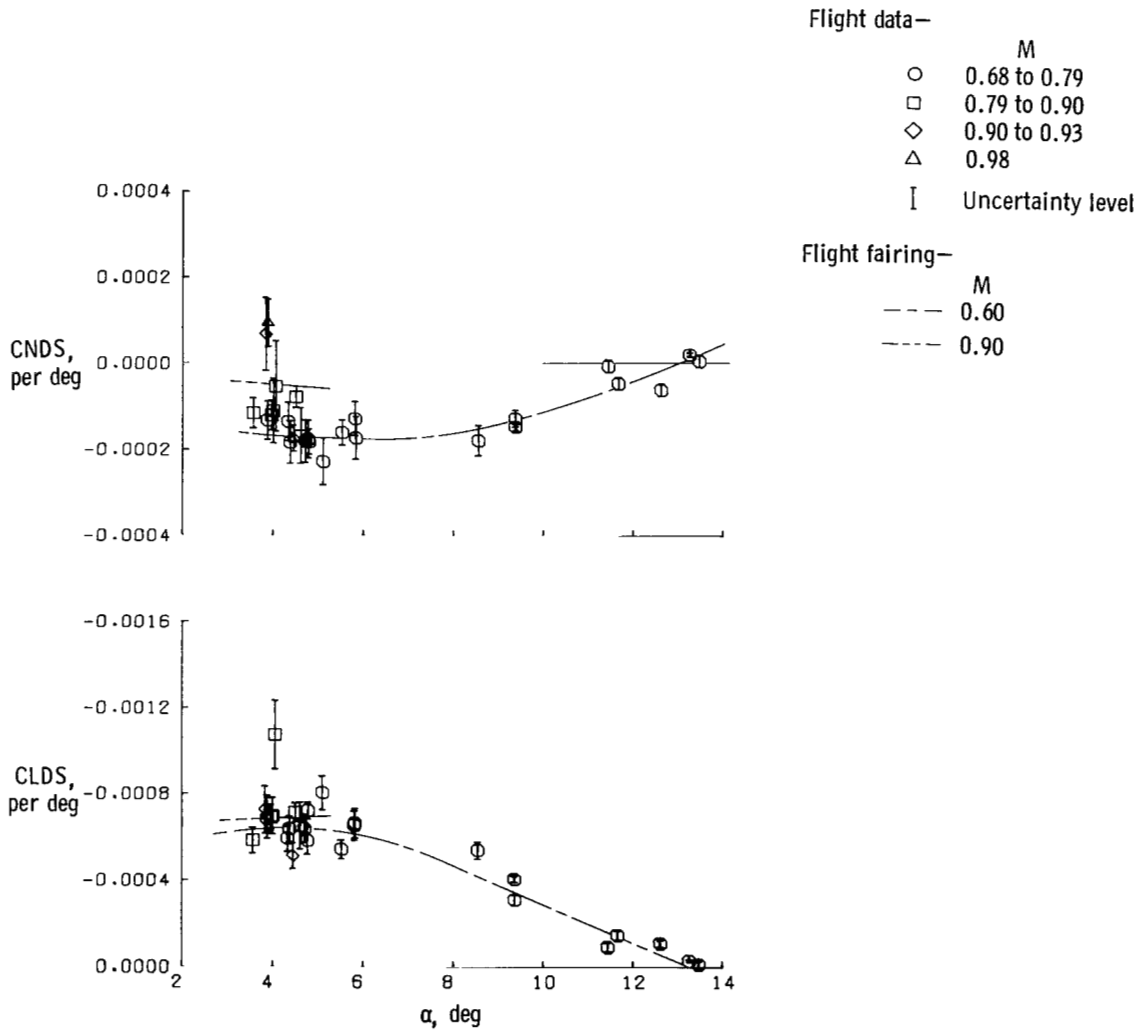

(f) CNDS, CLDS.

Figure 16. Continued.

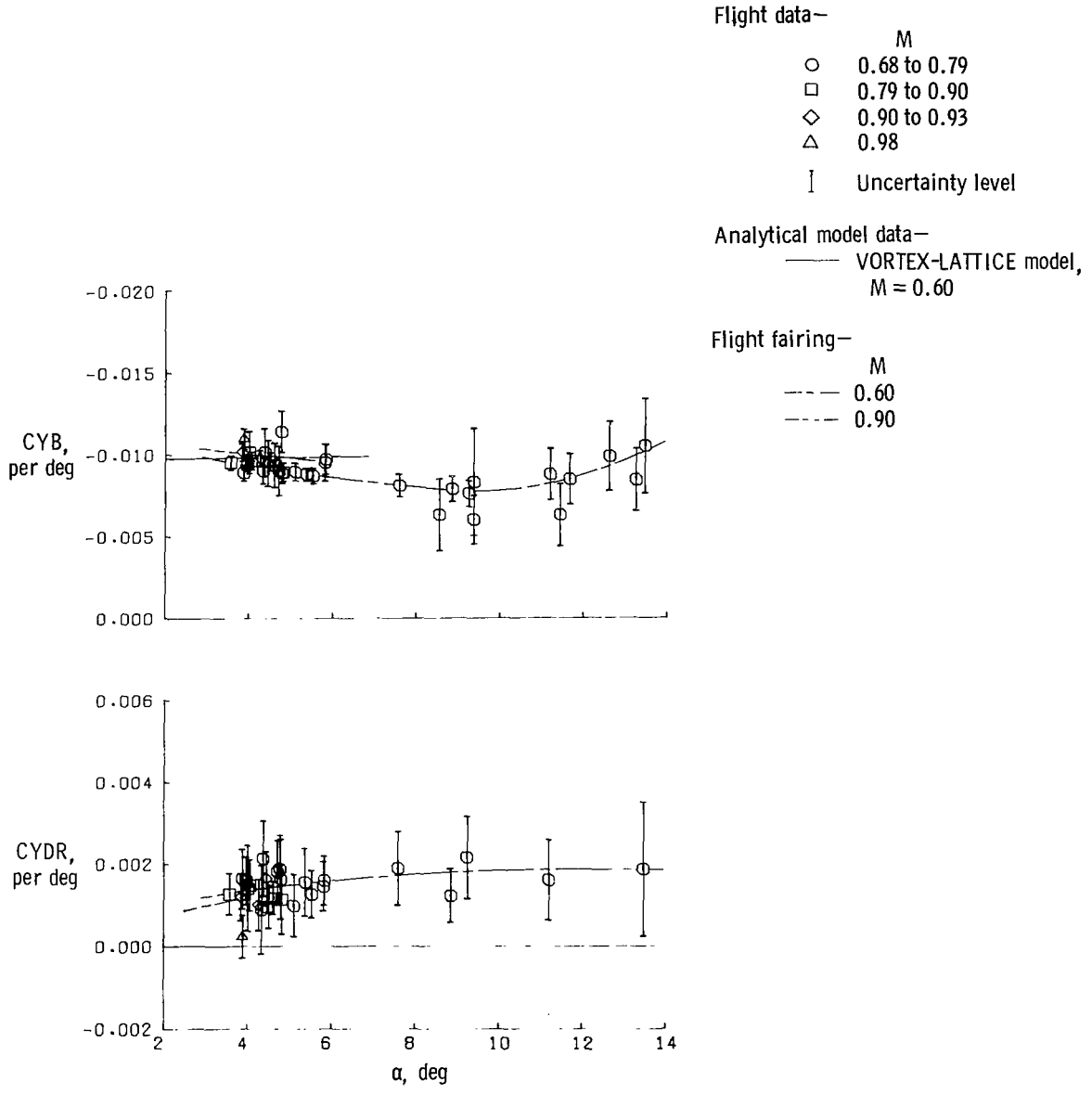

(g) CYB, CYDR.

Figure 16. Continued.

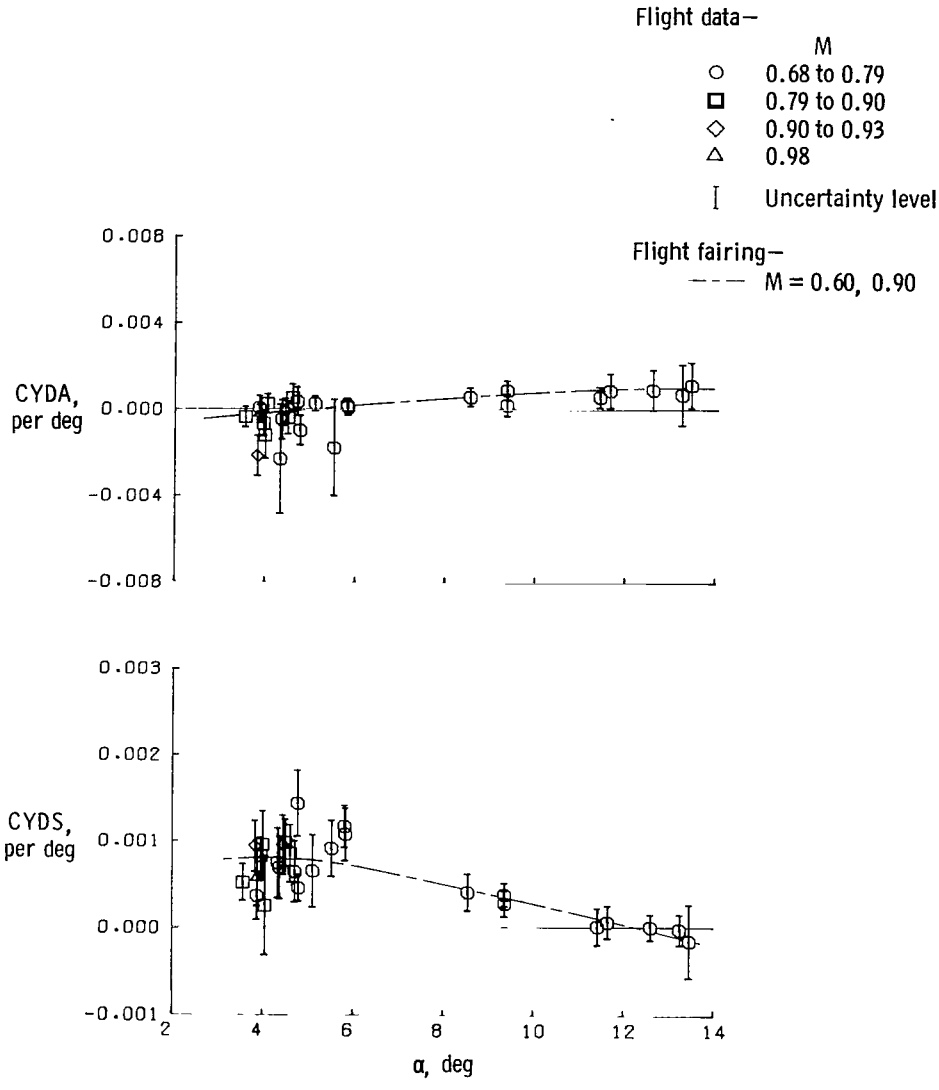

(h) CYDA, CYDS.

Figure 16. Concluded.

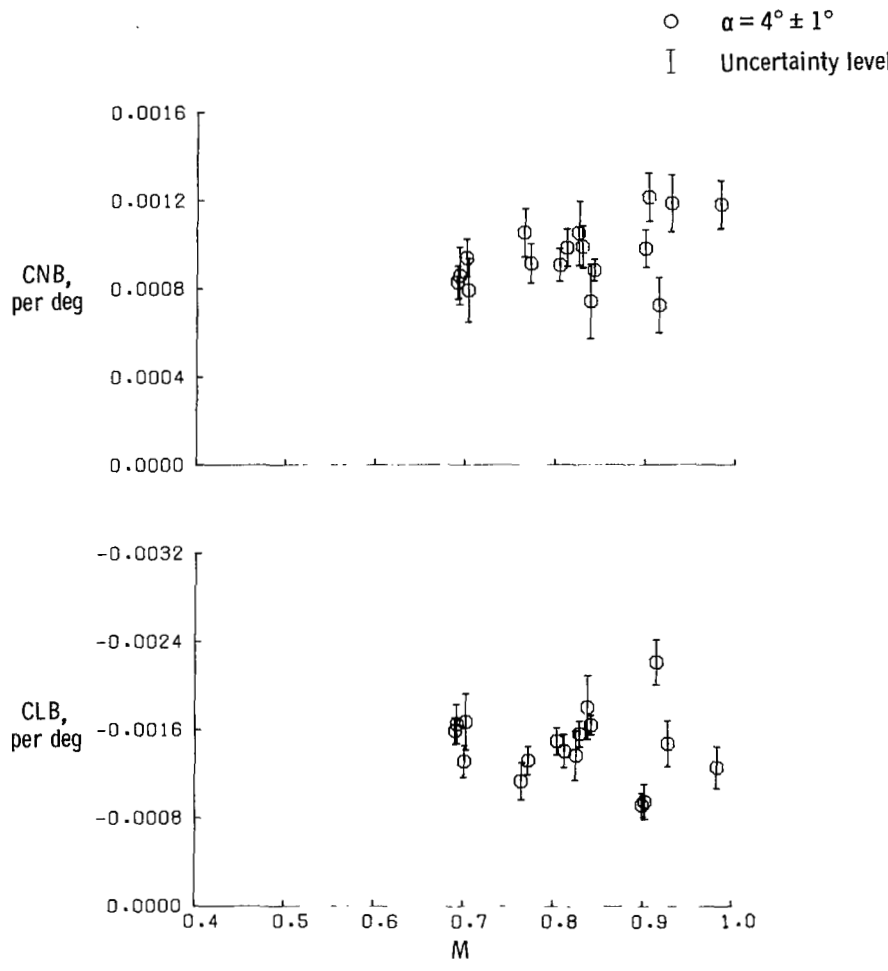

(a) CNB, CLB.

Figure 17. Lateral-directional derivatives obtained from flight data as a function of Mach number. λ = 35°; clean configuration.

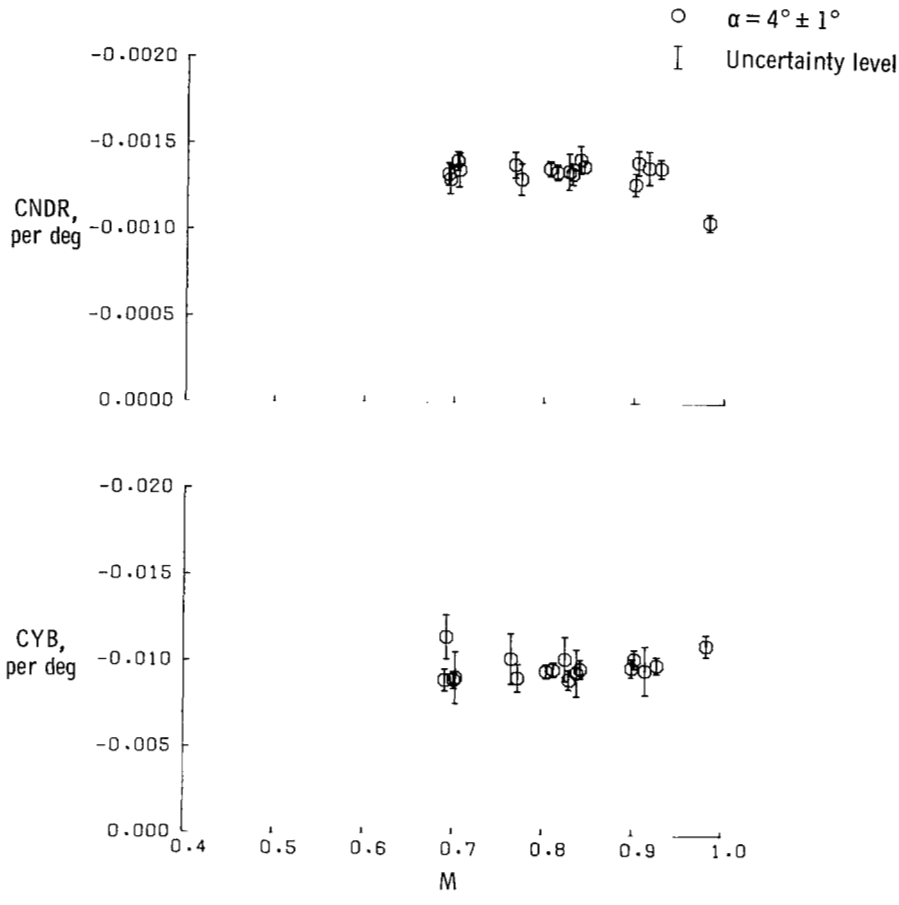

(b) CNDR, CYB.

Figure 17. Continued.

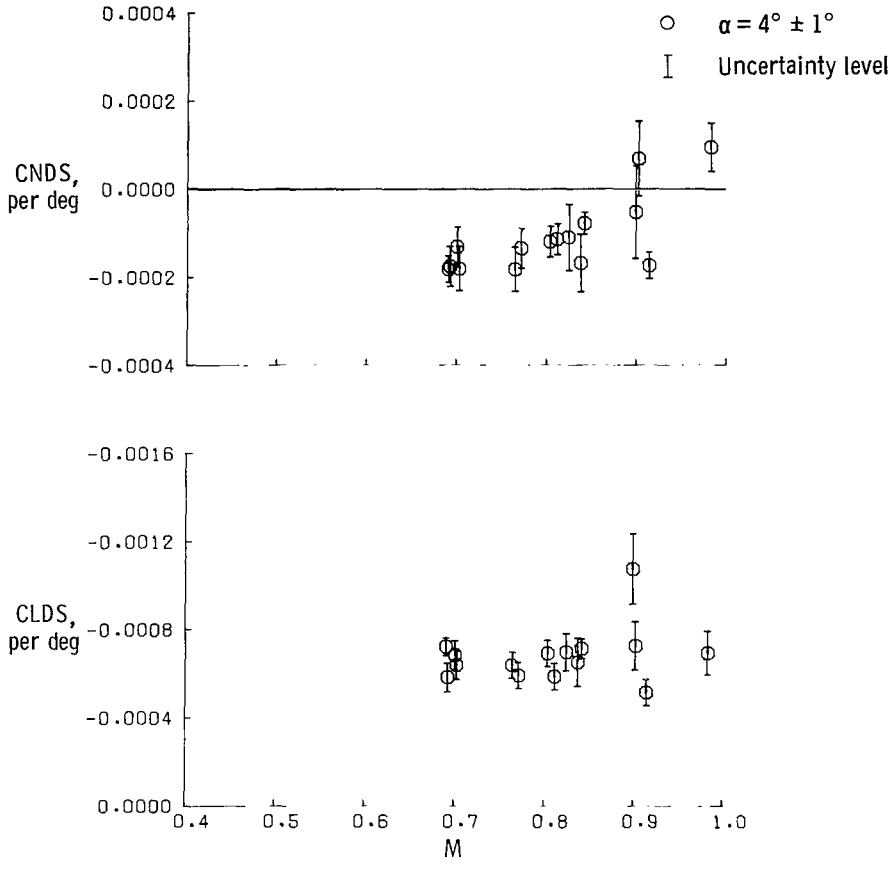

(c) CNDS, CLDS.

Figure 17. Concluded.

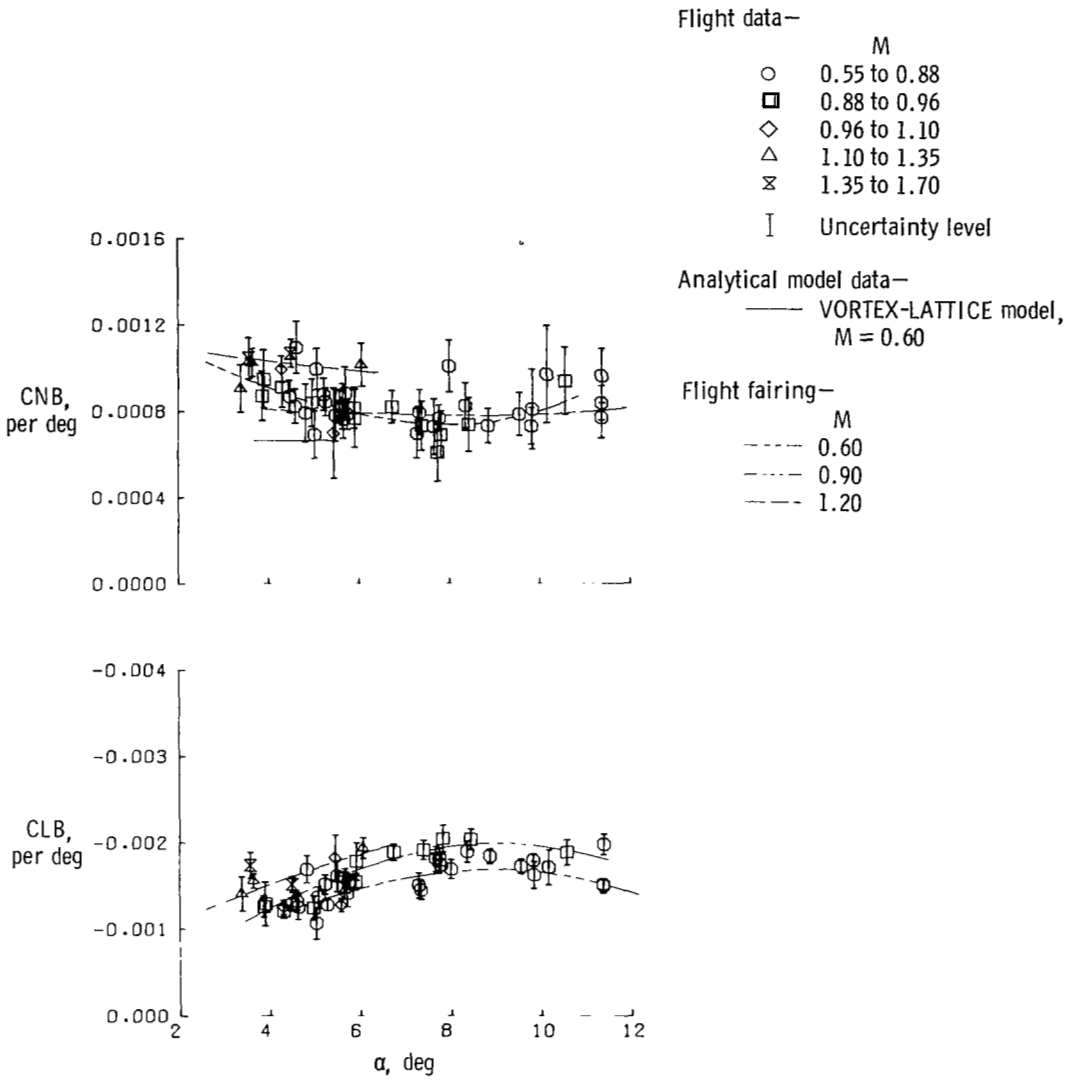

(a) CNB, CLB.

Figure 18. Lateral-directional derivatives obtained from flight data as a function of angle of attack and comparison with analytical model results. λ = 58°; clean configuration.

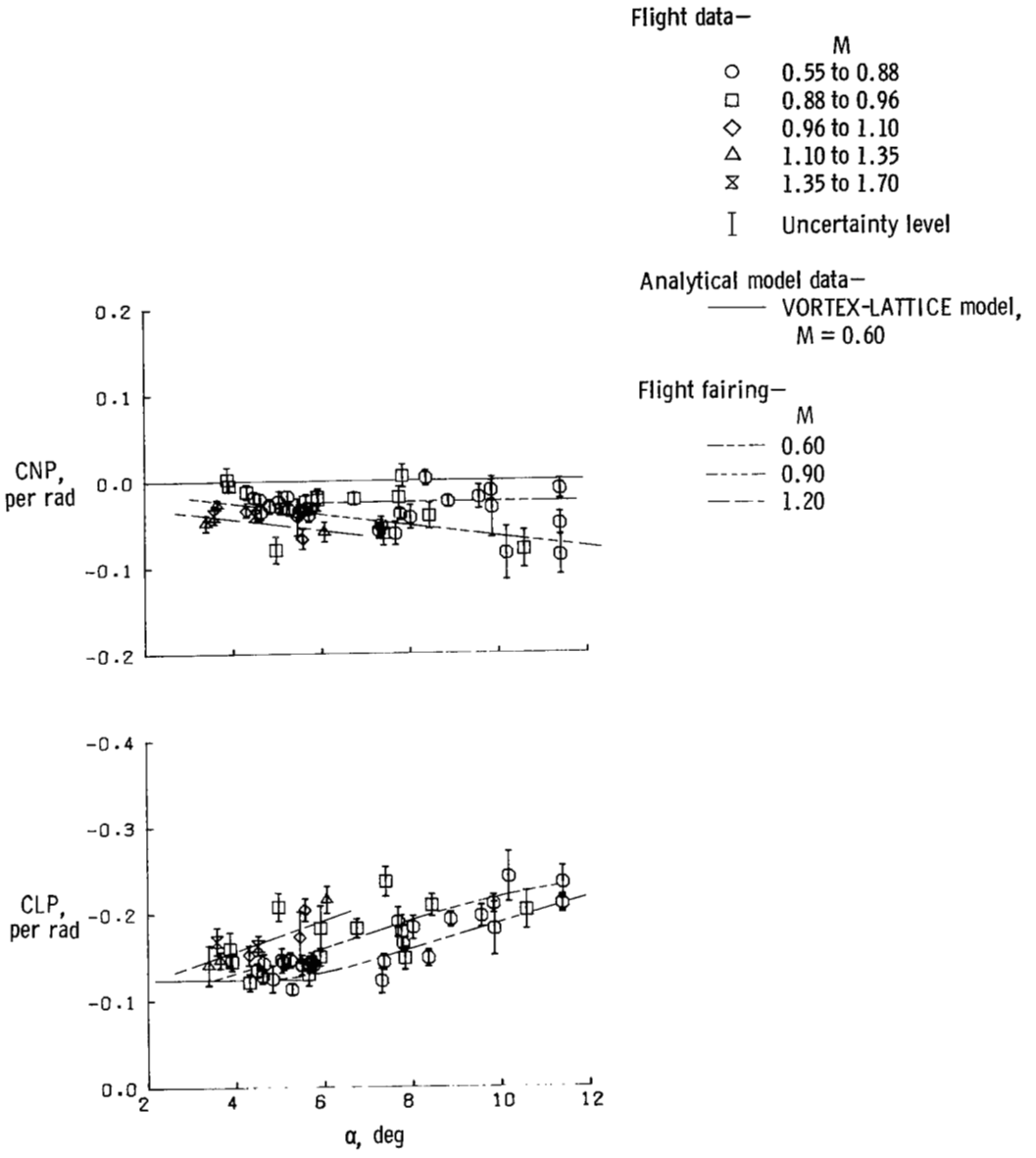

(b) CNP, CLP.

Figure 18. Continued.

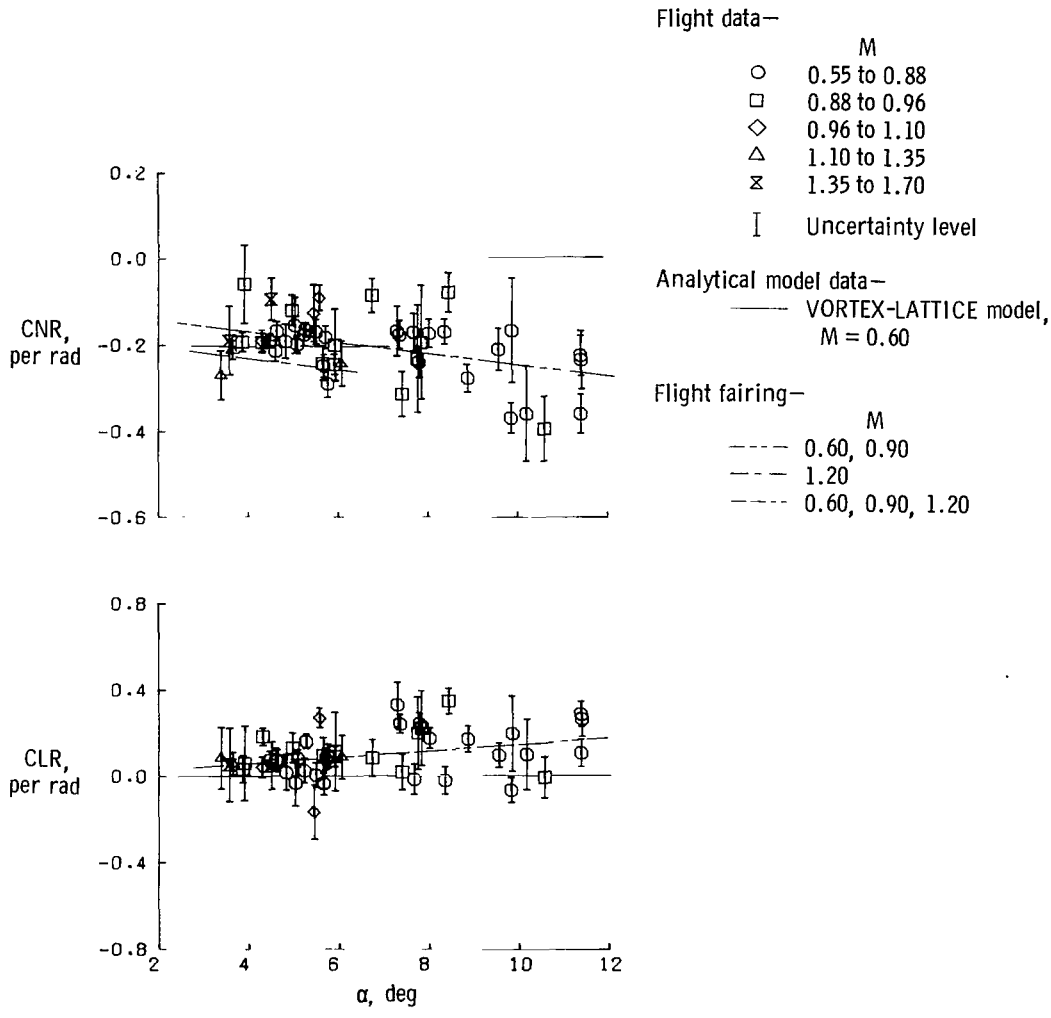

(c) CNR, CLR.

Figure 18. Continued.

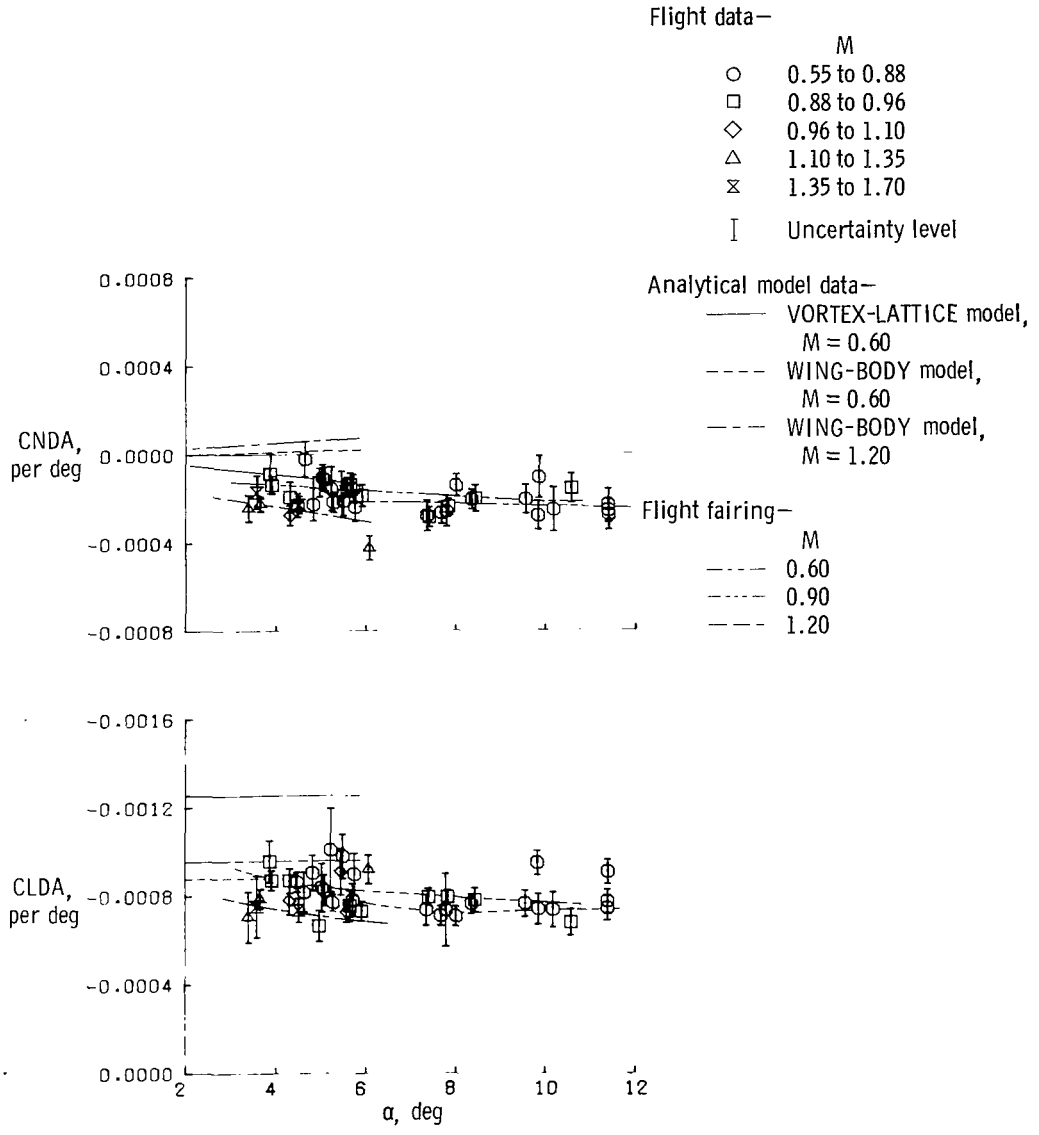

(d) CNDA, CLDA.

Figure 18. Continued.

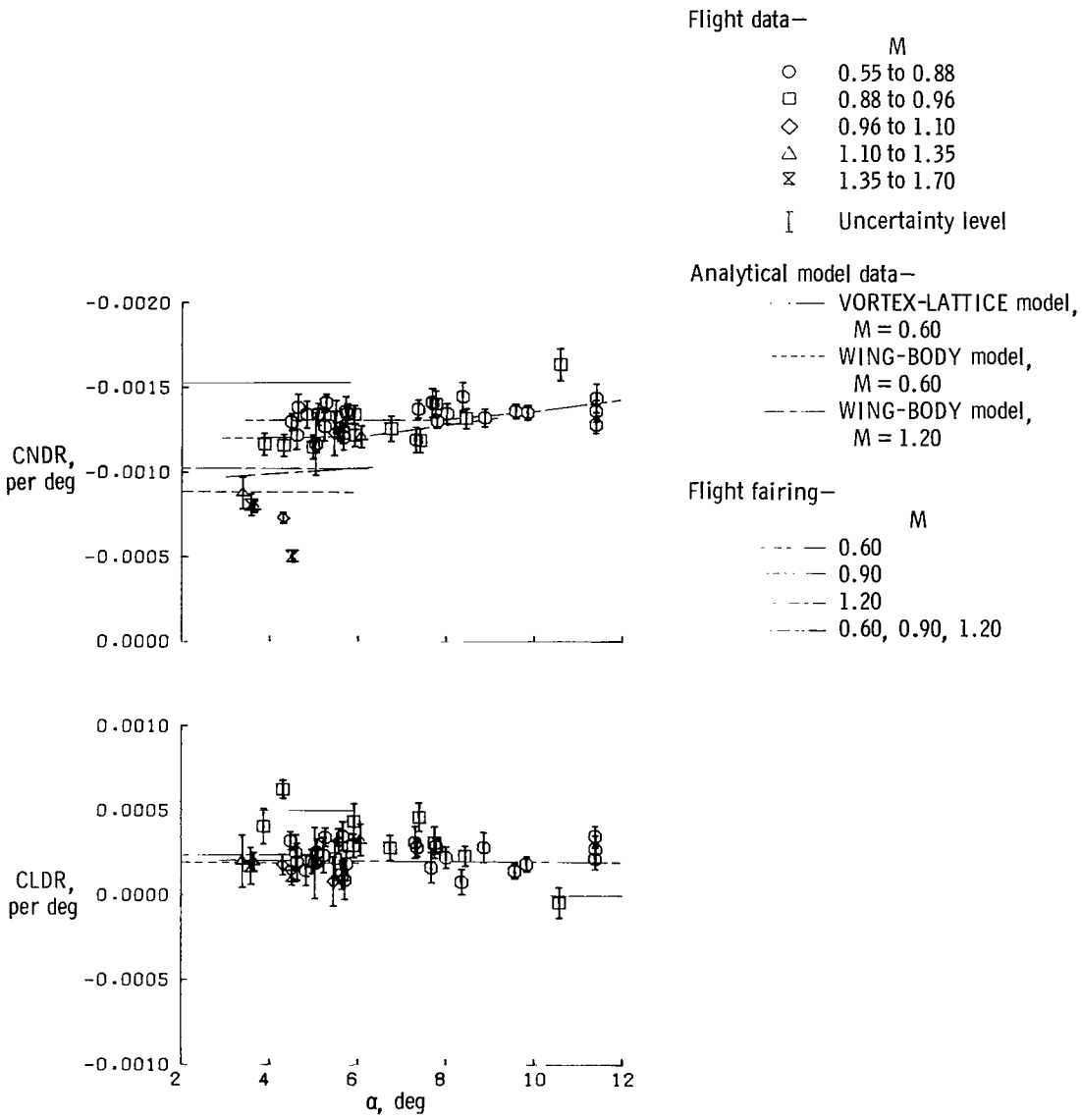

(e) CNDR, CLDR.

Figure 18. Continued.

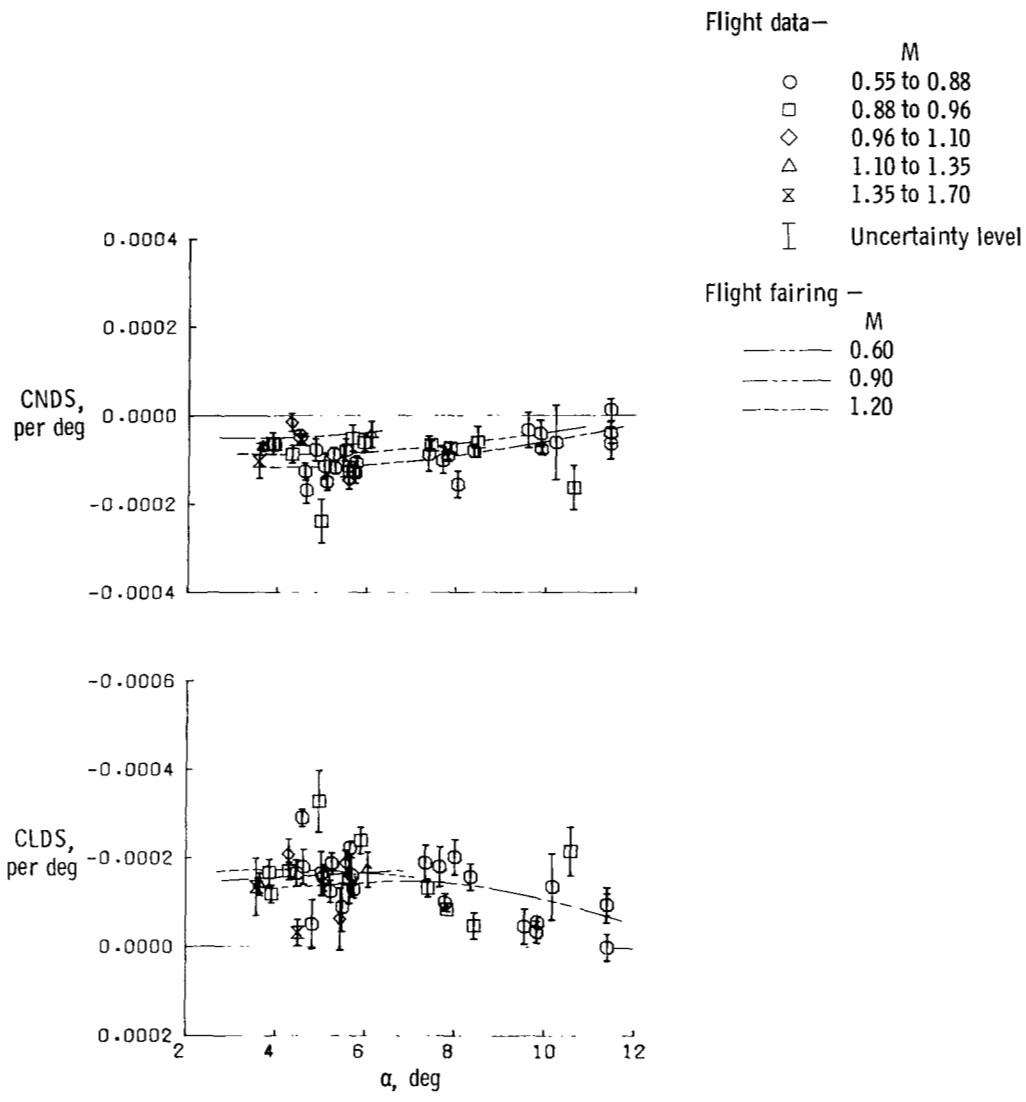

(f) CNDS, CLDS.

Figure 18. Continued.

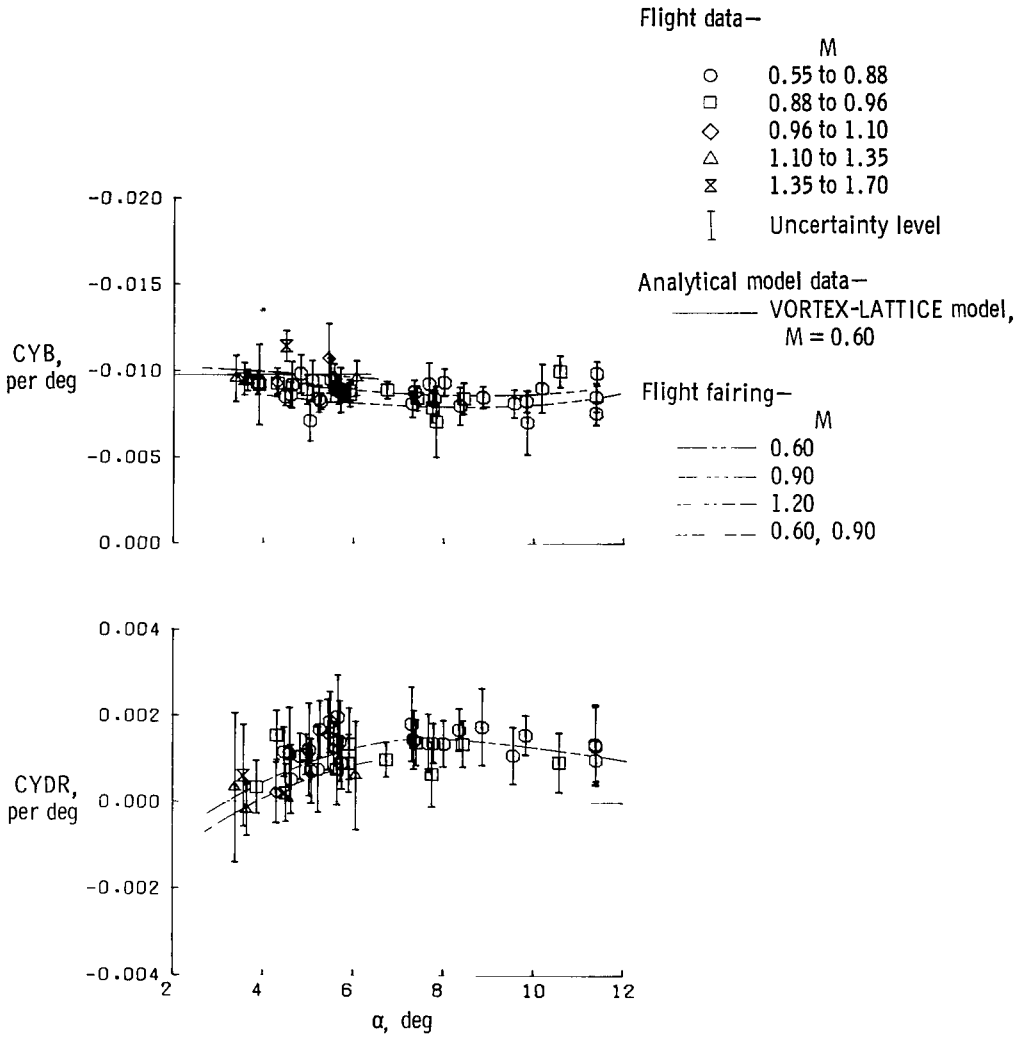

(g) CYB, CYDR.

Figure 18. Continued.

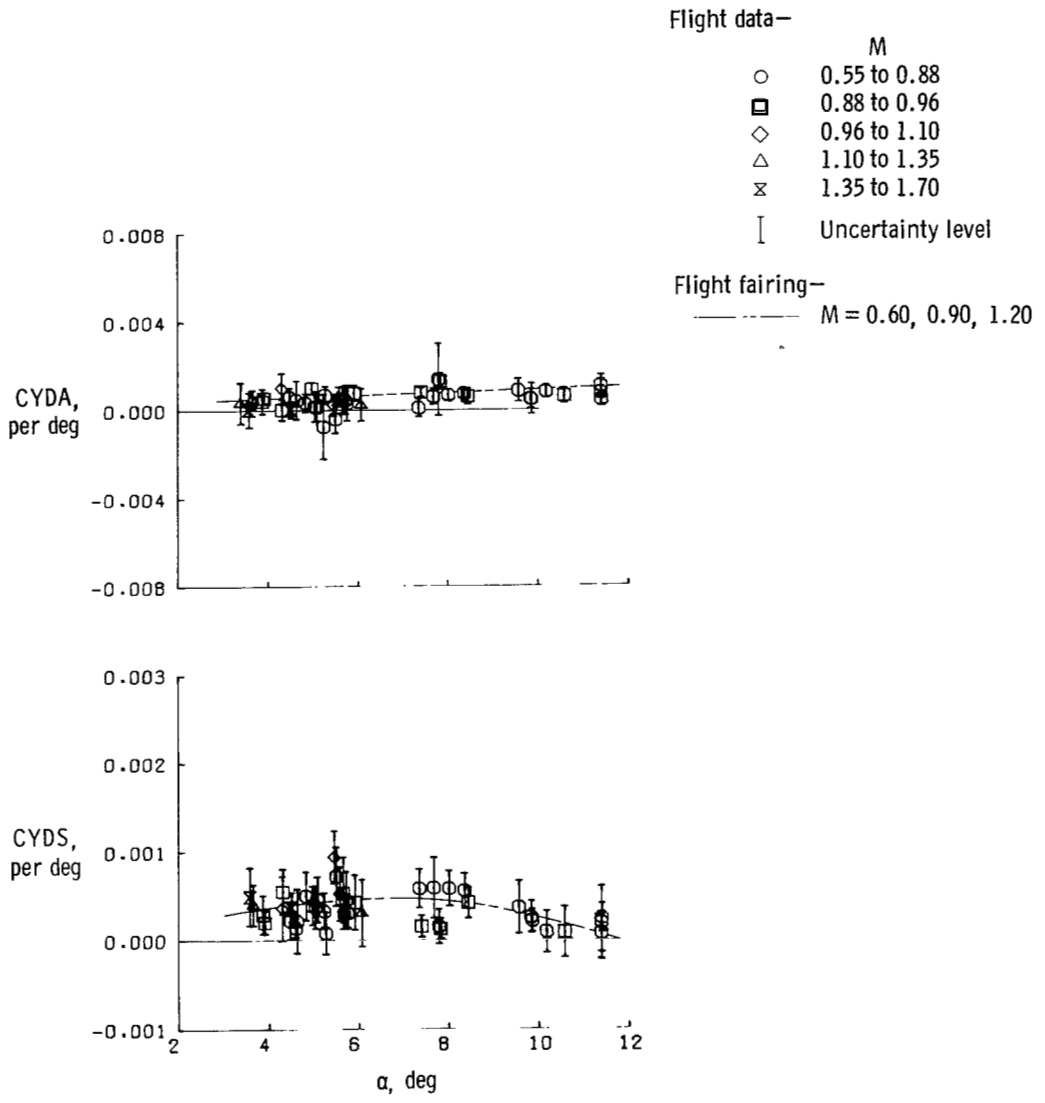

(h) CYDA, CYDS.

Figure 18. Concluded.

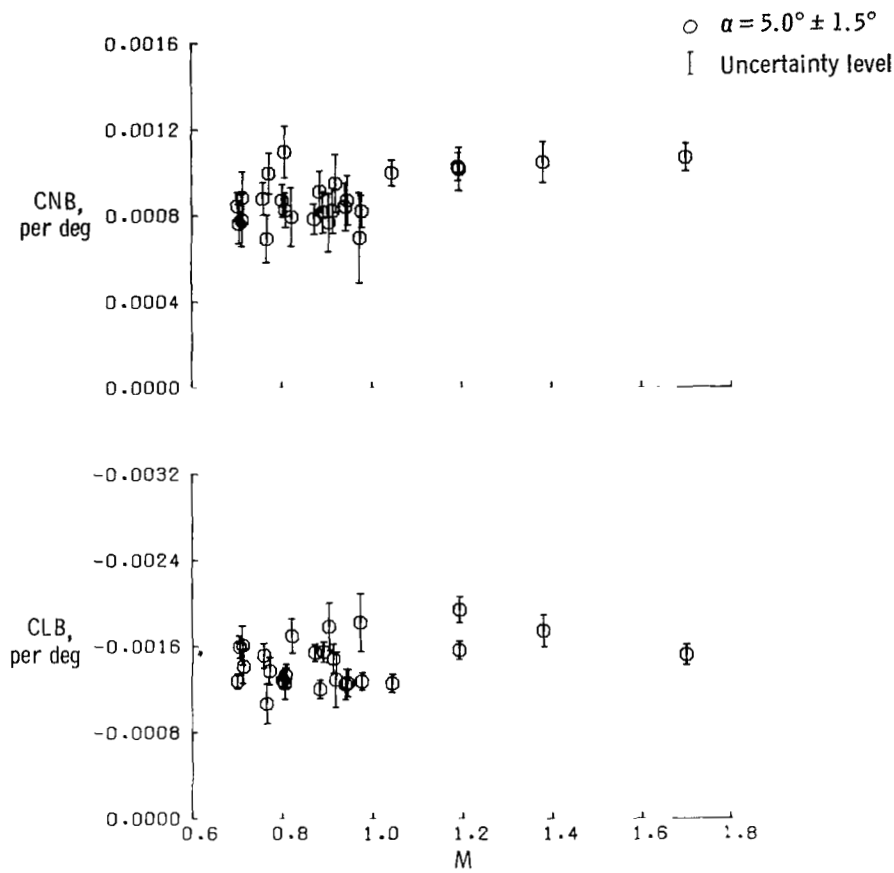

(a) CNB, CLB.

Figure 19. Lateral-directional derivatives obtained from flight data as a function of Mach number. λ = 58°; clean configuration.

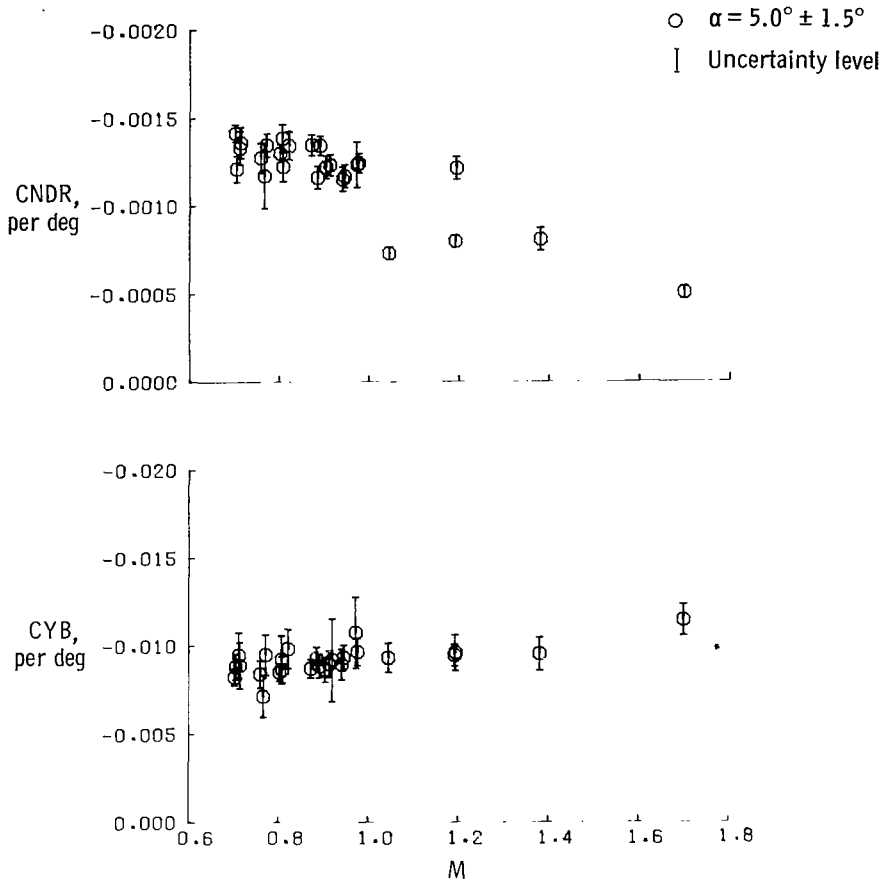

(b) CNDR, CYB.

Figure 19. Continued.

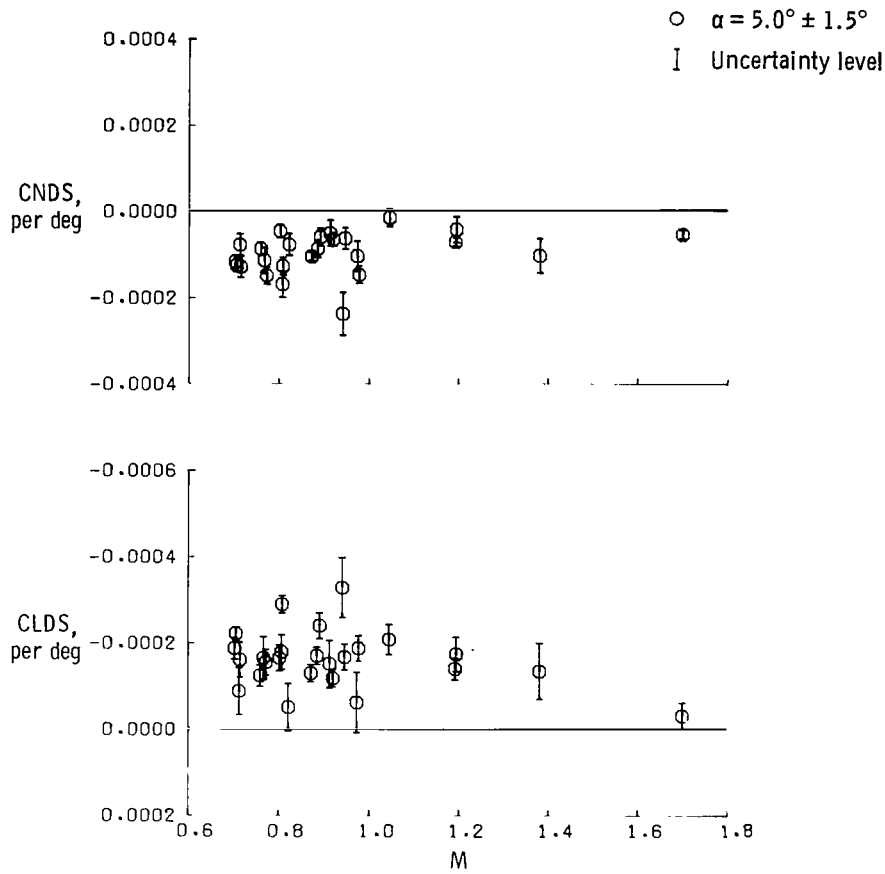

(c) CNDS, CLDS.

Figure 19. Concluded.

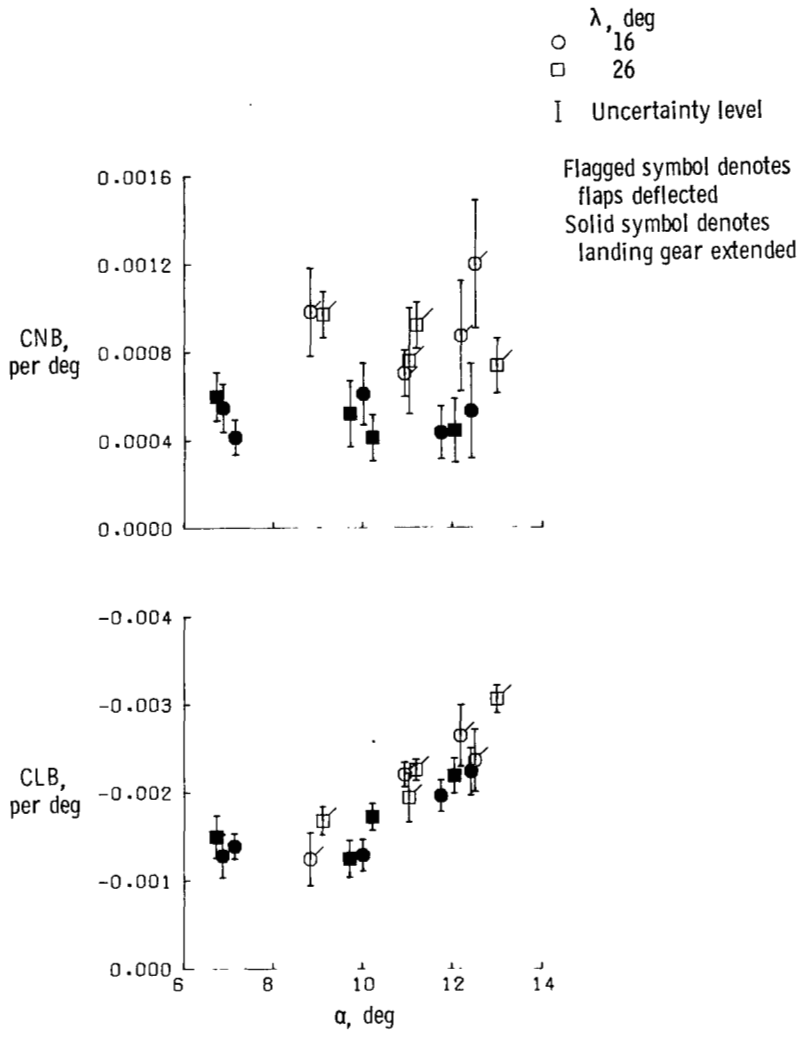

(a) CNB, CLB.

Figure 20. Lateral-directional derivatives obtained from flight data for various combinations of landing gear and flap positions. Low speed.

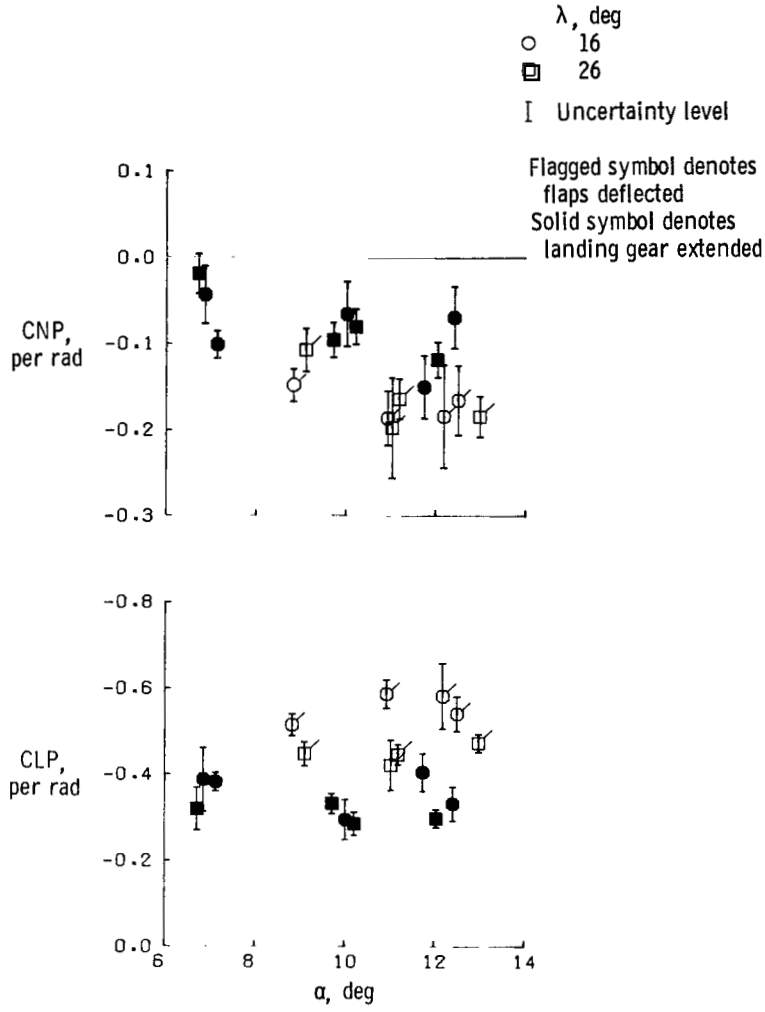

(b) CNP, CLP.

Figure 20. Continued.

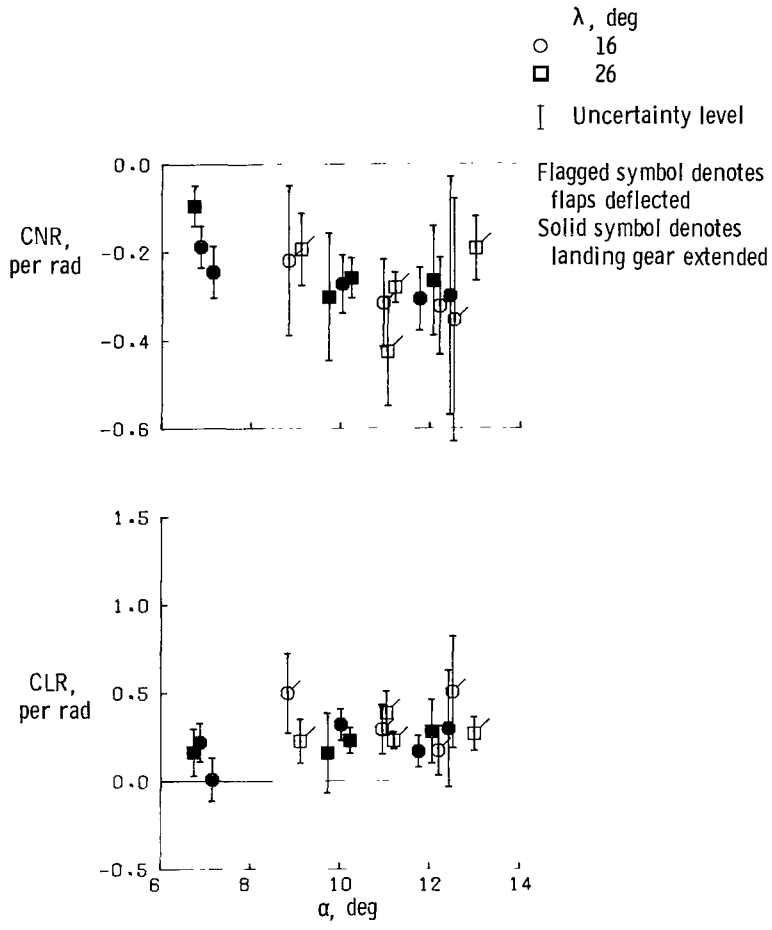

(c) CNR, CLR.

Figure 20. Continued.

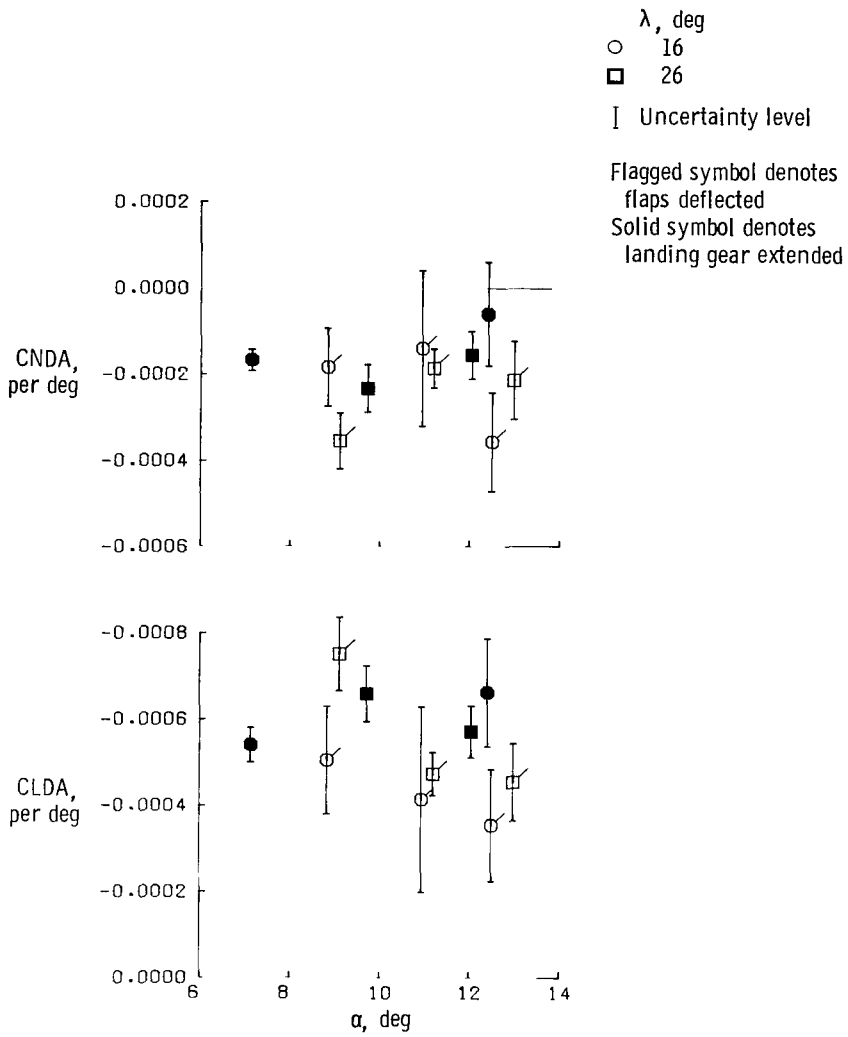

(d) CNDA, CLDA.

Figure 20. Continued.

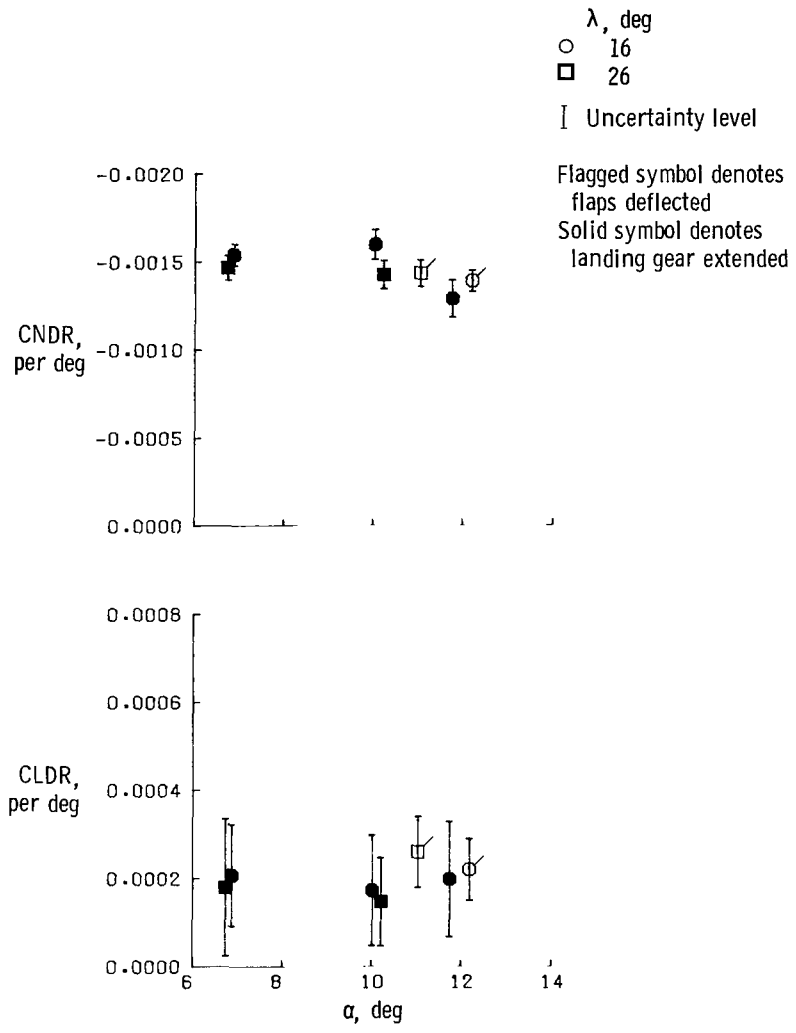

(e) CNDR, CLDR.

Figure 20. Continued.

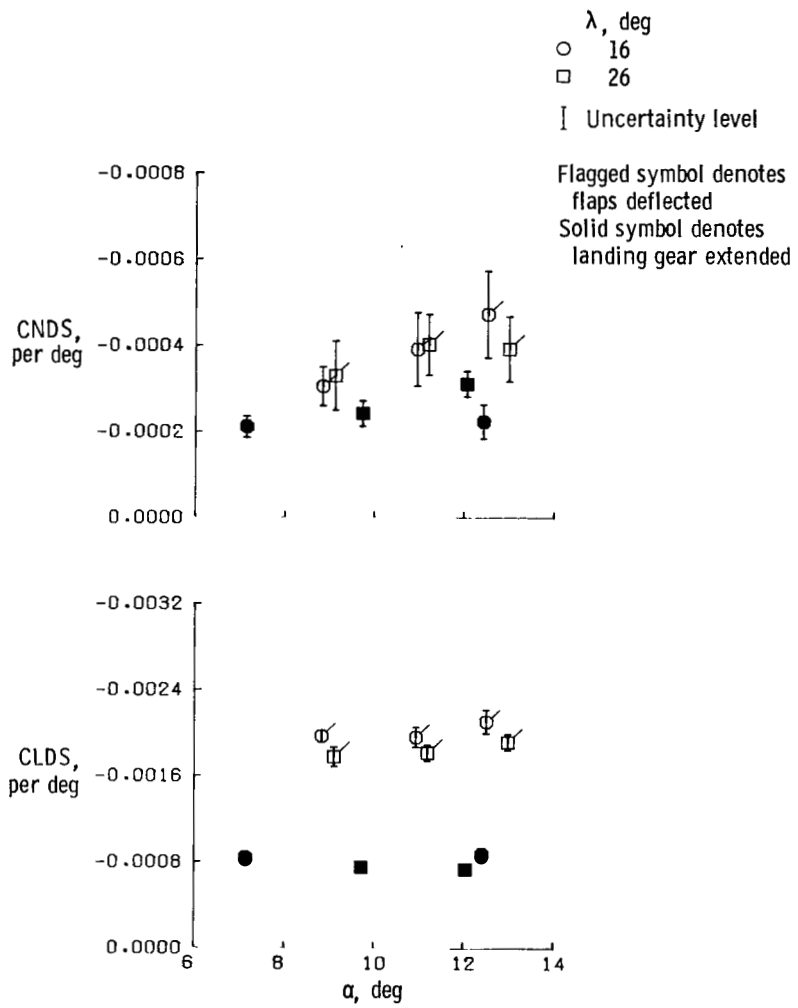

(f) CNDS, CLDS.

Figure 20. Continued.

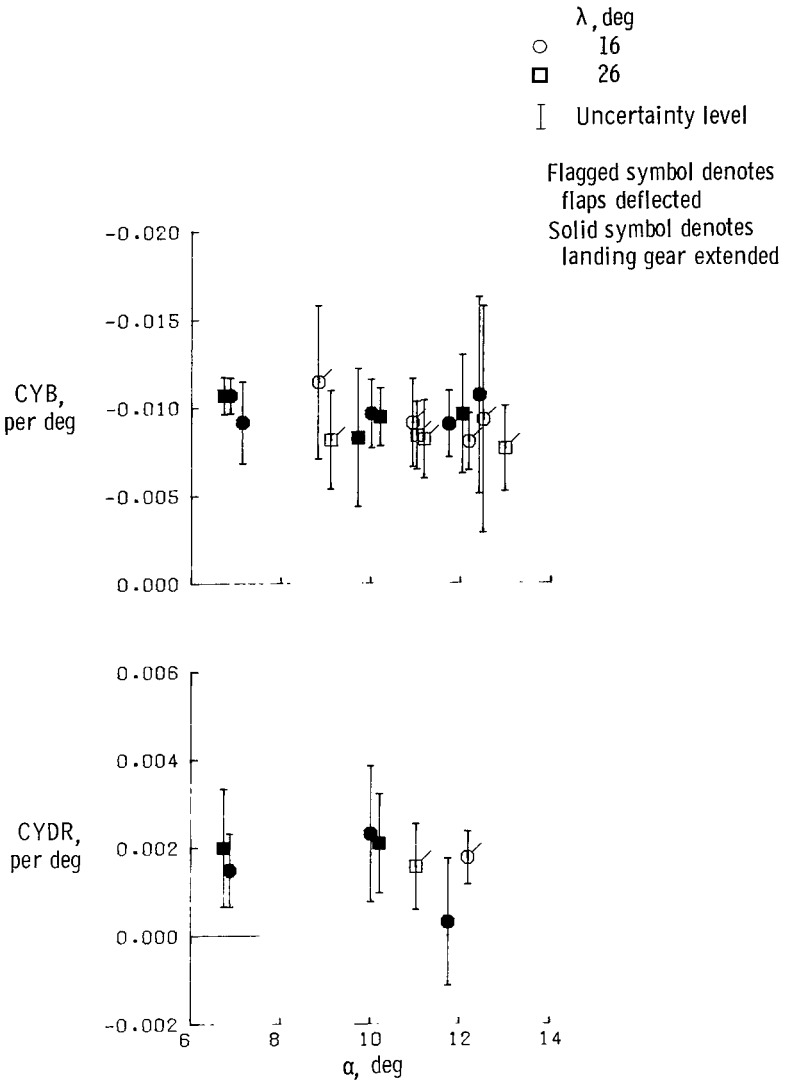

(g) CYB, CYDR.

Figure 20. Continued.

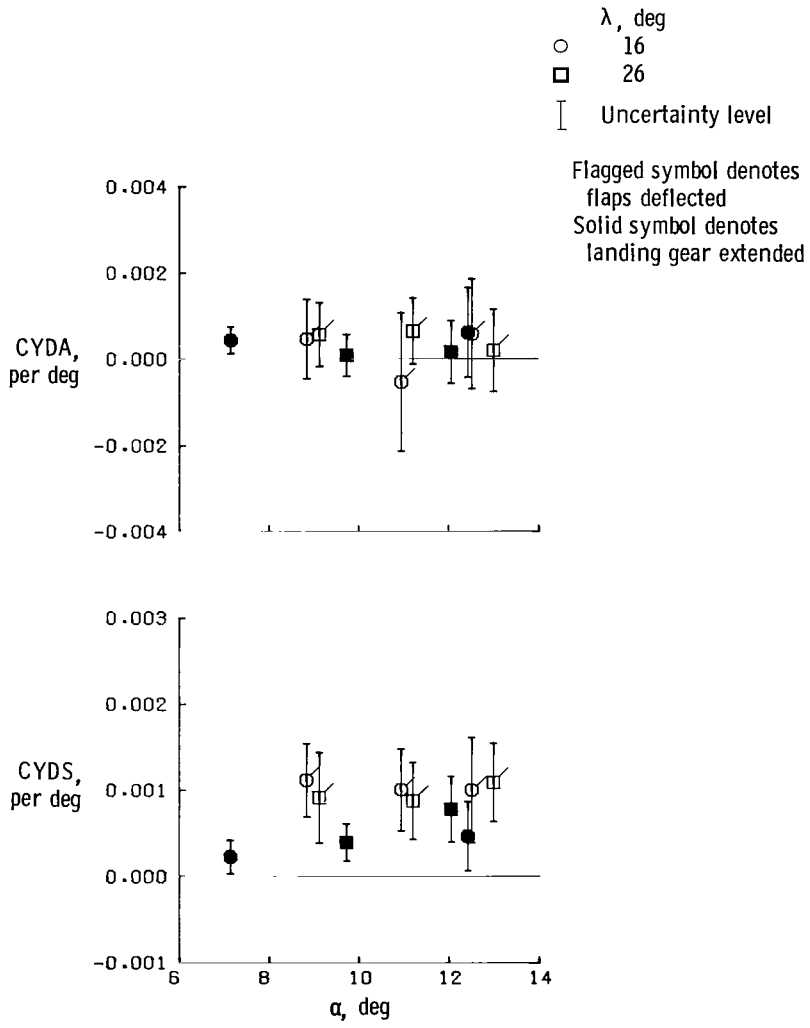

(h) CYDA, CYDS.

Figure 20. Concluded.

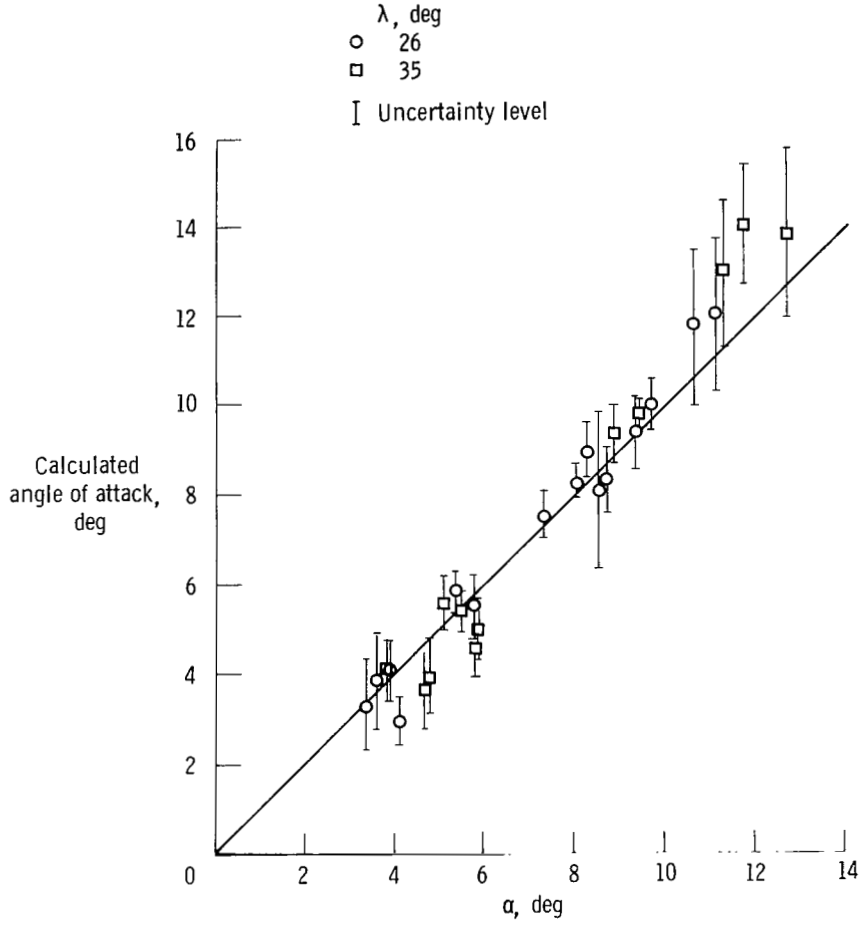

Figure 21. Correlation of calculated and reference angle of attack. M = 0.70.

1. Report No.	2. Government Accession No.	3. Recipient's Catalog No.
NASA TP-1350		

4. Title and Subtitle

FLIGHT-DETERMINED STABILITY AND CONTROL DERIVATIVES FOR THE F-111 TACT RESEARCH AIRCRAFT

5. Report Date: October 1978

6. Performing Organization Code: H-1004

7. Author(s)

Alex G. Sim and Robert E. Curry

8. Performing Organization Report No.

9. Performing Organization Name and Address

NASA Dryden Flight Research Center
P.O. Box 273
Edwards, California 93523

10. Work Unit No.: 505-11-24

11. Contract or Grant No.

12. Sponsoring Agency Name and Address

National Aeronautics and Space Administration
Washington, D.C. 20546

13. Type of Report and Period Covered: Technical Paper

14. Sponsoring Agency Code

15. Supplementary Notes

16. Abstract

A flight investigation was conducted to provide a stability and control derivative data base for the F-111 transonic aircraft technology (TACT) research aircraft. Longitudinal and lateral-directional data were obtained as functions of Mach number, angle of attack, and wing sweep. For selected derivatives, the flight results were correlated with derivatives calculated based on vehicle geometry. The validity of the angle of attack measurement was independently verified at a Mach number of 0.70 for angles of attack between 3° and 10°.

17. Key Words (Suggested by Author(s))

Transonic aircraft technology, supercritical wing, maximum likelihood, derivative extraction, computational aerodynamics, Woodward panel method, vortex-lattice method

18. Distribution Statement

Unclassified—Unlimited

STAR Category: 08

19. Security Classif. (of this report)	20. Security Classif. (of this page)	21. No. of Pages	22. Price*
Unclassified	Unclassified	80	$4.75

*For sale by the National Technical Information Service, Springfield, Virginia 22161

NASA-Langley, 1978

National Aeronautics and
Space Administration

Washington, D.C.
20546

Official Business
Penalty for Private Use, $300

THIRD-CLASS BULK RATE

Postage and Fees Paid
National Aeronautics and
Space Administration
NASA-451

9 1 10,A, 100678 S00903DS
DEPT OF THE AIR FORCE
AF WEAPONS LABORATORY
ATTN: TECHNICAL LIBRARY (SUL)
KIRTLAND AFB NM 87117

POSTMASTER: If Undeliverable (Section 158 Postal Manual) Do Not Return